



HAL
open science

Search for non-minimal Higgs bosons in Z^0 decays

O. Adriani, M. Aguilar-Benitez, S. Ahlen, J. Alcaraz, A. Aloisio, G. Alverson,
M.G. Alviggi, G. Ambrosi, Q. An, H. Anderhub, et al.

► **To cite this version:**

O. Adriani, M. Aguilar-Benitez, S. Ahlen, J. Alcaraz, A. Aloisio, et al.. Search for non-minimal Higgs bosons in Z^0 decays. *Zeitschrift für Physik C Particles and Fields*, 1993, 57, pp.355-381. 10.1007/BF01474331 . in2p3-00001222

HAL Id: in2p3-00001222

<https://hal.in2p3.fr/in2p3-00001222>

Submitted on 9 Mar 1999

HAL is a multi-disciplinary open access archive for the deposit and dissemination of scientific research documents, whether they are published or not. The documents may come from teaching and research institutions in France or abroad, or from public or private research centers.

L'archive ouverte pluridisciplinaire **HAL**, est destinée au dépôt et à la diffusion de documents scientifiques de niveau recherche, publiés ou non, émanant des établissements d'enseignement et de recherche français ou étrangers, des laboratoires publics ou privés.

**Search for Non-Minimal Higgs Bosons
in Z^0 Decays**

The L3 Collaboration

ABSTRACT

We report on a search for the neutral and charged Higgs bosons predicted by models of spontaneous symmetry breaking with more than one Higgs doublet field. No signals are observed. We set model-independent limits on masses or branching ratios of singly and pair-produced neutral and charged Higgs bosons. In addition, we interpret our results in the framework of a general two-doublet Higgs model and the Minimal Supersymmetric extension of the Standard Model.

Contents

1	Introduction	2
2	L3 Detector and Simulation	3
3	Search for Higgs Boson Bremsstrahlung	5
3.1	Search in the $Z^0 \rightarrow h^0 Z^{0*} \rightarrow h^0 \nu \bar{\nu}$ Channel	7
3.2	Search in the $Z^0 \rightarrow h^0 Z^{0*} \rightarrow h^0 \mu^+ \mu^-$ Channel	8
3.2.1	Mass Range $2 \text{ GeV} < m_h < 15 \text{ GeV}$	8
3.2.2	Mass Range $2m_\mu < m_h < 2 \text{ GeV}$	9
3.2.3	Mass Range $0 < m_h < 2m_\mu$	11
3.3	Search in the $Z^0 \rightarrow h^0 Z^{0*} \rightarrow h^0 e^+ e^-$ Channel	12
3.3.1	Mass Range $2 \text{ GeV} < m_h < 30 \text{ GeV}$	12
3.3.2	Mass Range $0 < m_h < 2 \text{ GeV}$	13
3.4	Search in the $Z^0 \rightarrow h^0 Z^{0*} \rightarrow A^0 A^0 Z^{0*}$ Channel	15
3.5	Results for $Z^0 \rightarrow h^0 Z^{0*}$ Searches	16
4	Search for Neutral Higgs Boson Pair-Production	17
4.1	Search in the $Z^0 \rightarrow h^0 A^0 \rightarrow b\bar{b}b\bar{b}$ Channel	17
4.1.1	Selection-Details	17
4.1.2	Results for $b\bar{b}b\bar{b}$ Channel	20
4.2	Search in the $Z^0 \rightarrow h^0 A^0 \rightarrow A^0 A^0 A^0 \rightarrow b\bar{b}b\bar{b}b\bar{b}$ Channel	23
4.2.1	Selection-Details	23
4.2.2	Results for $b\bar{b}b\bar{b}b\bar{b}$ Channel	24
4.3	Search in the $Z^0 \rightarrow h^0 A^0 \rightarrow \tau^+ \tau^- b\bar{b}$ Channel	26
4.3.1	Selection-Details	26
4.3.2	Mass Reconstruction of the τ -Pair	28
4.3.3	Results for $\tau^+ \tau^- b\bar{b}$ Channel	30
4.4	Search in the $Z^0 \rightarrow h^0 A^0 \rightarrow \tau^+ \tau^- \tau^+ \tau^-$ Channel	32
4.4.1	Selection-Details	34
4.4.2	Results for $\tau^+ \tau^- \tau^+ \tau^-$ Channel	35
5	Search for Charged Higgs Boson Pair-Production	38
5.1	Search in the $Z^0 \rightarrow H^+ H^- \rightarrow c\bar{s}c\bar{s}$ Channel	38
5.1.1	Selection-Details	38
5.1.2	Results for $c\bar{s}c\bar{s}$ Channel	40
5.2	Search in the $Z^0 \rightarrow H^+ H^- \rightarrow cs\tau\nu$ Channel	41
5.2.1	Selection-Details	41
5.2.2	Results for $cs\tau\nu$ Channel	44
5.3	Search in the $Z^0 \rightarrow H^+ H^- \rightarrow \tau^+ \nu \tau^- \bar{\nu}$ Channel	44
5.3.1	Selection-Details	44
5.3.2	Results for $\tau^+ \nu \tau^- \bar{\nu}$ Channel	48
6	Interpretation in the Two-Doublet Higgs Model	49
6.1	Constraints from Higgs Bremsstrahlung	51
6.2	Constraints from the Z^0 Line-Shape	52
6.3	Excluded Region in the (m_h, m_A) Plane	52

6.4	Combined Limit on Charged-Higgs Production	52
7	Interpretation in the Minimal Supersymmetric Standard Model	53
8	Conclusions	58

1 Introduction

In the Standard Model of electroweak interactions [1], the Higgs mechanism [2] generates masses for gauge bosons and charged fermions via spontaneous breaking of the local gauge symmetry. At least one doublet of Higgs fields is required, leading to one physical particle, the Higgs boson H_{SM}^0 . Its production and decay rates depend only on its mass. The L3 collaboration has searched for this Standard Model Higgs boson and excluded it for masses up to 52 GeV [3].

In this paper we report on searches for neutral and charged Higgs bosons in the framework of more general models with more than one Higgs doublet [4]. In such models, production rates and decay properties depend not only on the Higgs boson masses, but also on additional parameters not predicted by the model. Rates for Higgs boson production by bremsstrahlung from the Z^0 could thus be significantly smaller than those predicted by the minimal Standard Model. Furthermore, neutral and charged Higgs bosons could be produced in pairs.

Possible extensions of the Higgs sector of the Standard Model are constrained by the fact that the ρ parameter, $\rho \equiv m_W/(m_Z \cos \theta_W)$, is measured to be close to unity [5] and stringent limits on the existence of flavor changing neutral currents [5]. However, models that group all Higgs fields into doublets of weak isospin do not modify the Standard Model prediction for ρ . They also allow cancellation of flavor-changing neutral current amplitudes without fine tuning. As a minimal implementation of such an extension, we consider a model with two Higgs doublets, also required in the Minimal Supersymmetric extension of the Standard Model (MSSM) [6].

The Higgs sector of a two-doublet model contains 5 physical Higgs bosons: one neutral CP-odd A^0 boson, two neutral CP-even bosons h^0 and H^0 , and two charged bosons H^\pm . The CP-odd nature of the A^0 boson forbids its bremsstrahlung emission off the Z^0 . The decays $Z^0 \rightarrow h^0 h^0$ and $Z^0 \rightarrow A^0 A^0$ are forbidden by Bose-symmetry. Defining h^0 as the lightest of the two neutral CP-even bosons, the dominant Higgs boson production processes at the Z^0 resonance which we investigate are:

- a) the bremsstrahlung process: $Z^0 \rightarrow Z^{0*} h^0$,
- b) neutral pair-production: $Z^0 \rightarrow h^0 A^0$,
- c) charged pair-production: $Z^0 \rightarrow H^+ H^-$.

We thus search for both singly and pair-produced Higgs bosons. Higgs bosons tend to decay into the heaviest kinematically allowed quark and lepton pairs.

In the two-doublet model, the rates of production via processes a) and b) depend on three types of parameters: the Higgs boson masses, the mixing angle α between the neutral scalar Higgs fields and $\tan \beta$, the ratio of the vacuum expectation values of the two Higgs doublets. The rate for process a) is proportional to $\sin^2(\beta - \alpha)$ while process b) has a cross section proportional to $\cos^2(\beta - \alpha)$.

For the bremsstrahlung production process a), we search for signatures of

$$Z^0 \rightarrow h^0 Z^{0*} \rightarrow h^0 \nu \bar{\nu}, h^0 \mu^+ \mu^-, h^0 e^+ e^-, \quad (1)$$

where the h^0 decays into quark and lepton pairs either directly, or via $h^0 \rightarrow A^0 A^0$. Decay modes of this kind have already been looked for in the search for the minimal Standard Model Higgs boson [3], but the limits obtained can be reinterpreted in terms of the additional parameters of the two-doublet model.

The neutral pair-production mechanism b) leads to multijet and/or multi-lepton final states. Searches are made for

$$\begin{aligned} Z^0 &\rightarrow h^0 A^0 \rightarrow b\bar{b}b\bar{b}, \quad \tau^+\tau^-\bar{b}\bar{b}, \quad \tau^+\tau^-\tau^+\tau^-, \\ Z^0 &\rightarrow h^0 A^0 \rightarrow A^0 A^0 A^0 \rightarrow b\bar{b}b\bar{b}b\bar{b} \end{aligned} \quad (2)$$

and results for each channel will be given as limits on:

$$\Gamma(Z^0 \rightarrow h^0 A^0) \text{BR}(h^0 A^0 \rightarrow X) / \Gamma(Z^0 \rightarrow q\bar{q}), \quad (3)$$

as a function of the masses of h^0 and A^0 under consideration, with X being one of the final states given in (2).

In the two-doublet Higgs model the partial width of the Z^0 into pairs of charged Higgs bosons c) is only a function of the charged Higgs boson mass and thus independent of the additional parameters α and β [4]:

$$\Gamma(Z^0 \rightarrow H^+ H^-) = \frac{G_F m_Z^3}{6\sqrt{2}\pi} \left(\frac{1}{2} - \sin^2 \theta_W\right)^2 \beta_{H^\pm}^3, \quad \beta_{H^\pm} = \sqrt{1 - \frac{4m_{H^\pm}^2}{m_Z^2}}, \quad (4)$$

Charged Higgs bosons are again expected to decay predominantly into the heaviest lepton allowed and its associated neutrino, or into the heaviest quark pair whose decay is not suppressed by the smallness of the corresponding CKM matrix element, i.e. $H^\pm \rightarrow \tau^\pm \nu$ or $H^\pm \rightarrow cs$. Therefore, searches for the processes relevant at the Z^0 -resonance are performed in the following three channels:

$$Z^0 \rightarrow H^+ H^- \rightarrow c\bar{s}\bar{c}s, \quad \tau\nu cs, \quad \tau^+\nu\tau^-\nu. \quad (5)$$

Lower limits on the mass of a charged Higgs boson will be presented as a function of its leptonic branching ratio.

This work extends previous searches for singly produced low-mass Higgs [7], neutral pair-produced Higgs [8] and charged pair-produced Higgs [9]. It is based on the L3 data sample collected in 1990 and 1991 corresponding to a total of 408,000 hadronic Z^0 decays at center-of-mass energies between 88.2 and 94.3 GeV.

2 L3 Detector and Simulation

The L3 detector consists of a central tracking chamber, a high resolution electromagnetic calorimeter composed of BGO crystals, a ring of scintillation counters, a uranium and brass hadron calorimeter with proportional wire chamber readout, and an accurate muon chamber system. These detectors are installed in a 12 m diameter magnet which provides a uniform field of 0.5 T along the beam direction. For hadronic jets the fiducial coverage is 99% of 4π .

The central tracking chamber (TEC) is a time expansion chamber which consists of two cylindrical layers of 12 (inner) and 24 (outer) sectors, with 62 wires measuring the $R-\phi$ coordinate. The single wire resolution is 58 μm averaged over the entire cell. The double-track resolution is 640 μm . The BGO electromagnetic calorimeter, which now includes endcaps installed in 1991, covers 85% of the solid angle. The fine segmentation of the BGO detector

and hadron calorimeter allows us to measure the direction of jets with an angular resolution of 2.1° , and to measure the total energy of hadronic events from Z^0 decay with a resolution of 10.2%. The muon detector consists of 3 layers of precise drift chambers, which measure 56 points on the muon trajectory in the bending plane, and 8 points in the non-bending direction. A detailed description of the detector and its performance is given in reference [10].

Events are recorded in the L3 detector if at least one of the following trigger requirements is fulfilled:

Energy trigger: At least 10 GeV is registered in the BGO calorimeter, or 15 GeV in the BGO and barrel hadron calorimeter, or 20 GeV in all calorimeters (including the end-cap calorimeters).

Dimuon trigger: At least two tracks are detected in the muon chambers in non-adjacent octants and at least one scintillation counter has fired.

Single muon trigger: At least one track with a transverse momentum greater than 1.5 GeV is detected in the muon chambers and at least one scintillation counter has fired.

Charged-track trigger: At least two tracks with a transverse momentum greater than 0.15 GeV and with an angular separation greater than 120° in the transverse plane are observed in the TEC.

Scintillation counter trigger: At least 5 out of the 30 barrel scintillation counters fire within 13 ns of the beam gate and at least one pair of the counters hit is separated by more than 45° in azimuth.

Cluster trigger: At least an energy of 6 GeV deposited in a solid angle subtended by one hadron calorimeter module (22.5° polar angle).

These trigger requirements have a large redundancy. Typically at least two trigger requirements are fulfilled. This allows a check on the trigger efficiency of the individual triggers. The combined trigger efficiency for all of the investigated reactions is larger than 99%.

The response of the L3 detector is modeled with the GEANT3 [11] detector simulation program which includes the effects of energy loss, multiple scattering and showering in the detector materials and in the beam pipe. Hadronic showers in the calorimeters are simulated with the GHEISHA [12] program. Generated events are passed through the detector simulation program and are reconstructed by the same program that is used to reconstruct the data for each of the physical processes studied. The database, which keeps track of the detector status, is used in the reconstruction of simulated events to compensate for time-dependent detector inefficiencies. Except where explicitly stated, all Monte Carlo studies mentioned in this article are made with events which have been tracked through the detector by the simulation program.

The right-handed coordinate system that we use to describe the detector is defined as follows: the z axis is along the direction of the incoming e^- , the y axis is vertical and the x axis points towards the center of LEP. The polar angle θ is determined with respect to the z axis, and the azimuthal angle ϕ is determined in the xy plane with respect to the x axis.

In the analysis we use the following Monte Carlo event generation programs: JETSET 7.3 [13] for $Z^0 \rightarrow q\bar{q}$ events; KORALZ [14] for $Z^0 \rightarrow \tau^+\tau^-$ and $Z^0 \rightarrow e^+e^-$ events; DIAG36 [15] for four-fermion final states and PYTHIA 5.6 [16] for the Higgs signal simulation.

The search for the Higgs bosons includes our 1991 data sample, corresponding to 296,000 Z^0 hadronic decays. Combined with the 1990 data this totals 408,000 Z^0 hadronic decays and 17.5 pb^{-1} integrated luminosity at center-of-mass energies between 88.2 and 94.3 GeV.

A quantity which is used in all searches is the number of calorimetric clusters. A cluster is defined as a group of neighboring calorimeter hits, which are likely to be produced by the same particle. Only clusters with a total energy above 100 MeV are used. The algorithm normally reconstructs one cluster for each particle produced near the interaction point. For a cluster energy of 2 GeV the angular resolution is approximately 0.4° for isolated electrons and photons and better than 3° for hadrons.

In all search channels for pair-produced Higgs bosons, jets are reconstructed from clusters in the calorimeters by using an invariant-mass jet algorithm [17]. For each pair of clusters i and j the invariant mass squared

$$y_{ij} = (p_i + p_j)^2/s \quad (6)$$

is then evaluated. p_i and p_j are the four momenta of the clusters, in which the mass of the clusters is included. The cluster pair for which y_{ij} is smallest is replaced by a pseudocluster $p_k = p_i + p_j$. This procedure is repeated until all scaled invariant masses squared, y_{ij} , exceed the jet resolution parameter y_{cut} . Two types of jets are defined, wide jets with minimum invariant mass of resolution of 13 GeV ($y_{\text{cut}} = 0.02$) and narrow jets with minimum mass resolution of 2.9 GeV ($y_{\text{cut}} = 0.001$).

The precision of the Monte Carlo simulations in reconstructing mass resolutions has been studied with $q\bar{q}\gamma$ events [18]. In order to compare the predicted mass resolution of hadronically decaying Higgs bosons with the data events, a sample of $q\bar{q}\gamma$ events with a hard photon is selected. After removing the photon from the reconstruction, their topology is similar to $Z^0 \rightarrow h^0\nu\bar{\nu}$ events. The quantity Δm_{qq} is defined as the difference between the invariant mass of the hadronic system and the mass of the hadronic system computed only from the photon energy imposing energy conservation. Figure 1 shows the result of the comparison as well as the obtained mass resolution for 15% on the invariant mass of the hadronic system. The energies of the hard photon in the $q\bar{q}\gamma$ data sample allow to investigate a hadronic invariant mass range of about 25 to 65 GeV. Data and Monte Carlo agree within the statistical error.

3 Search for Higgs Boson Bremsstrahlung

We search for Higgs bosons with masses ranging up to 60 GeV. To be as independent as possible on the modelling of the hadronic Higgs boson decays, we only use leptonic channels below 2 GeV Higgs mass and we search for final state which are tagged by the decay of the off-shell Z^0 into a pair of electrons or muons.

The search for the Higgs bosons in the 30 GeV to 60 GeV mass range has been recently updated in a published paper [3]. We have searched in the $h^0\nu\bar{\nu}$, $h^0e^+e^-$, $h^0\mu^+\mu^-$, ($h^0 \rightarrow \tau^+\tau^-$)($Z^0 \rightarrow q\bar{q}$), ($h^0 \rightarrow q\bar{q}$)($Z^0 \rightarrow \tau^+\tau^-$) channels. The selection efficiencies for these different channels are given in Table 1.

Only one event passes the selection criteria in the $h^0e^+e^-$ search, described in [3]. The missing mass recoiling against the electron pair, corresponding to a Higgs boson mass, is 31.4 ± 1.5 GeV. This event is consistent with the four-fermion background, expected to be 1.6 ± 0.3 events. In the $h^0\mu^+\mu^-$ search, one event with a well isolated muon pair and a recoiling mass of 70.4 ± 0.7 GeV survives the selection criteria. It is also consistent with the four-fermion background, expected to be 1.7 ± 0.2 events in this channel.

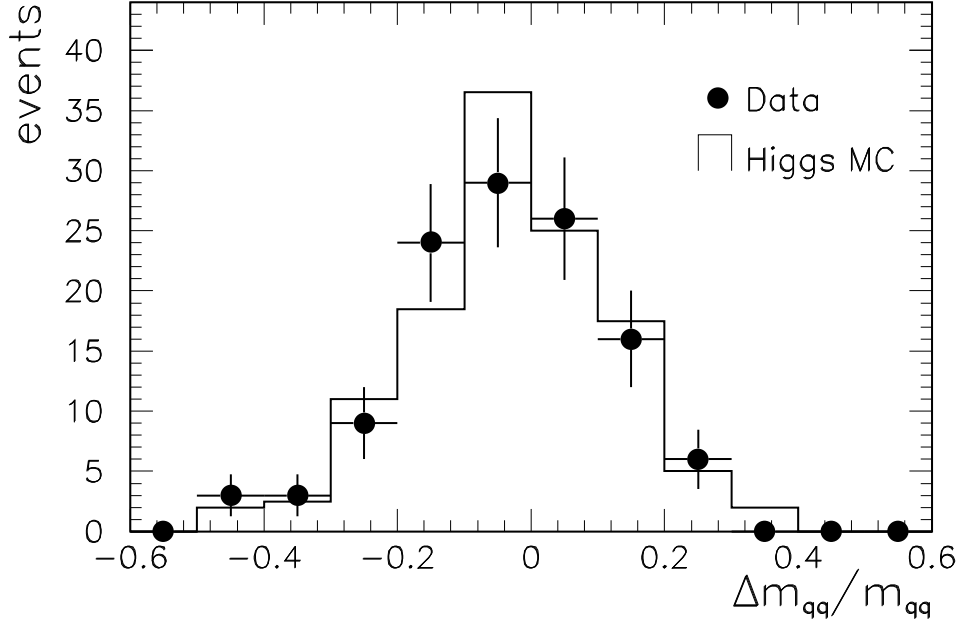


Figure 1: Comparison of data and simulation for Higgs mass reconstruction. After removing the hard photon from a $q\bar{q}\gamma$ data sample, the difference between the invariant mass of the hadronic system and the mass of the hadronic system computed only from the photon energy is compared. For the simulated Higgs bosons δm_{qq} is the resolution of the reconstructed Higgs boson mass. The mass resolution is 15%.

Higgs Mass (GeV)	30	40	50	55	60
$h^0\nu\bar{\nu}$ channel	36.4	60.6	59.0	50.3	37.4
$h^0e^+e^-$ channel (1991)	58.2	55.2	52.2	50.5	49.4
$h^0e^+e^-$ channel (1990)	45.5	38.0	35.0	32.0	29.0
$h^0\mu^+\mu^-$ channel	62.6	61.2	61.6	60.6	55.4
$(h^0 \rightarrow \tau^+\tau^-)(Z^0 \rightarrow q\bar{q})$ (1991)	3.8	10.2	15.6	17.8	14.8
$(h^0 \rightarrow q\bar{q})(Z^0 \rightarrow \tau^+\tau^-)$ (1991)	14.6	8.6	4.0	2.2	1.4
$(h^0 \rightarrow \tau^+\tau^-)(Z^0 \rightarrow q\bar{q})$ (1990)	2.4	5.4	9.4	12.4	8.8
$(h^0 \rightarrow q\bar{q})(Z^0 \rightarrow \tau^+\tau^-)$ (1990)	8.0	4.2	2.2	1.4	1.2

Table 1: Selection efficiencies (in %) for Higgs bosons with masses between 30 GeV and 60 GeV.

3.1 Search in the $Z^0 \rightarrow h^0 Z^{0*} \rightarrow h^0 \nu \bar{\nu}$ Channel

In this channel the mass range $2 \text{ GeV} < m_h < 30 \text{ GeV}$ is investigated. If the Higgs boson has a low mass compared to the Z^0 it gets a large Lorentz boost. For $Z^{0*} \rightarrow \nu \bar{\nu}$, the event has large missing energy and momentum. Such events are characterized by a single jet or two or more acolinear jets.

To reject most of the hadronic events ($e^+e^- \rightarrow q\bar{q}$), we require that the total event energy is less than 70 GeV, the invariant mass of the event less than 65 GeV and the transverse imbalance more than 15% of the total energy and more than 7 GeV. In addition, the energy measured in the region $|\cos \theta| > 0.75$ should be less than 40 GeV. These cuts, associated with the requirement that the longitudinal energy imbalance be less than 80% of the total energy, reject most of the events coming from two-photon interactions ($e^+e^- \rightarrow e^-e^+\gamma\gamma \rightarrow e^+e^-q\bar{q}$). Such events have high longitudinal and low transverse energy imbalance, and sometimes one or both of the final state electrons scatters into the detector. $Z^0 \rightarrow \tau^+\tau^-$ events that may have large transverse imbalance are rejected by requiring that the angle between the two most energetic jets should be less than 2.95 radians.

Events should have at least one-fourth of the tracks with transverse momentum larger than 100 MeV and a distance of closest approach to the interaction point in the plane transverse to the beam (d.c.a.) less than 10 mm. These cuts reject beam-gas and beam-wall interactions in which tracks do not come from the vertex.

Events with muons must have at least 10 GeV calorimetric energy and the sum of the muon momenta should be less than 20 GeV in order to reject cosmic ray events and $e^+e^- \rightarrow \mu^+\mu^-(\gamma)$ events.

For single-jet events we require at least two tracks (one or more of which has transverse momentum more than 100 MeV and d.c.a. less than 10 mm) and at least three calorimetric clusters. No track should be present in the 45° half-angle sector opposite to the jet axis. This cut rejects the $\tau\tau$ events in which there is a single-jet plus a low-energy track opposite to the jet, due to the large momentum taken away by the neutrino in the tau decay.

For multi-jet events there should be at least one track in each of the two most energetic jets. The third jet, if present, should have an energy less than 5 GeV. The variable θ_{123} defined as: zero for one jet, θ_{12} for two jets, (where θ_{12} is the angle between jet₁ and jet₂), and $(\theta_{12} + \theta_{23} + \theta_{31})/2$ for three jets; is a measure of acollinearity and acoplanarity of the most energetic jets ($\theta_{123}=\pi$ if 3 jets are planar or 2 jets are collinear). The distribution of θ_{123} is shown in Figure 2 for real data, for background simulation of Z^0 decaying into $f\bar{f}$, (where $f\bar{f}$ can be e^+e^- or $\mu^+\mu^-$ or $\tau^+\tau^-$ or $q\bar{q}$) and for Higgs signal simulation.

An event is finally accepted if it satisfies the following criteria:

- θ_{123} is less than 2.5 radians,
- the angle in $r\text{-}\phi$ plane between the two most energetic jets is larger than 0.64 radians.

The efficiencies for Higgs boson masses ranging between 2 GeV and 20 GeV are shown in Table 3. No event in the data pass the selection. From a Monte Carlo study of $Z^0 \rightarrow f\bar{f}$ events we expect to see less than one event.

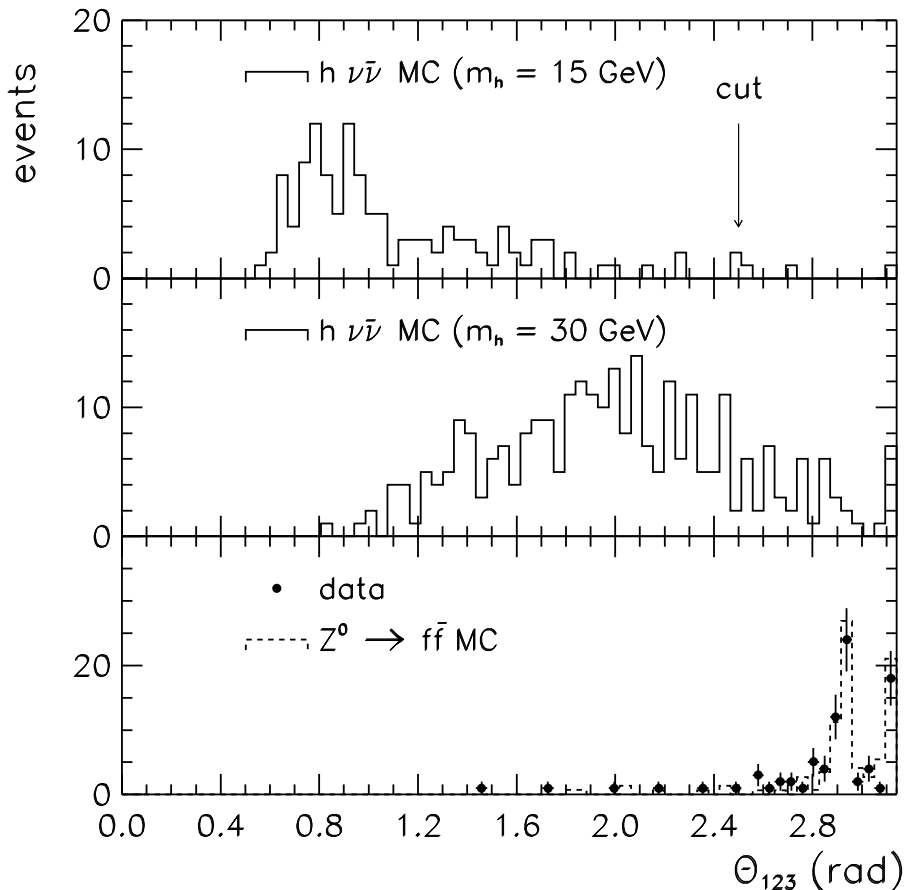


Figure 2: Distribution of θ_{123} for data, simulated background and Higgs signal in the $h^0\nu\bar{\nu}$ channel. See text for a definition of θ_{123} .

3.2 Search in the $Z^0 \rightarrow h^0 Z^{0*} \rightarrow h^0 \mu^+ \mu^-$ Channel

3.2.1 Mass Range $2 \text{ GeV} < m_h < 15 \text{ GeV}$

As one search for the Higgs bosons in the intermediate mass range, we select events with two high-momentum, well isolated muons together with other charged tracks produced in the decay of the Higgs boson. The event must have two muon tracks matching with the vertex, the total number of charged tracks in the TEC must be larger than 2, and the number of calorimetric clusters must be larger than 5.

In order to determine the isolation of the muons, we define for each muon the variable:

$$\mathcal{D} = \frac{E_{\mu \text{ jet}} - p_{\mu}}{p_{\mu}}, \quad (7)$$

where $E_{\mu \text{ jet}}$ is the energy of the jet containing the muon and p_{μ} is the muon momentum. The isolation conditions are:

$$\max(\mathcal{D}_1, \mathcal{D}_2) < 0.75 \quad , \quad \min(\mathcal{D}_1, \mathcal{D}_2) < 0.4 \quad (8)$$

and in each jet containing the muons there must be at most 2 charged tracks.

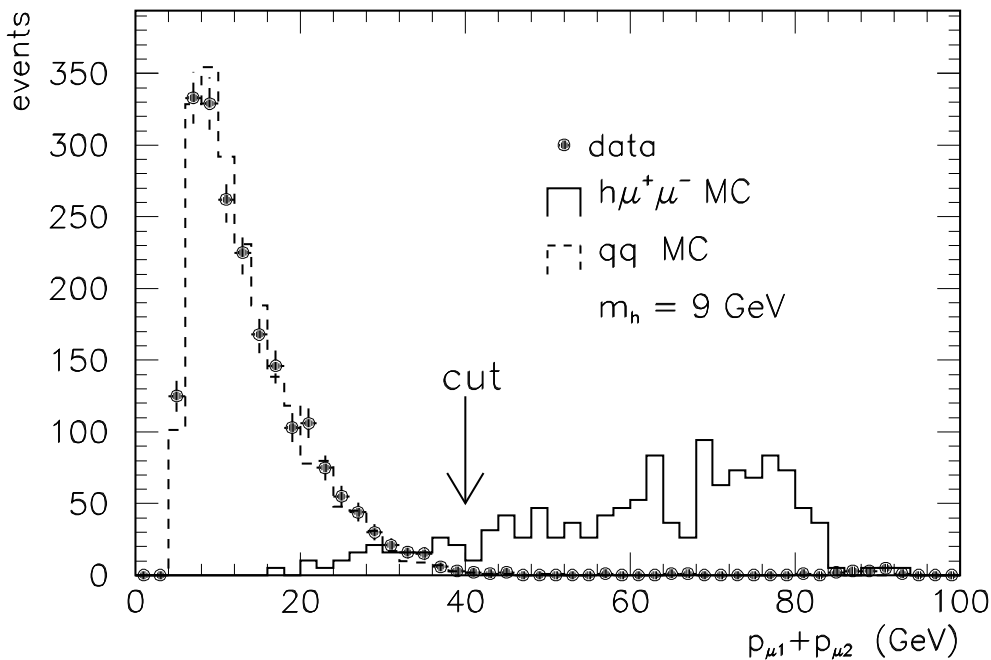


Figure 3: Distribution of the sum of the two muon momenta for data, simulated background and Higgs signal in the $h^0\mu^+\mu^-$ channel.

To reduce the background due to semileptonic decays of the hadrons, we require the sum of the two muon momenta to be larger than 40 GeV: this cut is shown in Figure 3.

After this cut no $e^+e^- \rightarrow q\bar{q}$ event is expected. The only background left is the four-fermion $e^+e^- \rightarrow \mu^+\mu^-\bar{f}f$ process, which is reduced by requiring the acollinearity angle between the two muons to be larger than 0.035 radians. After this selection about 0.6 events are expected from four-fermion processes, and no event in the data survives. The efficiencies for the signal as a function of the Higgs boson mass are shown in Table 3.

3.2.2 Mass Range $2m_\mu < m_h < 2$ GeV

The selection in this mass range is based on the requirement of the presence of two muons and two additional charged tracks.

We require the presence of two muons (μ_1 and μ_2), at least one of which has momentum $p_\mu > 15$ GeV. In order to reject the cosmic background, at least one of the two muons is required to have a d.c.a. from the interaction point less than 100 mm in the plane perpendicular to the beam and less than 200 mm in the z plane. In addition, we require either a 4 ns cut on the scintillator time (after correction for time of flight), or at least one TEC track matching with a muon and with a d.c.a. less than 2 mm.

In order to suppress beam-gas and $\tau^+\tau^-$ background, the total energy of the event is required to be greater than 74 GeV, or greater than 55 GeV if a muon with momentum higher than 40 GeV is present. To remove the $Z^0 \rightarrow q\bar{q}$ background and to select the Higgs boson decay with two tracks, we apply the following cuts, the total number of tracks has to be between 3 and 5 and the transverse momentum of a possible fifth track is required to be less than 0.5 GeV. From this sample we select events which contain at least two oppositely charged TEC tracks

not associated with the two high-momentum muons. In order to increase the efficiency in the $h^0 \rightarrow \mu^+\mu^-$ channel, we also keep events containing an extra muon associated with a TEC track.

Most of the selected events are due to γ conversion in the beam pipe or in the TEC. To reject this background we reconstruct the secondary vertex of the two additional tracks and we require its distance from the interaction point to be less than 20 mm. The remaining background comes from four-fermion decays of the Z^0 . In order to reduce this background we require θ_{tr}^m , the minimum angle between each of the two high-momentum muons and the two additional tracks (or the remaining pair of muons in the four-muon events), to be greater than 20° . The distribution of θ_{tr}^m is shown in Figure 4.

In order to calculate the efficiency of this selection cut, we simulated Higgs boson decays into pairs of e, μ, π, K at different masses between 220 MeV and 2 GeV. The efficiencies are given in Table 2.

Higgs Mass (GeV)	0.01	0.1	0.22	0.3	1.0	3.6
$h^0 \rightarrow e^+e^-$	14.	7.	-	-	40.	-
$h^0 \rightarrow \mu^+\mu^-$	-	-	36.	-	42.	44.
$h^0 \rightarrow \pi^+\pi^-$	-	-	-	34.	35.	38.
$h^0 \rightarrow K^+K^-$	-	-	-	-	31.	35.

Table 2: Selection efficiencies (in %) for light Higgs boson in the $h^0\mu^+\mu^-$ channel.

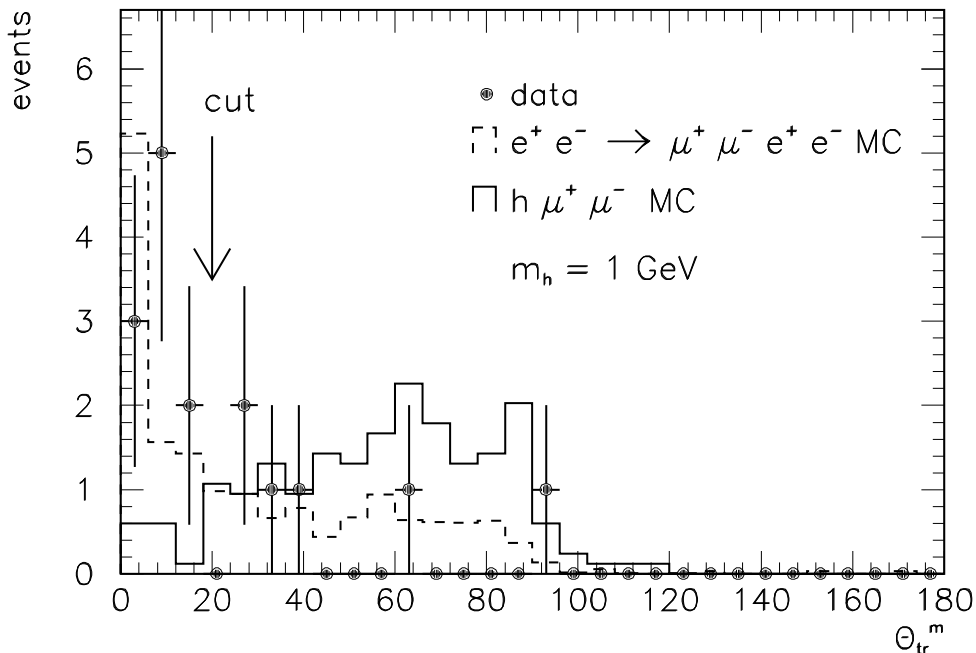


Figure 4: Distribution of the minimum angle between each of the two high-momentum muons

and the two additional tracks, θ_{tr}^m , for data, simulated background and Higgs signal in the $h^0\mu^+\mu^-$ channel.

Six data events survive after applying this cut. We simulated $e^+e^- \rightarrow e^+e^-\mu^+\mu^-$ and $e^+e^- \rightarrow \mu^+\mu^-\mu^+\mu^-$ events, using the four-fermion generator. The expected background is 5.8 ± 1.2 events from $e^+e^- \rightarrow e^+e^-\mu^+\mu^-$, and 1.9 ± 0.2 from $e^+e^- \rightarrow \mu^+\mu^-\mu^+\mu^-$.

3.2.3 Mass Range $0 < m_h < 2m_\mu$

Below the $\mu^+\mu^-$ threshold the Higgs boson decays predominantly into an e^+e^- pair. We have used the selection method described in the previous section also to search for $h^0 \rightarrow e^+e^-$ events. For Higgs boson masses below 100 MeV, however, this method becomes inefficient due to the absence of tracks in the 50 cm radius vertex chamber. In this case we developed a complementary method. It relies on the fact that if the Higgs boson decays outside the volume of the electromagnetic calorimeter, the event will contain only two acoplanar muons with no other detected particle balancing the missing momentum. To select events with 2 muons we first apply the following set of cuts:

- The event is required to have two tracks in the muon chambers in the fiducial volume defined by $|\cos\theta| < 0.8$ satisfying:
 - a) The tracks must have an acoplanarity angle of less than 90° in order to match the dimuon trigger requirements.
 - b) At least one track must extrapolate to within 100 mm of the nominal vertex position in both the transverse and longitudinal planes.
- Both muon chamber tracks must have a measured momentum greater than 30 GeV.
- At least one of the scintillation counters hit by the muons must give a signal which, after correction for time of flight, must be within 4 ns of the beam gate.
- The event is required to have at least one and no more than five TEC tracks with a transverse distance of closest approach to the beam axis of less than 5 mm.
- When the TEC is not operational the event is selected if both muons have an associated scintillator hit in time and the number of calorimetric clusters in the event is less than 15.

Most of the cuts are the same as those used in the standard $\mu^+\mu^-$ selection. We require high momentum for both muons in order to suppress the contribution from two-photon processes and $\tau^+\tau^-$ events decaying into $\mu^+\mu^-$.

A potential background comes from $\mu^+\mu^-(\gamma)$ events, where the photon leaves all the energy in the first 22 radiation lengths of the detector. The requirements for the selection of the signal are the following:

- There must be at most one TEC track within a cone of 30° around each muon-chamber track (extrapolated back to the TEC). This cut rejects four-fermion events arising from final-state bremsstrahlung processes.

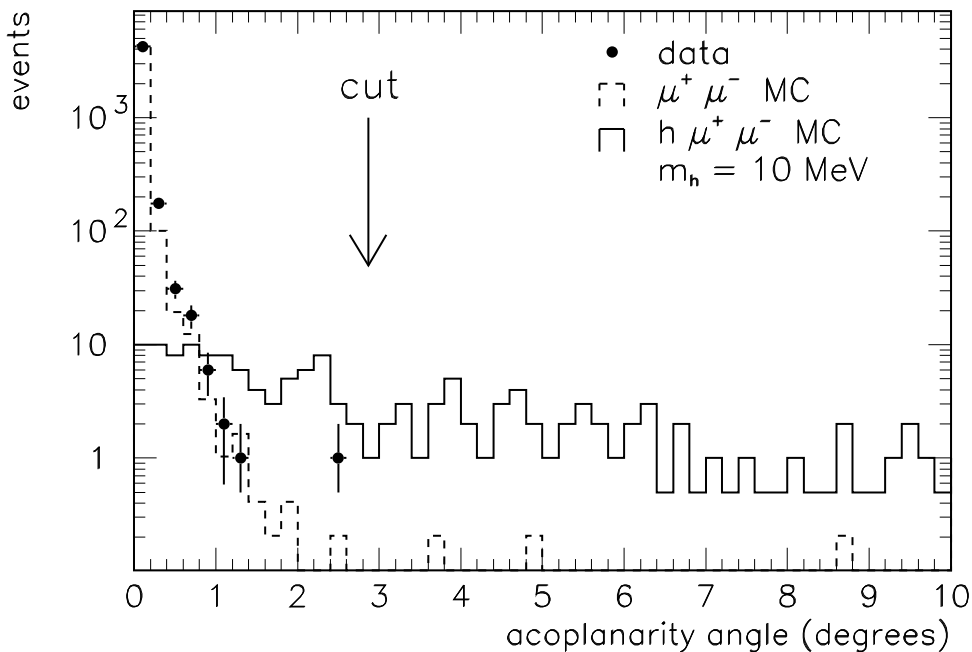


Figure 5: *Acoplanarity angle distribution for data, simulated background and Higgs signal in the $h^0\mu^+\mu^-$ channel.*

- The acoplanarity between both muons must be greater than 50 mrad (2.86°). The distribution of this acoplanarity angle is shown in Figure 5.
- Events with significant deposition of energy in the first 22 radiation lengths of the detector are rejected. In order to be insensitive to noise, we only consider depositions above 0.5 GeV in the electromagnetic calorimeter and above 1.0 GeV in the hadronic calorimeter.

The detection efficiency for a 10 MeV Higgs boson is given in Table 2. For higher masses (~ 100 MeV), the Higgs boson can also decay inside the TEC chamber. Therefore we have used the complementary selection of the mass range $2 m_\mu < m_h < 2$ GeV. The result is also shown in Table 2.

The expected background from $e^+e^- \rightarrow \mu^+\mu^-(\gamma)$ events has been estimated to be less than one. No candidates were found in the data.

3.3 Search in the $Z^0 \rightarrow h^0 Z^{0*} \rightarrow h^0 e^+e^-$ Channel

3.3.1 Mass Range $2 \text{ GeV} < m_h < 30 \text{ GeV}$

The distinctive signature of the process $Z^0 \rightarrow h^0 e^+e^-$ is two high-energy well separated electrons recoiling against one or two hadronic jets coming from the h^0 decay products. The main background is the four-fermion process $e^+e^- \rightarrow e^+e^-q\bar{q}$.

In order to remove low-multiplicity events, mainly e^+e^- and $\tau^+\tau^-$ pairs, we require at least 3 clusters in the BGO electromagnetic calorimeter and more than two tracks in the TEC. To remove hadronic background, we select events where the sum of the energy of the two most energetic electromagnetic clusters is larger than 40 GeV. The distribution of this sum is shown

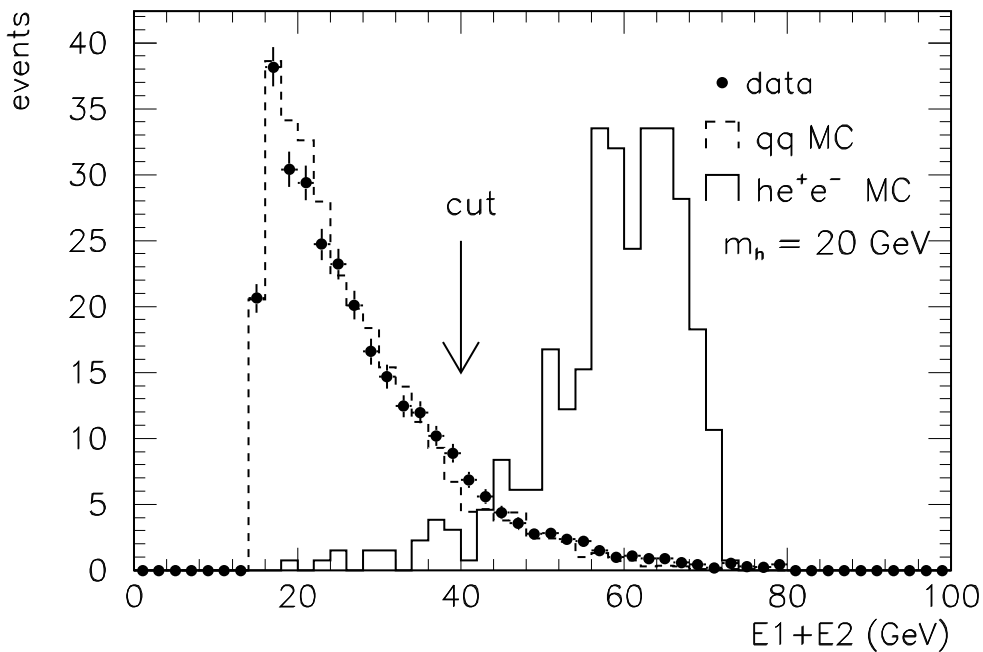


Figure 6: *Distribution of the sum of the energy of the two most energetic electromagnetic clusters for data, simulated background and Higgs signal in the $h^0 e^+ e^-$ channel.*

in Figure 6. The lowest energy cluster of the two must have an energy greater than 13 GeV. In addition the opening angle between these two clusters must be larger than 40° .

The selection of isolated electromagnetic particles and their identification as electrons use the same criteria as in the high-mass range [3]. To identify the Higgs boson decay products, we require the number of jets in the event to be larger than two and the third most energetic jet to have a thrust lower than 0.9985. Then we examine the hadronic jets in the event. Defining P_t as the transverse momentum of an electron with respect to the nearest jet, we require the sum of the two P_t to be greater than 30 GeV and lower than 75 GeV. The Higgs boson selection efficiencies are shown in Table 3.

One data event passes the above selection criteria. This event, corresponding to a mass of 31.4 GeV, is already described in the 30 GeV to 60 GeV mass range section. This event is consistent with the four-fermion background from which, using these cuts, we expect 1.6 ± 0.3 events.

We have also generated $Z \rightarrow b\bar{b} \rightarrow e^+ e^- X$ background events corresponding to 1.6×10^6 $Z^0 \rightarrow q\bar{q}$. No event passed the selection. In addition, no background from hadronic events was found in a sample of 340,000 simulated $q\bar{q}$ events, and no background event appeared from $\tau^+ \tau^-$ simulated events corresponding to 1.4×10^6 $Z^0 \rightarrow q\bar{q}$ and from Bhabhas corresponding to 0.5×10^6 $Z^0 \rightarrow q\bar{q}$.

3.3.2 Mass Range $0 < m_h < 2$ GeV

We search for a low-mass Higgs boson decaying into electrons, muons or hadrons. The main backgrounds with a similar signature are the four-fermion process and the radiative Bhabha with a photon converting in the beam pipe or in the material of the TEC chamber. For masses

Higgs Mass (GeV)	2	5	9	15	20
$h^0\nu\bar{\nu}$ Channel	24.0	37.0	35.0	44.0	48.0
$h^0e^+e^-$ Channel	22.6	40.8	51.8	57.0	62.0
$h^0\mu^+\mu^-$ Channel	24.6	27.6	31.8	46.2	54.2

Table 3: *Selection efficiencies (in %) for intermediate Higgs boson masses.*

below 100 MeV, due to the long life time of the Higgs boson, an event is expected to contain only two acoplanar electrons with no other detected particle balancing the missing momentum. The background for such events is mainly radiative Bhabha and $\tau^+\tau^-$ with the photon escaping detection.

In order to remove the high-multiplicity events (for example $e^+e^- \rightarrow q\bar{q}(\gamma)$) we require at most 15 clusters in the BGO electromagnetic detector. We require at least two high-energy electromagnetic clusters in the BGO calorimeter, the second most energetic having an energy greater than 30 GeV. The identification of isolated electrons is performed exactly as in the high-mass range [3]. Radiative Bhabhas are rejected by requiring the acoplanarity angle of the two electrons is required to be larger than 0.05 radians. The distribution of this acoplanarity angle is similar to the one of the $h^0\mu^+\mu^-$ channel shown in Figure 5.

We require the number of charged tracks to be less than five and, if there are no good tracks other than the two associated with the two highly energetic electromagnetic clusters, we require no electromagnetic cluster with energy above 3 GeV. If the number of tracks is less than 3, then we reject events with hadronic activity in the angular acceptance not covered by the electromagnetic calorimeter.

We construct the missing energy vector to the two electrons and require that it lies more than 10° from the beam. We construct a cone of 30° around the missing energy vector and require that:

- one of the two most energetic clusters does not lie inside the cone,
- at least one electromagnetic cluster with an associated track lies inside the cone,
or
no electromagnetic cluster with energy larger than 100 MeV lies inside the cone and the ratio of the number of electromagnetic clusters to the number of charged tracks is less than two,
or
at least one hadronic cluster larger than 3 GeV lies inside the cone.

In addition, if there is in the cone only one electromagnetic cluster with two associated tracks, and if the hadronic energy in this cone is less than 4% of the electromagnetic cluster energy, we reject the event.

We have performed several Monte Carlo simulations with the Higgs boson decaying into pairs of μ, π, K at various masses in the range $m_\mu < m_h < 2$ GeV. The corresponding selection efficiencies are given in Table 4.

Five data events satisfy the above selection. These five events are consistent with the expected backgrounds and have the following probable interpretations:

- $e^+e^- \rightarrow \mu^+\mu^-e^+e^-$, one event with 7.6 GeV invariant mass of the muon-pair which is above the mass region investigated here; from 4-fermion background we expect 0.5 ± 0.1 event.

Higgs Mass (GeV)	0.01	0.1	0.22	0.3	1.0	3.6
$h^0 \rightarrow e^+e^-$	14.	14.	-	-	25.	-
$h^0 \rightarrow \mu^+\mu^-$	-	-	26.	-	30.	33.
$h^0 \rightarrow \pi^+\pi^-$	-	-	-	20.	26.	28.
$h^0 \rightarrow K^+K^-$	-	-	-	-	28.	28.

Table 4: Selection efficiencies (in %) for light Higgs boson in the $h^0 e^+e^-$ channel.

- $e^+e^- \rightarrow e^+e^-$ hadrons, one event with a hadronic invariant mass around 2.0 GeV, from 4-fermion background we expect 2.2 ± 0.4 events.
- $e^+e^- \rightarrow e^+e^- \gamma$, three events where the radiative photon reaches the hadron calorimeter without interaction in the electromagnetic calorimeter. From radiative background ($e^+e^- \rightarrow e^+e^- \gamma$), we expect 4.3 ± 0.4 events.

3.4 Search in the $Z^0 \rightarrow h^0 Z^{0*} \rightarrow A^0 A^0 Z^{0*}$ Channel

Possible decays of a Higgs boson into a pair of CP-odd Higgs bosons lead to new signatures in Higgs boson decays. Searches for Higgs bremsstrahlung involving $h^0 \rightarrow A^0 A^0$ are summarized. The leptonic channels $h^0 \ell \ell$, $\ell \ell = \nu \bar{\nu}, \mu^+ \mu^-, e^+ e^-$ have been investigated. Based on the event selection for the high mass minimal Standard Model Higgs [3], the change in detection efficiencies for a possible $h^0 \rightarrow A^0 A^0$ decay has been studied. The selection is optimized in four m_A mass regions:

- $2m_b < m_A < 30$ GeV: Above the $b\bar{b}$ threshold the search developed for the high mass Higgs boson can be applied. In the $h^0 \nu \bar{\nu}$ channel, the number of hadronic clusters is expected to be larger than for the SM Higgs boson due to four b-quarks in the final states. In the $h^0 \mu^+ \mu^-$ and $h^0 e^+ e^-$ channels the selection relies on the identification of the lepton pair and only minor modifications on the selection compared to the searches for the Standard Model Higgs are made.
- $2m_\tau < m_A < 2m_b$: In this mass region the relative ratio of $c\bar{c}$ and $\tau^+ \tau^-$ in A^0 decays is unknown. In order to stay model independent the four- τ final state with lower selection efficiency is assumed to be dominant. The selection takes into account that two tau pairs lead to larger missing energy and smaller cluster multiplicity in the $h^0 \nu \bar{\nu}$ channel compared with signatures from $h^0 \rightarrow q\bar{q}$ decays.
- $2m_\mu < m_A < 2m_\tau$: The decay modes of A^0 in this mass range are unknown and low-mass quark final states at various masses have been investigated using a similar method as that used for direct h^0 decays. Both A^0 bosons can decay into these particles, therefore typically four charged tracks in addition to a lepton pair are expected.
- $0 < m_A < 2m_\mu$: A very light A^0 can either decay outside the detector or it can decay into electrons or photons. The event characteristic in the first case is identical to signature expected without $h^0 \rightarrow A^0 A^0$ decays. In the latter case the same search as in the very low mass range described before has been applied.

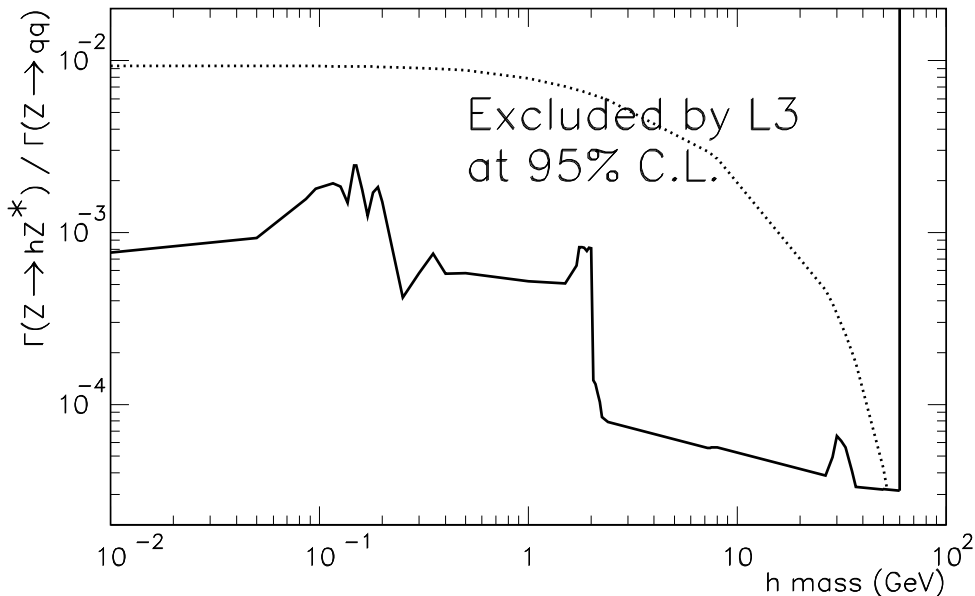


Figure 7: Limit on $\Gamma(Z^0 \rightarrow h^0 Z^{0*})/\Gamma(Z^0 \rightarrow q\bar{q})$ from searches with the Higgs bremsstrahlung process. The dotted line shows the Higgs branching ratio expected in the minimal Standard Model.

3.5 Results for $Z^0 \rightarrow h^0 Z^{0*}$ Searches

No indication of a Higgs boson signal is observed. The number of events that pass the selection are consistent with the expected background. The selection efficiencies are given in Table 1 for the 30 GeV to 60 GeV mass range, in Table 3 for the 2 GeV to 30 GeV mass range and in Tables 2 and 4 for the mass range lower than 2 GeV.

The results of the searches are presented as a 95% CL limit on the branching ratio for Higgs bremsstrahlung from the Z^0 :

$$\Gamma(Z^0 \rightarrow h^0 Z^{0*})/\Gamma(Z^0 \rightarrow q\bar{q}) < \frac{N^l}{N^{had} \times \epsilon} \quad (9)$$

where $N^l = 3.0$ if there is no candidate event. If there are candidate events, N^l is increased according to Poisson statistics. $N^{had} (= 408,000)$ is the total number of collected hadronic Z^0 decays and $\epsilon = \sum_f \text{BR}(h^0 \rightarrow f\bar{f}) \times \epsilon_{f\bar{f}}$ is the global Higgs boson selection efficiency. To set the limit on each investigated decay channel we have reduced the efficiencies to account for systematic errors (5%) coming from the Monte Carlo simulation and statistical errors due to Monte Carlo statistics (5% to 9%). Figure 7 shows the limit as a function of the Higgs boson mass.

The searches involving $h^0 \rightarrow A^0 A^0$ decays have similar efficiencies to those in the minimal Standard Model Higgs search. In the mass range $m_A > 2m_b$, typically the selection efficiency is increased by 5% with respect to the direct h^0 decay channel described before, while in the range $2m_\tau < m_A < 2m_b$ the efficiency is reduced by 10%. For $m_A < 2m_\tau$ the selection efficiency is increased by about 15% in the $h^0 \nu\bar{\nu}$ channel and is reduced by about 5% in both leptonic channels. Interpretations will be given as effects on excluded mass regions in the framework of the two-doublet model.

4 Search for Neutral Higgs Boson Pair-Production

Searches for pair-produced Higgs bosons are presented in the channels $b\bar{b}b\bar{b}$, $b\bar{b}b\bar{b}b\bar{b}$, $\tau^+\tau^-b\bar{b}$ and $\tau^+\tau^-\tau^+\tau^-$. No assumption on the cross section is made and results are shown as limits on individual branching ratios for the Higgs production in Z^0 decays.

4.1 Search in the $Z^0 \rightarrow h^0 A^0 \rightarrow b\bar{b}b\bar{b}$ Channel

The search for $Z^0 \rightarrow h^0 A^0 \rightarrow b\bar{b}b\bar{b}$ is made in the hadronic event sample using the following cuts:

$$E_{\parallel}/E_v < 0.60, \quad E_{\perp}/E_v < 0.60, \quad 0.4 < E_v/\sqrt{s} < 1.4, \quad N_{cl} \geq 7, \quad (10)$$

where E_{\parallel} is the energy imbalance along the beam direction, E_{\perp} the transverse energy imbalance, E_v the total measured calorimetric energy and N_{cl} the number of calorimetric clusters. In order to distinguish the signal from the main background due to $Z^0 \rightarrow q\bar{q}$ decays, use is made of both the different topological properties of the events and of the higher inclusive semileptonic branching ratio of the b quarks compared to lighter quarks in Z^0 decays. The mass region from 18 GeV up to the $m_Z = m_h + m_A$ kinematical limit is investigated. The 18 GeV limit results from the limit set by the cluster algorithms ($y_{cut} = 0.02$, see section 2); it exceeds this limit by two standard deviations of the mass resolution.

4.1.1 Selection-Details

Events with either 4 or 5 jets are selected. The $Z^0 \rightarrow q\bar{q}$ background contribution is normalized to the data. More than 85% of the signal events in the (m_h, m_A) mass range of interest and about 8% of the background events from $Z^0 \rightarrow q\bar{q}$ survive the cut on the number of jets. The 5-jet events are transformed into 4-jet events by combining the two jets with the smallest invariant mass. The next step is to identify the two jets potentially coming from the $h^0 \rightarrow b\bar{b}$ decay and those coming from the $A^0 \rightarrow b\bar{b}$ decay and to select events corresponding to a given (m_h, m_A) mass combination. For this purpose, a mass- χ^2 is calculated for each $h^0 \rightarrow \text{jet jet}$ and $A^0 \rightarrow \text{jet jet}$ combination:

$$\chi_i^2 = \frac{(m_h^{rec} - m_h)^2}{\sigma_h^2} + \frac{(m_A^{rec} - m_A)^2}{\sigma_A^2} \quad (11)$$

where runs over the three possible jet-jet combinations, m_h^{rec}, m_A^{rec} are the reconstructed masses, (m_h, m_A) the mass point under investigation and σ_h, σ_A the mass resolutions at (m_h, m_A) . The mass resolutions are determined from the simulated signal events by taking the reconstructed mass distribution with the minimum χ^2 . An example of such a distribution for the (m_h, m_A) point (22 GeV, 52 GeV) is shown in Figure 8. The two mass peaks are clearly separated with mass resolutions of 3.7 GeV and 7.7 GeV, respectively. These resolutions agree with the 15% mass resolution obtained in the data by the study of $q\bar{q}\gamma$ events described in section 2. The procedure is repeated for each of the nine (m_h, m_A) points for which signal events were simulated. The resolutions σ_h and σ_A are then parameterized as a function of (m_h, m_A) . Figure 9 shows the χ^2 -distributions for a (22 GeV, 52 GeV) signal, the $Z^0 \rightarrow q\bar{q}$ background and the data. As expected, the χ^2_{min} distribution for the signal is steeper than for the background. Having selected the best jet-jet combination using the χ^2_{min} -criterion, events are rejected with $\chi^2_{min} > 2$. At this stage the full event is reconstructed since the jets coming from the decays of h^0 and A^0 are identified.

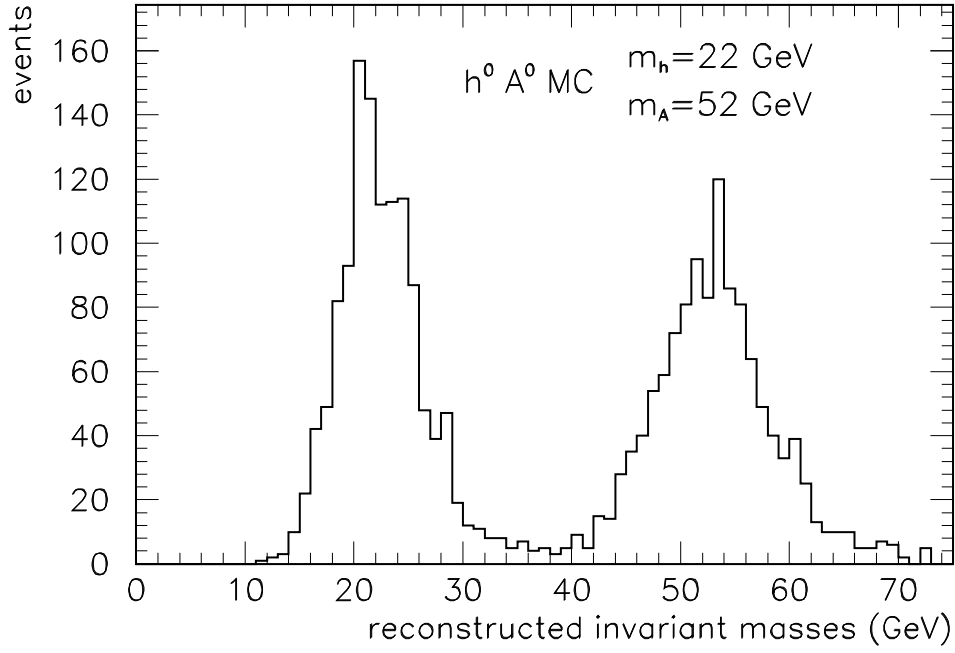


Figure 8: *Reconstructed Higgs masses for a simulated (22 GeV, 52 GeV) Higgs signal.*

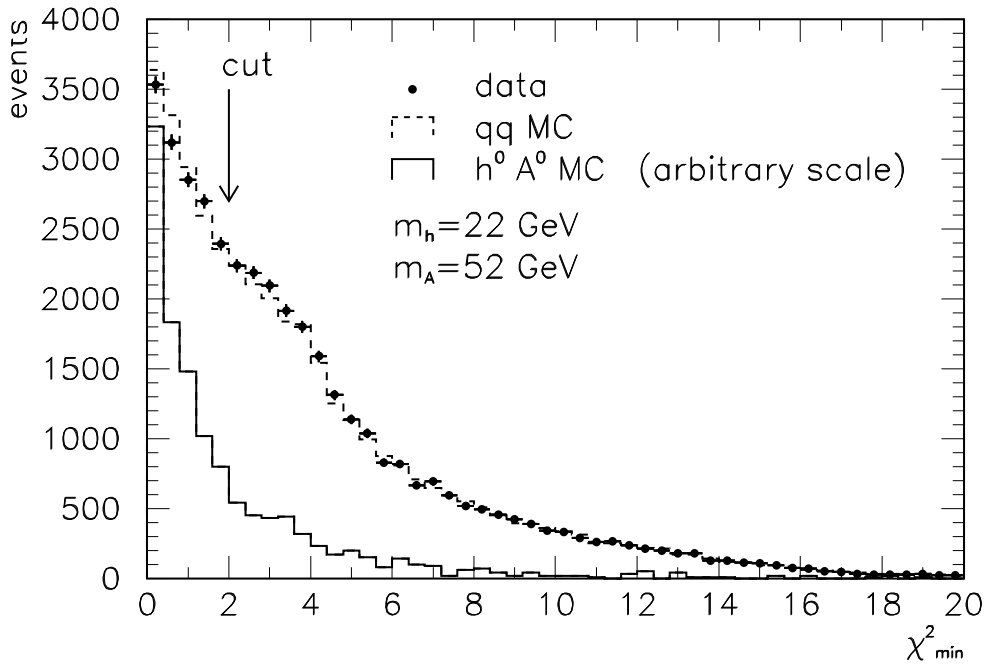


Figure 9: *Distribution of χ^2_{min} for data, simulated background and Higgs signal in the $bbbb$ channel. See text for a definition of χ^2_{min} .*

Additional topological cuts are applied to reduce the $Z^0 \rightarrow q\bar{q}$ background. These cuts are optimized at simulated signal points (m_h, m_A) and subsequently parameterized as a function of (m_h, m_A) . The cut values are then interpolated for any arbitrary point in the (m_h, m_A) plane. The variables used in this analysis are:

- The production angle, θ_p , of the h^0 and A^0 bosons defined as the angle between the Higgs direction and the beam axis in the laboratory. The $Z^0 \rightarrow h^0 A^0$ events are expected to follow a $\sin^2 \theta_p$ distribution whereas the $Z^0 \rightarrow q\bar{q}$ background events should have a $(1 + \cos^2 \theta_p)$ distribution.
- The decay angle, θ_d , defined as the angle between the direction of the jets with respect to the Higgs direction in the rest frame of the Higgs. The signal distribution is expected to be flat, while for $Z^0 \rightarrow q\bar{q}$ background the distribution should be peaked at small angles due to gluon bremsstrahlung.
- The event thrust, T , which discriminates against large Higgs masses. Figure 10 shows the T -distribution for events with $m_h = 52$ GeV and $m_A = 22$ GeV Higgs masses after the χ^2_{min} , $\cos \theta_p$ and $\cos \theta_d$ cuts are applied. The signal is concentrated at smaller thrust values than the $Z^0 \rightarrow q\bar{q}$ background.
- The minimum angle between any jet-pair, θ_{min}^{jj} . The signal has a flatter $\cos \theta_{min}^{jj}$ distribution than the $Z^0 \rightarrow q\bar{q}$ background.
- The angle, ψ_{pl} , between the normal to the plane of the two jets from h^0 and the normal to the plane of the two jets from the A^0 decays: 4-jet events from QCD processes tend to have a smaller ψ_{pl} angles than the one for the signal events.

The values of the cuts used for each (m_h, m_A) signal simulated are given in Table 5. The

bbbb Channel					
Masses (GeV)	$ \cos \theta_p $	$ \cos \theta_d $	T	$ \cos \theta_{min}^{jj} $	$ \cos \psi_{pl} $
m_h, m_A	\leq	\leq	\leq	\leq	\leq
22,22	0.6	0.8	0.9	0.8	1.0
22,32	0.75	0.8	0.84	0.65	0.95
22,42	0.7	0.8	0.76	0.60	0.95
22,52	0.75	0.8	0.79	0.60	0.95
22,62	0.5	0.8	0.82	1.0	0.80
32,32	0.9	0.7	0.78	0.5	1.0
32,42	1.0	0.7	0.78	0.5	1.0
32,52	0.8	0.7	0.78	1.0	0.8
42,42	0.8	0.7	0.78	1.0	0.8

Table 5: Values of topological cuts applied to select $Z^0 \rightarrow h^0 A^0 \rightarrow b\bar{b}b\bar{b}$ events at the various (m_h, m_A) values for which the signal Monte Carlo was generated.

$Z^0 \rightarrow h^0 A^0 \rightarrow b\bar{b}b\bar{b}$ signal is expected to have a larger number of leptons from inclusive semileptonic decays compared to 4-jet events from QCD background. Both electrons and muons are used in this analysis. A requirement is made of at least one lepton with high momentum (≥ 3 GeV) and high p_T with respect to the nearest jet (≥ 1.5 GeV). The quality cuts for lepton

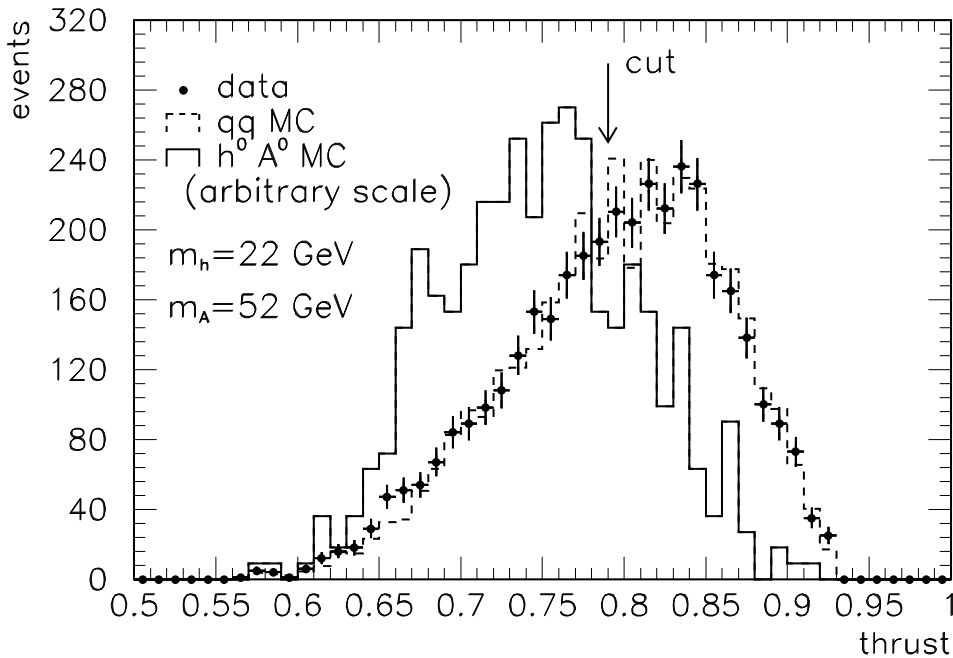


Figure 10: *Thrust distribution for data, simulated background and Higgs signal in the $b\bar{b}b\bar{b}$ channel.*

selection as described in the inclusive lepton analyses [19] are imposed. For the electron sample the lateral shower profile, the BGO shower shape χ^2 and the azimuthal angle and energy-momentum matching between the TEC detector and the electromagnetic calorimeter are used. For the muon sample, a track reconstruction is required both in the muon chamber and in the TEC; the two measurements should match. The effects of the cuts, the expected signals, the background and the data are summarized in Table 6.

4.1.2 Results for $b\bar{b}b\bar{b}$ Channel

The numbers of surviving events in the simulated signal, in the $Z^0 \rightarrow q\bar{q}$ background and in the data are shown in Table 7 for the 1990 and 1991 runs.

The systematic errors and their effects on the predicted signal acceptances for the $b\bar{b}b\bar{b}$ channel are given in Table 8. For the available signal Monte Carlo samples, the statistical error is about 15%. The resulting total uncertainty is estimated to be 27%, which is used to reduce the signal efficiency by one sigma of error in order to obtain a 95% CL limits on the $Z^0 \rightarrow h^0 A^0 \rightarrow b\bar{b}b\bar{b}$ branching ratio

$$\frac{\Gamma(Z^0 \rightarrow h^0 A^0 \rightarrow b\bar{b}b\bar{b})}{\Gamma(Z^0 \rightarrow q\bar{q})} \quad (12)$$

as function of m_h and m_A . Figure 11 shows the regions in the (m_h, m_A) plane excluded at 95% CL for values of the branching ratio larger or equal to 1×10^{-3} and 2×10^{-3} , respectively. Interpretations of these limits in the MSSM are discussed in Section 7.

bbbb Channel						
Selection Cuts $m_h = m_A = 32$ GeV	Signal Acc. (%)	$Z^0 \rightarrow q\bar{q}$ Events	Data Events	Signal Acc. (%)	$Z^0 \rightarrow q\bar{q}$ Events	Data Events
	1991			1990		
			296k			116k
Preselection	84.9	39855	39480	87.0	16195	16782
$\chi^2 \leq 2$	60.8	12007	12264	60.4	4958	5220
$ \cos \theta_p \leq 0.9$	60.0	11796	12042	59.6	4874	5131
$ \cos \theta_d \leq 0.7$	31.1	1658	1820	32.1	651	713
$T \leq 0.78$	28.6	1113	1137	30.0	426	545
$ \cos \theta_{min}^{jj} \leq 0.5$	26.6	782	846	26.1	301	336
incl. lepton	4.4	27	23	5.3	8.9	4

Table 6: Cuts and the corresponding event numbers in the $bbbb$ channel for the different steps of the selection in the $b\bar{b}b\bar{b}$ channel for data and for background, compared with the acceptances for a $m_h = m_A = 32$ GeV signal. The details of the preselection are given in the text. 1600 Higgs events are simulated for the 1991 data sample and 872 for the 1990 data sample.

bbbb Channel						
Masses (GeV)	Signal Acc. (%)	$Z^0 \rightarrow q\bar{q}$ Events	Data Events	Signal Acc. (%)	$Z^0 \rightarrow q\bar{q}$ Events	Data Events
m_h, m_A	1991			1990		
22,22	3.9	19	13	3.3	3	5
22,32	3.1	20	19	2.4	9	5
22,42	2.4	21	19	3.2	7	9
22,52	2.6	27	24	—	7	11
22,62	1.3	21	22	—	9	11
32,32	4.4	27	23	5.8	9	4
32,42	3.5	28	23	3.9	10	5
32,52	2.1	21	24	—	4	7
42,42	2.3	13	15	1.9	4	4

Table 7: Surviving events after all cuts in the $bbbb$ channel. At each mass point 1600 signal events have been simulated. The expected $Z^0 \rightarrow q\bar{q}$ background is normalized to the data.

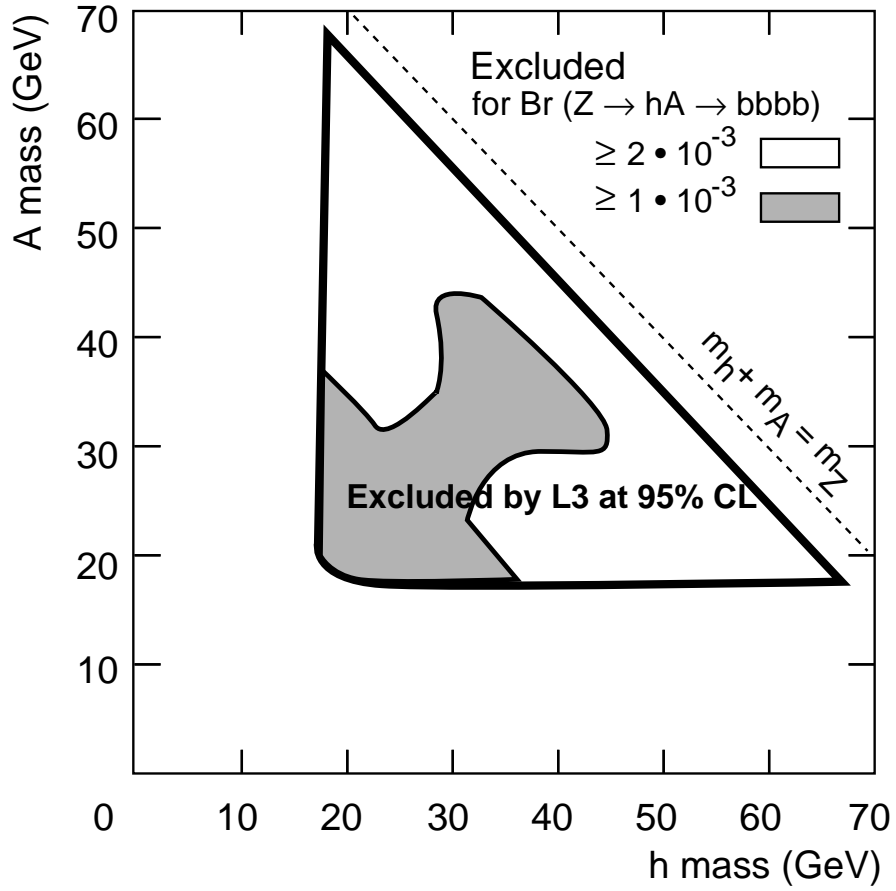


Figure 11: Regions of the (m_h, m_A) plane excluded at 95% CL for values of the branching ratio $\Gamma(Z^0 \rightarrow h^0 A^0 \rightarrow b\bar{b}b\bar{b})/\Gamma(Z^0 \rightarrow q\bar{q}) \geq 1 \times 10^{-3}$ (dark region), $\geq 2 \times 10^{-3}$ (region inside heavy contour line).

bbbb Channel		
Selection Cuts $m_h = m_A = 32$ GeV	Variation	Acceptance Reduction (%)
Preselection	–	< 3
$N_J = 4$ or 5	20%	20
$\chi^2 \leq 2$	0.2	9
$ \cos \theta_p \leq 0.9$	0.02	1.7
$ \cos \theta_d < 0.7$	0.04	4.0
$T \leq 0.78$	0.01	5.0
$ \cos \theta_{\min}^{jj} \leq 0.5$	0.044	2.9
incl. leptons	5%	5
TOTAL		23

Table 8: Reduction of expected Higgs acceptance in the $bbbb$ channel due to modeling of the detector response for each quantity used in the analysis. For continuous quantities the variation is taken as one standard deviation on the measured quantity and for discrete quantities as one standard deviation on the normalization of the event rate. The reductions are summed in quadrature.

4.2 Search in the $Z^0 \rightarrow h^0 A^0 \rightarrow A^0 A^0 A^0 \rightarrow b\bar{b}b\bar{b}b\bar{b}$ Channel

The process $Z^0 \rightarrow h^0 A^0 \rightarrow A^0 A^0 A^0 \rightarrow b\bar{b}b\bar{b}b\bar{b}$ is possible if $m_h > 2m_A$. At the parton level one expects six jets in the event, however, the number of reconstructed jets can be different. A study of a simulated signal for (m_h, m_A) values in GeV (50, 22), (60, 22) and (60, 27) shows that more than 80 % of the events led to $N_J \geq 5$ jets in the final state. The $Z^0 \rightarrow q\bar{q}$ background is normalized to the 5-and-more-jet-rate in the data.

4.2.1 Selection-Details

The thrust distribution for events passing the jet-number cut peaks at low values; a cut of $T < 0.8$ is imposed. This requirement provides a very effective way of suppressing the QCD background: only about 2.1% of the background events and about 70% signal events survive the cut.

Since most of the events lead to only 5 jets in the final state, the reconstruction of the full event topology is not possible. The search strategy is therefore based on the reconstruction of two A^0 bosons of a specific mass. Following the procedure adopted for the 4-jet analysis, a mass- χ^2 is defined as to reconstruction the A^0 boson:

$$\chi_i^2 = \frac{(m_{A_1}^{rec} - m_A)^2}{\sigma_{A_1}^2} + \frac{(m_{A_2}^{rec} - m_A)^2}{\sigma_{A_1}^2} \quad (13)$$

where i runs over six possible jet-pairing, $m_{A_1}^{rec}$ and $m_{A_2}^{rec}$ are reconstructed invariant masses of the jet-pairings and $\sigma_{A_{1,2}}$ are the corresponding mass resolutions. From a study of signal Monte Carlo events a resolution of 2.7 GeV is obtained in the mass range of interest (20 to 27 GeV). Combinations of $A^0_1 \rightarrow \text{jet}_i \text{jet}_j$ and $A^0_2 \rightarrow \text{jet}_k \text{jet}_l$ are then selected for which the χ^2 is minimum; events with $\chi_{\min}^2 \geq 3$ are rejected.

Additional cuts are applied:

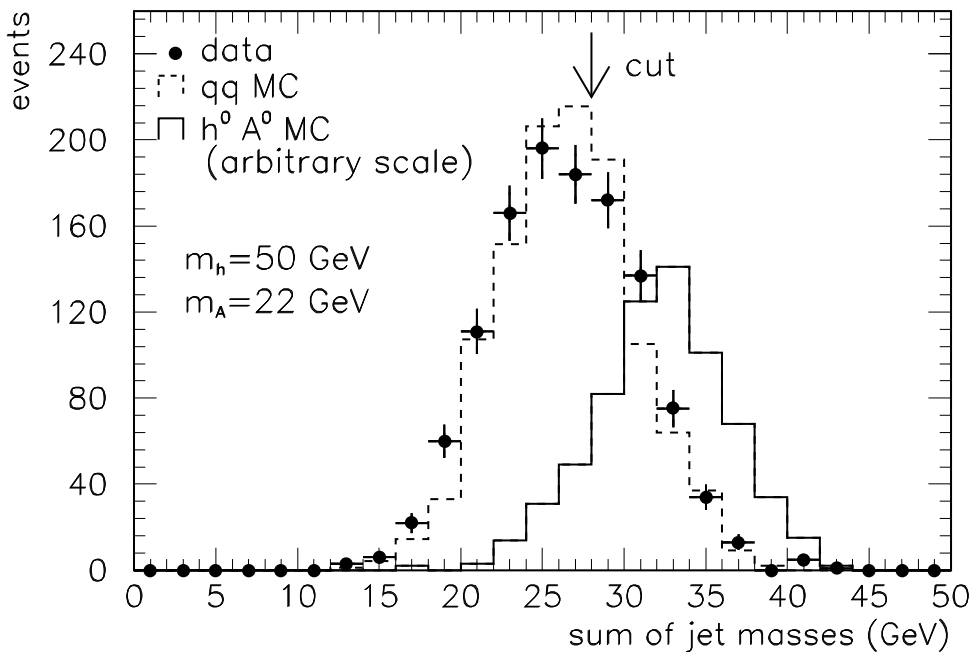


Figure 12: *Distribution of the sum of jet masses for data, simulated background and Higgs signal in the bbbbbb channel.*

- $|\cos \theta_p| \leq 0.9$, where $\cos \theta_p$ is the production angle of A^0 . Although only one A^0 is directly produced, a cut on the production angle of the two reconstructed A^0 bosons distinguishes the expected signal from background.
- $|\cos \theta_{min}^{jj}| \leq 0.8$, where $\cos \theta_{min}^{jj}$ is the minimum angle between any two jets.
- $\sum M_{jet}^{rec} \geq 28$ GeV cut is applied, where $\sum M_{jet}^{rec}$ is the sum of jet masses. The signal final state (consisting of 6 b-quarks) leads to higher values of the $\sum M_{jet}^{rec}$ compared to the $Z^0 \rightarrow q\bar{q}$ background. Figure 12 shows the $\sum M_{jet}^{rec}$ distributions for data, $Z^0 \rightarrow q\bar{q}$ background and for a (50 GeV, 22 GeV) simulated signal.

Finally, at least one semileptonic b decay (e or μ) is required with the same lepton characteristic as for the $Z^0 \rightarrow h^0 A^0 \rightarrow b\bar{b}b\bar{b}$ final state. With six b-quarks in the final state the probability of observing a semi-leptonic decay of one of the b quarks is large. The effects of the cuts and the expected signal, background and data are summarized in Table 9.

4.2.2 Results for $b\bar{b}b\bar{b}b\bar{b}$ Channel

After applying the above cuts on the simulated signal, the selection efficiency is found to be 6.3% in the (m_h, m_A) range of interest. The comparison between data events surviving the cuts and the QCD expectation is given in Table 10. The systematic errors and their effects on the predicted signal acceptances for the $b\bar{b}b\bar{b}b\bar{b}$ channel are given in table 11.

For the mass range $20 \leq m_A \leq 27$ GeV and $m_h > 2m_A$, model independent limits on the branching rate for the $Z^0 \rightarrow h^0 A^0 \rightarrow A^0 A^0 A^0 \rightarrow b\bar{b}b\bar{b}b\bar{b}$ process are derived from the numbers of surviving events given in Table 10. For the available signal Monte Carlo samples, the

bbbbbb Channel					
Selection Cuts $m_h = 60$ GeV, $m_A = 27$ GeV	Signal Acc. (%)	$Z^0 \rightarrow q\bar{q}$ Events	Data Events	$Z^0 \rightarrow q\bar{q}$ Events	Data Events
	1991			1990	
			296k		116k
Preselection	82.4	78287	58887	29018	25018
N_J, T	67.1	2907	2997	1328	1289
$\chi^2 \leq 3.0$	51.4	1786	1936	804	837
$ \cos \theta_p \leq 0.9$	46.8	1535	1641	677	703
$ \cos \theta_{min}^{jj} \geq 0.8$	38.4	983	1122	427	474
$\sum M_{jet}^{rec} \geq 28$.	34.3	376	452	187	198
incl. lepton	6.8	12	16	12	6

Table 9: The cuts and the corresponding event numbers in the different steps of the selection in the bbbbb channel for data and background compared with acceptances for $m_h = 60$ GeV, $m_A = 27$ GeV signal. The details of the preselection are given in the text. 1600 Higgs signal events are simulated.

bbbbbb Channel								
m_A (GeV)	20	21	22	23	24	25	26	27
1990+1991 Data (Events)	18	21	20	22	19	17	18	22
$Z^0 \rightarrow q\bar{q}$ (Events)	25	26	29	25	22	22	23	24

Table 10: Surviving events after all cuts as a function of m_A . The selection is independent of m_h .

bbbbbb Channel		
Selection Cuts $m_h = 60$ GeV, $m_A = 27$ GeV	Variation	Acceptance Reduction (%)
Preselection	–	< 3
$N_J = 5$ or 6	20%	20
$\chi^2 \leq 3$	0.4	8.0
$ \cos \theta_p \leq 0.9$	0.04	5.5
$ \cos \theta_{min}^{jj} < 0.8$	0.044	5.5
$\sum M_{jet}^{rec} \geq 28$ GeV	1.7	12
incl. leptons	5%	5
TOTAL		26

Table 11: Reduction of expected Higgs acceptance due to modeling of the detector response for each quantity used in the analysis. For continuous quantities the variation is taken as one standard deviation on the resolution in the measured quantity and for discrete quantities as one standard deviation on the normalization of the event rate. The reductions are summed in quadrature.

statistical error is about 11%. The resulting total uncertainty is estimated to be 28%, which is used to reduce the signal efficiency in order to obtain a 95% CL limit on the branching ratio: a limit at 95% CL is set:

$$\frac{\Gamma(Z^0 \rightarrow h^0 A^0 \rightarrow A^0 A^0 A^0 \rightarrow b\bar{b}b\bar{b}b\bar{b})}{\Gamma(Z^0 \rightarrow q\bar{q})} \leq 9.1 \times 10^{-4}. \quad (14)$$

4.3 Search in the $Z^0 \rightarrow h^0 A^0 \rightarrow \tau^+ \tau^- b\bar{b}$ Channel

The events from $Z^0 \rightarrow h^0 A^0 \rightarrow \tau^+ \tau^- b\bar{b}$ are characterized by an isolated pair of narrow jets, associated with a small number of tracks (2 in 74% and 4 in 25% of the tau pair final states) and a large amount of missing momentum, recoiling against two broad hadronic jets. The main background comes from hadronic Z^0 decays.

The analysis presented here concentrates on the identification and the mass reconstruction of the $\tau^+ \tau^-$ pair. As a first step in the identification of the $\tau^+ \tau^-$ pair, the event is divided into two hemispheres using the plane perpendicular to the thrust axis and counting the number of calorimetric clusters in each of them. The hemisphere with the lower number of clusters (hereafter referred to as the tau-hemisphere) should contain the $\tau^+ \tau^-$ pair. In the tau-hemisphere, the calorimetric clusters are combined into jets using $y_{cut} = 0.001$; this allows the separation of two jets down to a mass of 2.9 GeV. In the hemisphere with the higher number of clusters (hereafter referred to as the jet hemisphere), a y_{cut} value of 0.02 is used. The identification of the $\tau^+ \tau^-$ pair is made by requiring two narrow jets and two tracks with opposite charge. The invariant mass of the $\tau^+ \tau^-$ pair is reconstructed and the $\tau^+ \tau^-$ mass distribution scanned in different mass windows to search for an excess of events over the expected hadronic background.

4.3.1 Selection-Details

The events have to pass a preselection similar to one used for the $b\bar{b}b\bar{b}$ channel:

$$E_{\parallel}/E_v < 0.40, \quad E_{\perp}/E_v < 0.60, \quad 0.4 < E_v/\sqrt{s} < 0.9, \quad |\cos \theta_T| < 0.7. \quad (15)$$

The cut on $\cos \theta_T$ selects events in the central region of the detector, enhancing the signal from $Z^0 \rightarrow h^0 A^0$, which has a $\sin^2 \theta_T$ distribution, over the background from $Z^0 \rightarrow q\bar{q}$ and $Z^0 \rightarrow \tau^+ \tau^-$, which has a $(1 + \cos^2 \theta_T)$ distribution. For the mass region under investigation, the acceptance for the simulated $Z^0 \rightarrow h^0 A^0 \rightarrow \tau^+ \tau^- b\bar{b}$ events after these cuts is about 65%.

In order to reject low-multiplicity events ($Z^0 \rightarrow e^+ e^-, \mu^+ \mu^-, \tau^+ \tau^-$) and to identify $\tau^+ \tau^-$ pairs in the tau-hemisphere, the following cuts are applied:

- $N_{cl} \geq 15$, where N_{cl} is the number of calorimetric clusters,
- $N_J \geq 2$, where N_J is the number of broad jets in the jet hemisphere,
- $N_{\tau} = 2$, where N_{τ} is the number of narrow jets in the tau hemisphere with $0.5 \leq E_{\tau} \leq 30$ GeV, where E_{τ} is the narrow jet energy,
- $N_{tr} = 2$, where N_{tr} is the number of tracks in the tau hemisphere,
- $N_q = 0$, where N_q is the total charge in the tau hemisphere.

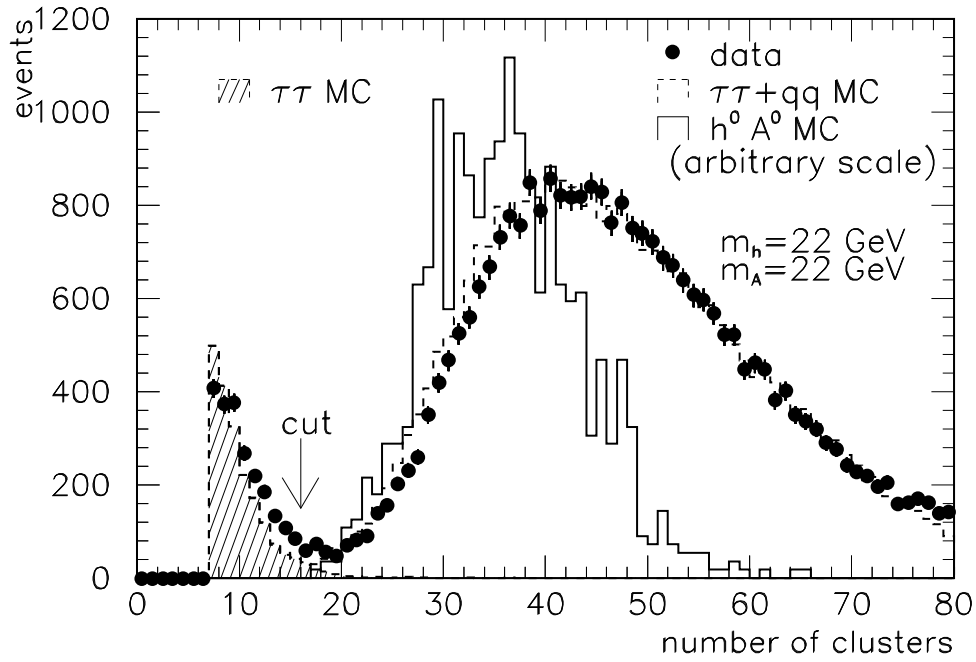


Figure 13: Distribution of the number of calorimetric clusters for data, simulated background and Higgs signal in the $\tau\tau bb$ channel.

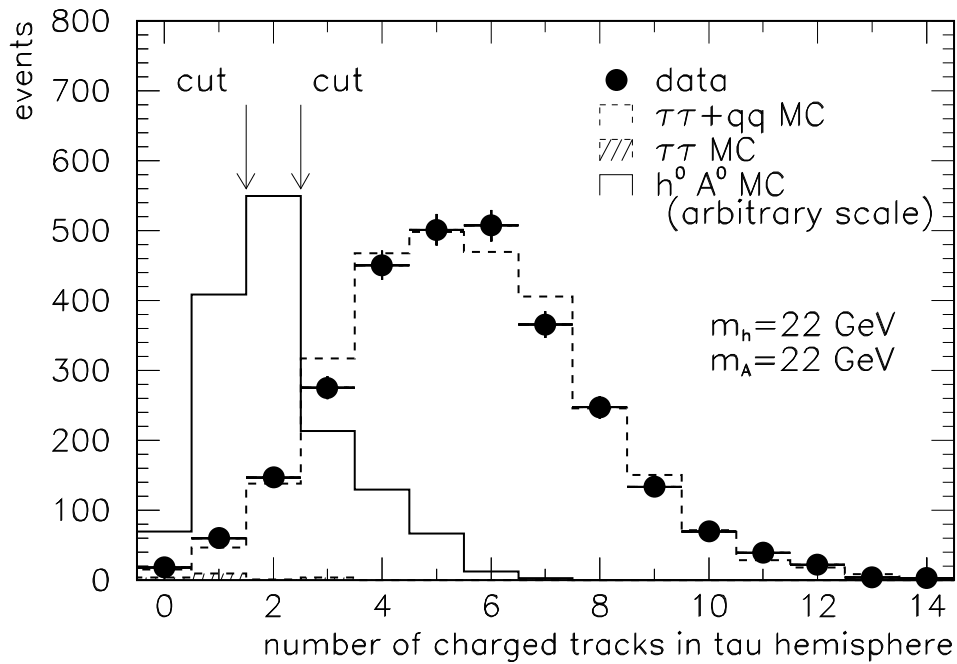


Figure 14: Distribution of number of charged tracks in the tau hemisphere for data, simulated background and Higgs signal in the $\tau\tau bb$ channel.

The distribution of the number of calorimetric clusters after the preselection is shown in Figure 13. The charged-track multiplicity is given in Figure 14 after the preselection and the first three cuts.

Finally, as described in the next section, the invariant mass of the identified $\tau^+\tau^-$ pair is reconstructed using the measured momenta of the two narrow jets and the missing momentum vector of the event.

4.3.2 Mass Reconstruction of the τ -Pair

The reconstruction of the invariant mass of the τ -pair is based on the fact that, in spite of the presence of (one or two) neutrinos among the τ -decay products, the momentum of each of the two τ 's can be fully reconstructed using the measured energy and direction of the visible τ -decay products and the missing momentum vector. If the masses of the particles from the τ -decay are small compared to their momenta, the direction of the τ 's is, to a good approximation, the same as that of its observable decay products (either a tau-jet or an electron or a muon). If the two τ 's are not back to back (in which case the reconstruction of the individual momenta of the two τ 's is not possible), the missing momentum vector can be used to determine the momentum carried by the neutrinos from the decay of each of the two τ 's, using the following relations:

$$\begin{aligned} P \cos \theta_{j_1 P} &= p_{\nu_1} + p_{\nu_2} \cos \theta_{j_1 j_2}, \\ P \sin \theta_{j_1 P} &= p_{\nu_2} \sin \theta_{j_1 j_2}, \end{aligned} \quad (16)$$

where P is the magnitude of the measured missing momentum vector \mathbf{P} , $\theta_{j_1 P}$ the angle between the missing momentum vector and one of the two τ -jets and $\theta_{j_1 j_2}$ the angle between the two τ -jets. (see Figure 16). The magnitudes p_{ν_1} and p_{ν_2} of the momenta carried by the neutrinos from the decay of the two τ 's can be calculated from the above equations, provided the two τ -jets are not collinear (*i.e.* if $\theta_{j_1 j_2} \neq 180^\circ$). The τ -pair invariant mass is given by:

$$m_{\tau\tau} = [2p_{\tau_1}p_{\tau_2}(1 - \cos \theta_{j_1 j_2})]^{1/2}, \quad (17)$$

in terms of the reconstructed τ -momenta $p_{\tau_{1,2}} = p_{j_{1,2}} + p_{\nu_{1,2}}$. Assuming that the two τ 's come from the decay of the h^0 , the h^0 mass resolution can be improved by constraining the energy of the τ -pair $E_{\tau\tau} = p_{\tau_1} + p_{\tau_2}$ to the energy of the h^0 from $Z^0 \rightarrow h^0 A^0$ decay:

$$E_h = \frac{1}{2}m_Z(1 - \frac{m_A^2 - m_h^2}{m_Z^2}). \quad (18)$$

For any (m_h, m_A) pair of mass values, the measured momenta of the two τ 's multiplied by a factor $E_h/E_{\tau\tau}$ are used to calculate of the τ -pair invariant mass. The resulting mass distribution is compared to the background prediction and to the simulated signal for the (m_h, m_A) mass point under investigation. In Figure 15 this comparison is shown for $Z^0 \rightarrow h^0 A^0$ events with $m_h = m_A = 22$ GeV. Events are kept if the τ -pair invariant mass is in the range $(m_h \pm \Delta m_h)$ with:

$$\begin{aligned} \Delta m_h &= 3 + 0.10(m_h - 12) \quad \text{for } m_h \geq 12 \text{ GeV}, \\ \Delta m_h &= 1 + 0.25(m_h - 4) \quad \text{for } m_h < 12 \text{ GeV}. \end{aligned} \quad (19)$$

In Table 12 all $\tau\tau b\bar{b}$ selection cuts and their effects on the data, the background and the simulated signal for $m_h = m_A = 22$ GeV and $m_h = m_A = 20$ GeV, both for the 1991

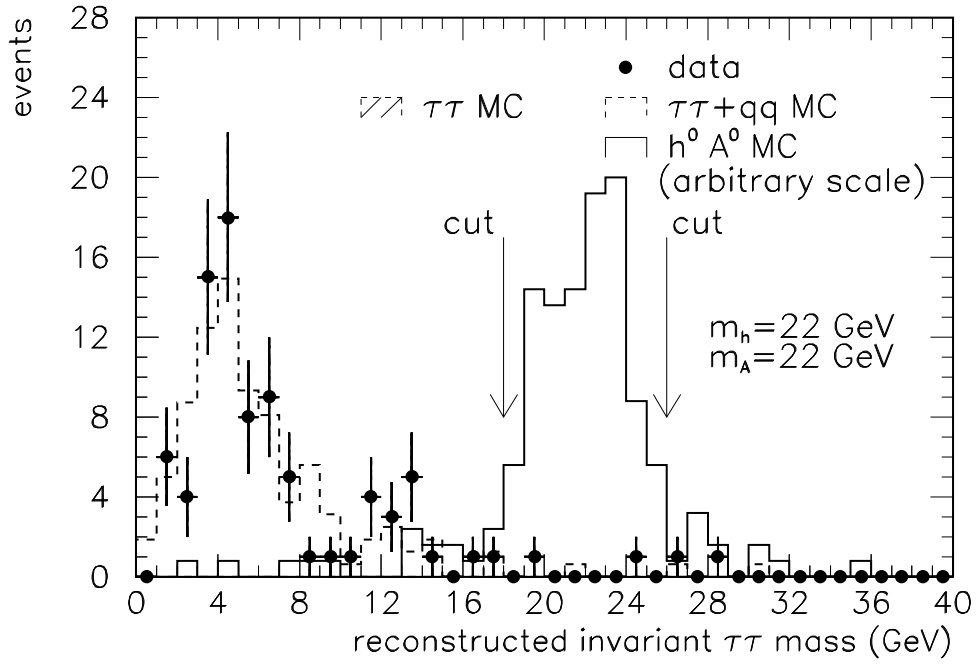


Figure 15: Distribution of the reconstructed invariant mass of identified $\tau^+\tau^-$ pairs for data, simulated background and Higgs signal in the $\tau\tau bb$ channel.

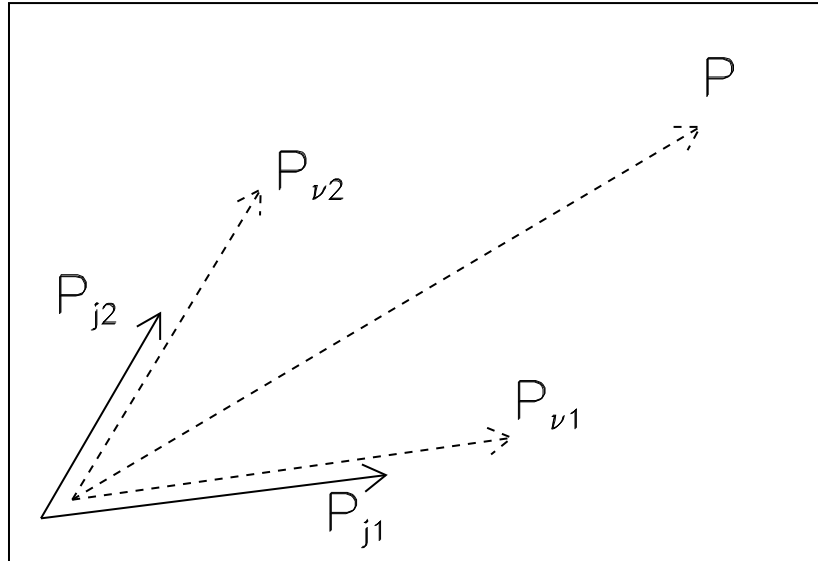


Figure 16: Reconstruction of the tau momenta $p_{\tau_{1,2}} = p_{j_{1,2}} + p_{\nu_{1,2}}$, using the direction of the tau jets $p_{j_{1,2}}$ and the missing energy vector \mathbf{P} .

and the 1990 detector configurations, are presented. For the Monte Carlo signal, 1500 and 1300 events are fully simulated in the 1991 and 1990 detector configurations, respectively. The $Z^0 \rightarrow q\bar{q}$ contribution is normalized to the data after preselection, taking the predicted $Z^0 \rightarrow \tau^+\tau^-$ contribution into account.

$\tau\tau b\bar{b}$ Channel				
Selection cuts	Signal Acc. (%)	$Z^0 \rightarrow q\bar{q}$ Events	$Z^0 \rightarrow \tau^+\tau^-$ Events	Data Events
1991				
$m_h=m_A=22$ GeV				296K
Preselection	65.7	29379	2013	31392
$N_{cl} \geq 15$	65.7	29370	129	29326
$N_J \geq 2$	63.1	21506	43	21485
$0.5 \text{ GeV} \leq E_\tau \leq 30 \text{ GeV}$	55.5	18504	30	18113
$N_\tau = 2$	26.8	2861	17	2841
$N_{tr} = 2$	12.6	137	1.4	146
$N_q = 0$	10.7	84	1	87
$18 \text{ GeV} \leq m_h \leq 26 \text{ GeV}$	8.5	1.2	0	2
1990				
$m_h=m_A=20$ GeV				116K
Preselection	72.1	15543	781	16324
$N_{cl} \geq 15$	72.1	15539	50	15551
$N_J \geq 2$	69.8	11400	17	11442
$0.5 \text{ GeV} \leq E_\tau \leq 30 \text{ GeV}$	62.5	9607	12	9448
$N_\tau = 2$	34.6	1259	7	1428
$N_{tr} = 2$	13.5	86	0.3	101
$N_q = 0$	10.8	46	0	67
$16.2 \text{ GeV} \leq m_h \leq 23.8 \text{ GeV}$	8.1	2	0	3

Table 12: Cuts and corresponding event numbers in the different steps of the selection in the $\tau\tau b\bar{b}$ channel for data and background compared with acceptances for $m_h=m_A=22$ GeV and for $m_h=m_A=20$ GeV signals for the 1991 and 1990 detector configurations, respectively. The details of the preselection are given in the text.

4.3.3 Results for $\tau^+\tau^-b\bar{b}$ Channel

The $Z^0 \rightarrow h^0 A^0 \rightarrow \tau^+\tau^-b\bar{b}$ acceptances for several combinations of h^0 and A^0 masses compared to data and background are given in Table 13 for the 1991 and 1990 detector configurations.

In the mass region for $m_h > 30$ GeV, we use the analysis developed for the minimal SM Higgs search [3] in the $h^0\tau^+\tau^-$ channel; this analysis was optimized for a Higgs of 55 GeV. The efficiencies resulting from this analysis are presented in Table 14 for a series of mass points. No data events pass the $\tau\tau b\bar{b}$ selection.

The predictions for the signal and the backgrounds are affected by a systematic uncertainty of 0.5% on the number of Z^0 hadronic decays used in the normalization and by a systematic

$\tau\tau b\bar{b}$ Channel			
Masses (GeV) m_h, m_A	Signal Acceptance (%)	$Z^0 \rightarrow q\bar{q}, \tau\tau$ Events	Data Events
1991			
4, 12	2.0	30	33
4, 22	2.9	31	33
4, 32	1.7	30	32
12, 12	6.2	12	15
12, 22	8.8	11	14
12, 32	5.3	8.8	14
12, 42	1.9	9.4	15
22, 22	8.5	1.2	2
22, 32	5.8	2.0	3
22, 42	1.0	2.0	3
1990			
4, 11	2.1	14	12
11, 11	6.6	8	16
11, 25	6.3	7	15
20, 20	8.1	2	3
20, 25	5.8	2	2
30, 30	4.1	0	0

Table 13: Acceptances for signal events from $Z^0 \rightarrow h^0 A^0$ $h^0 \rightarrow \tau^+ \tau^-$ and $A^0 \rightarrow b\bar{b}$ for several h^0 and A^0 mass combinations after applying the cut on the τ -pair invariant mass and corresponding number of events for the data and for the expected background.

$\tau\tau b\bar{b}$ Channel	
Masses (GeV) m_h, m_A	Signal Acceptance (%)
32, 32	11.3
42, 12	20.0
42, 22	19.9
42, 42	11.0
52, 12	26.5
52, 22	21.6
52, 32	16.4
62, 12	23.2
62, 22	15.3

Table 14: Acceptances for events with $Z^0 \rightarrow h^0 A^0$ $h^0 \rightarrow \tau^+ \tau^-$ and $A^0 \rightarrow b\bar{b}$ decays for a series of h^0 and A^0 mass combinations, after applying the selection for the search for Higgs bremsstrahlung in the $h^0 \tau^+ \tau^-$ channel. This selection is used to search for $Z^0 \rightarrow h^0 A^0 \rightarrow \tau^+ \tau^- b\bar{b}$ in the region $m_h > 30$ GeV. No data event survive this selection.

uncertainty on the modeling of the detector response. The latter is estimated by varying the cuts over amounts equal to the error on the measured quantity.

The main systematic errors affecting the predicted signal acceptances are listed in Table 15. For the available signal Monte Carlo samples, the statistical error lies between 10% and 30% depending on the signal acceptances. The resulting total uncertainty is used to reduce the signal efficiency in order to obtain a 95% CL limits on the $Z^0 \rightarrow h^0 A^0 \rightarrow \tau\tau b\bar{b}$ branching ratio as function of the (m_h, m_A) masses.

$\tau\tau b\bar{b}$ Channel		
Selection Cuts $m_h=m_A=22$ GeV	Variation	Acceptance Reduction (%)
Preselection	–	< 3
$N_{cl} \geq 15$	1	< 1
$N_J \geq 2$	5%	5.0
$0.5 \leq E_\tau \leq 30$ GeV	11%	2.0
$N_\tau = 2$	5%	5.0
$N_{tr} = 2$	< 3%	3.0
$N_q = 0$	< 3%	3.0
$18 \text{ GeV} \leq m_h \leq 26 \text{ GeV}$	$\sigma \pm 30\%$	9.7
TOTAL		13.0

Table 15: Reduction of expected Higgs acceptance in the $\tau\tau b\bar{b}$ channel due to modeling of the detector response for each quantity used in the analysis. For continuous quantities the variation is taken as one standard deviation on the measured quantity and for discrete quantities as one standard deviation on the normalization of the event rate. The reductions are summed in quadrature.

The agreement between the measured distributions and those of known physics processes shows that there is no evidence in our data for the decay $Z^0 \rightarrow h^0 A^0 \rightarrow \tau^+ \tau^- b\bar{b}$. Thus upper limits for the branching ratio

$$\frac{\Gamma(Z^0 \rightarrow h^0 A^0 \rightarrow \tau^+ \tau^- b\bar{b})}{\Gamma(Z^0 \rightarrow q\bar{q})} \quad (20)$$

can be derived as function of m_h and m_A . Figure 17 shows the regions in the (m_h, m_A) plane excluded at 95% CL for values of the branching ratio larger or equal to 2×10^{-3} , 1×10^{-3} and 2×10^{-4} , respectively. The analysis has been performed for $h^0 \rightarrow \tau^+ \tau^-$ and $A^0 \rightarrow b\bar{b}$. In the region $m_h > 30$ GeV the search for Higgs bremsstrahlung in the $h^0 \tau^+ \tau^-$ channel [3] is used.

4.4 Search in the $Z^0 \rightarrow h^0 A^0 \rightarrow \tau^+ \tau^- \tau^+ \tau^-$ Channel

The signature of a $Z^0 \rightarrow h^0 A^0 \rightarrow \tau^+ \tau^- \tau^+ \tau^-$ event consists of 4 low-mass jets associated with a low number of charged tracks. Requiring small calorimetric activity in the event strongly reduces the $Z^0 \rightarrow q\bar{q}$ background. The additional requirement that there is one isolated pair of narrow jets associated with two tracks of opposite charge, reduces the background from $Z^0 \rightarrow \tau^+ \tau^-$ decays. In fact, in such events a τ -jet can be split into two narrow jets, but the number of tracks associated with the jet pair is mostly 1 or 3 (the case of 2 tracks arises only as a result of detector inefficiencies). In the case of a real τ -pair the number of associated tracks

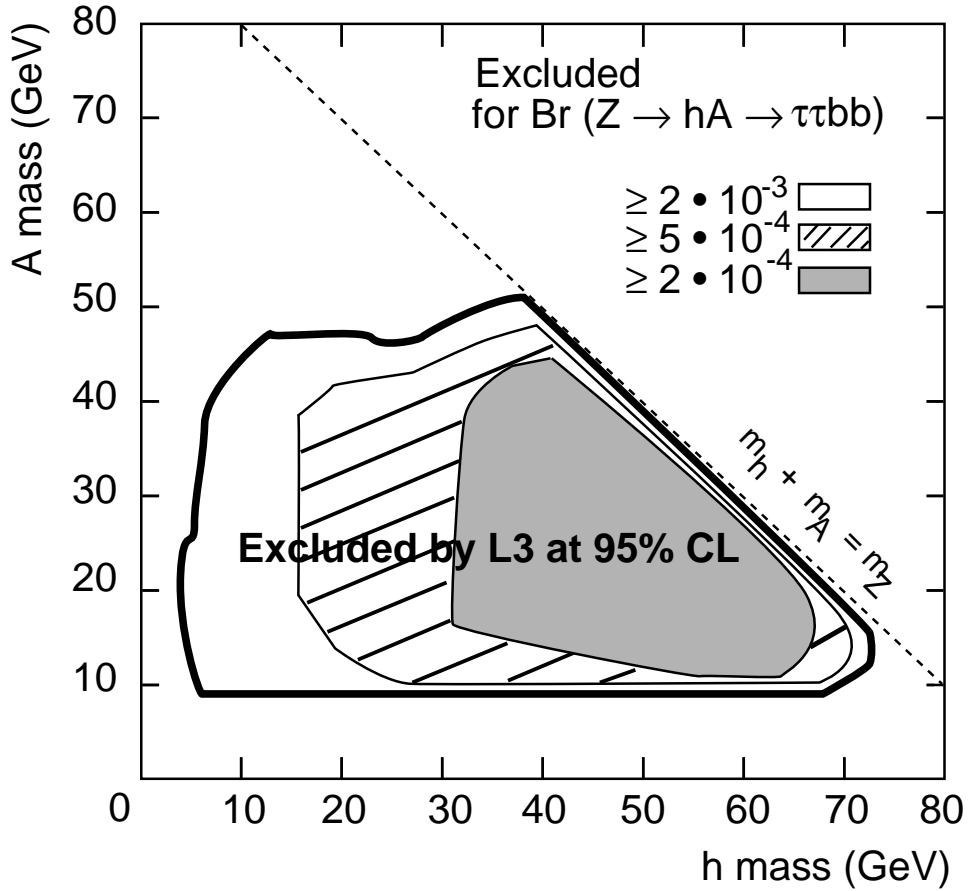


Figure 17: Regions of the (m_h, m_A) plane excluded at 95% CL for values of the branching ratio $\Gamma(Z^0 \rightarrow h^0 A^0 \rightarrow \tau^+ \tau^- b \bar{b}) / \Gamma(Z^0 \rightarrow q \bar{q}) \geq 2 \times 10^{-4}$ (dark region), $\geq 5 \times 10^{-4}$ (hatched region) and $\geq 2 \times 10^{-3}$ (region inside heavy contour line). The analysis has been performed for $h^0 \rightarrow \tau^+ \tau^-$ and $A^0 \rightarrow b \bar{b}$. The same efficiencies are obtained if h^0 and A^0 are interchanged, i.e. $h^0 \rightarrow b \bar{b}$, $A^0 \rightarrow \tau^+ \tau^-$.

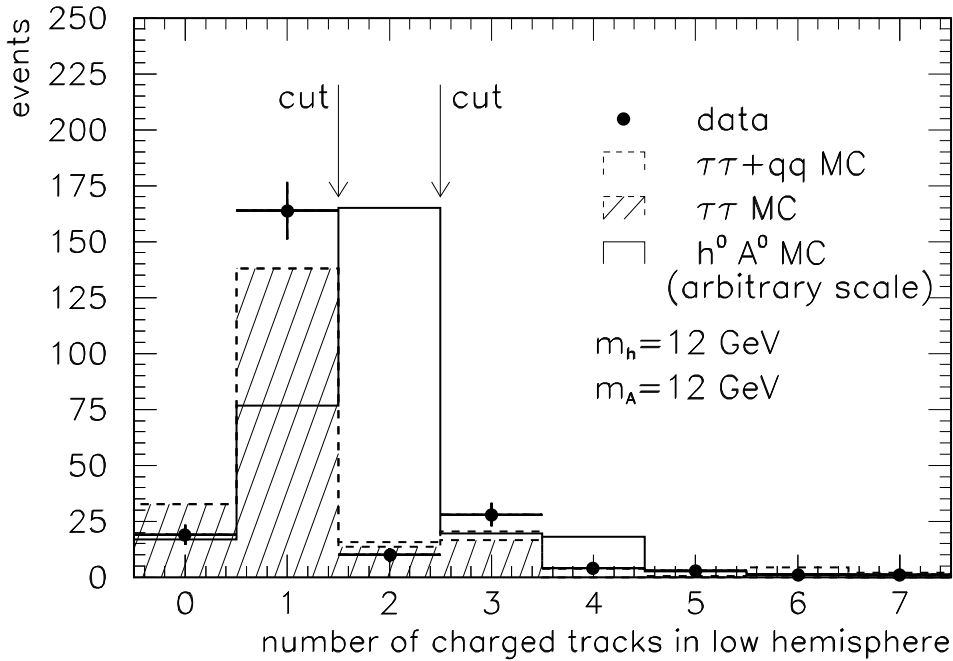


Figure 18: Number of charged tracks in the low-multiplicity hemisphere for data, simulated background and Higgs signal in the $\tau\tau\tau\tau$ channel.

is mostly 2. In the present search, again we adopt the method of dividing the event into two hemispheres, in order to select events with two well separated pairs of jets. The hemisphere with the lower number of clusters (hereafter referred to as the low-multiplicity hemisphere) should contain the $\tau^+\tau^-$ pair with the smaller track multiplicity.

4.4.1 Selection-Details

The events have to pass the same preselection as for $\tau\tau b\bar{b}$ channel. Events with low calorimetric cluster multiplicity are selected in order to remove $Z^0 \rightarrow q\bar{q}$ background by requiring:

- $7 \leq N_{cl} \leq 20$.

At this stage of the selection, the data sample is dominated by low cluster multiplicity events ($Z^0 \rightarrow e^+e^-, \mu^+\mu^-, \tau^+\tau^-$). The acceptance for the simulated $Z^0 \rightarrow h^0 A^0 \rightarrow \tau^+\tau^-\tau^+\tau^-$ events after these cuts is about 55%.

Events with 4 or 5 narrow jets and a two-prong final state for τ -pair are selected by requiring:

- $N_\tau^l = 2$ and $N_\tau^h = 2$ or 3, where N_τ^l and N_τ^h refer to the number of narrow jets with $0.5 \text{ GeV} \leq E_\tau \leq 30 \text{ GeV}$ in the low-multiplicity hemisphere and in the high hemisphere respectively,
- $N_{tr} = 2$, where N_{tr} is the number of tracks in the low-multiplicity hemisphere. The distribution of the number of charged tracks in the low hemisphere after the previous cuts is shown in Figure 18.
- $N_q = 0$, where N_q is the total charge in the low-multiplicity hemisphere.

In Table 16 the $\tau\tau\tau\tau$ selection cuts and their effects on the data, the background and the simulated signal for $m_h = m_A = 12$ GeV and $m_h = m_A = 11$ GeV are presented for the 1991 and the 1990 detector configurations, respectively.

$\tau\tau\tau\tau$ Channel				
Selection cuts	Signal Acceptance (%)	$Z^0 \rightarrow q\bar{q}$ Events	$Z^0 \rightarrow \tau^+\tau^-$ Events	Data Events
1991				
$m_h = m_A = 12$ GeV				296K
Preselection	55.1	29391	2005	31392
$7 \leq N_{cl} \leq 20$	51.4	182	1989	2455
$0.5 \text{ GeV} \leq E_\tau \leq 30 \text{ GeV}$	31.1	49	470	628
$N_\tau^l = 2$ and $N_\tau^h = 2$ or 3	15.4	17	200	230
$N_{tr} = 2$	8.4	1.9	10	10
$N_q = 0$	8.0	1.2	7.2	7
1990				
$m_h = m_A = 11$ GeV				116K
Preselection	42.7	15526	788	16324
$7 \leq N_{cl} \leq 20$	37.4	97	782	994
$0.5 \text{ GeV} \leq E_\tau \leq 30 \text{ GeV}$	23.3	19	185	237
$N_\tau^l = 2$ and $N_\tau^h = 2$ or 3	12.6	5.3	79	96
$N_{tr} = 2$	7.1	0.7	5.4	7
$N_q = 0$	6.5	0.7	4.0	4

Table 16: Cuts and corresponding numbers of events in the different steps of the selection in the $\tau\tau\tau\tau$ channel for data and background compared with acceptances for $m_h = m_A = 12$ GeV and for $m_h = m_A = 11$ GeV signals for the 1991 and 1990 detector configurations, respectively. The details of the preselection are given in the text.

4.4.2 Results for $\tau^+\tau^-\tau^+\tau^-$ Channel

The signal acceptances are given in Table 17. In the 1991 data sample 7 events survive the $\tau\tau\tau\tau$ selection and 8.4 are predicted from background processes. In the 1990 data sample 4 events are selected and 4.7 predicted as background. For the Monte Carlo signal, 1500 and 1300 events are fully simulated in the 1991 and the 1990 detector configuration, respectively.

The systematic errors affecting the predicted signal acceptances for the $\tau\tau\tau\tau$ channel are given in Table 18. Statistical errors on the signal predictions vary between 9% and 18%, depending on the (m_h, m_A) mass point, are taken into account.

The comparison between the data and the predictions for background shows no evidence for signal from $Z^0 \rightarrow h^0 A^0 \rightarrow \tau^+\tau^-\tau^+\tau^-$ decay. Thus limits on the branching ratio

$$\frac{\Gamma(Z^0 \rightarrow h^0 A^0 \rightarrow \tau^+\tau^-\tau^+\tau^-)}{\Gamma(Z^0 \rightarrow q\bar{q})} \quad (21)$$

can be set as function of the h^0 and A^0 masses. Figure 19 shows the regions in the (m_h, m_A) plane excluded at 95% CL for values of the branching ratio larger or equal to 2×10^{-3} , 1×10^{-3} and 5×10^{-4} , respectively.

$\tau\tau\tau\tau$ Channel	
Masses (GeV) m_h, m_A	Signal Acceptance (%)
1991	
4, 4	8.0
4, 12	8.3
4, 32	6.3
4, 42	4.5
4, 52	1.9
12, 12	8.0
12, 22	7.5
12, 32	7.0
12, 42	3.7
12, 52	1.9
22, 22	6.3
22, 42	2.5
32, 42	3.2
42, 42	4.9
1990	
4, 4	7.2
4, 11	6.9
11, 11	6.5

Table 17: Acceptances for simulated $Z^0 \rightarrow h^0 A^0$, $h^0 \rightarrow \tau^+ \tau^-$ and $A^0 \rightarrow \tau^+ \tau^-$ for several h^0 and A^0 mass combinations, after applying the selection for the $\tau\tau\tau\tau$ channel.

$\tau\tau\tau\tau$ Channel		
Selection Cuts $m_H=40$ GeV	Variation	Acceptance Reduction (%)
Preselection	–	< 3
$N_{cl} \leq 15$	1	9
$0.5 \leq E_\tau \leq 30$ GeV	+0.5 GeV, -2 GeV	11
$N_\tau^l = 2$ $N_\tau^h = 2$ or 3	10%	10
$N_{tr} = 2$	< 3%	3
$N_q = 0$	< 3%	3
TOTAL		19

Table 18: Reduction of expected Higgs acceptance in the $\tau\tau\tau\tau$ channel due to modeling of the detector response for each quantity used in the analysis. For continuous quantities the variation is taken as one standard deviation on the measured quantity and for discrete quantities as one standard deviation on the normalization of the event rate. The reductions are summed in quadrature.

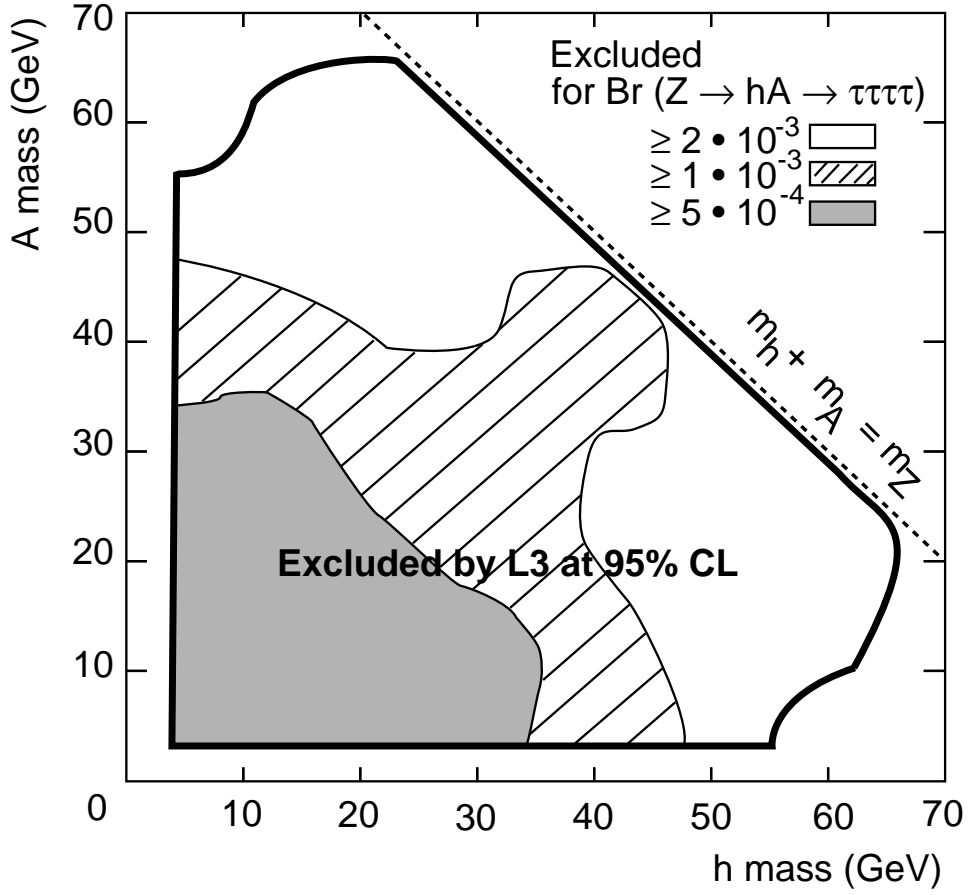


Figure 19: Regions of the (m_h, m_A) plane excluded at 95% CL for values of the branching ratio $\Gamma(Z^0 \rightarrow h^0 A^0 \rightarrow \tau^+ \tau^- \tau^+ \tau^-) / \Gamma(Z^0 \rightarrow q\bar{q}) \geq 5 \times 10^{-4}$ (dark region), $\geq 1 \times 10^{-3}$ (hatched region) and $\geq 2 \times 10^{-3}$ (region inside heavy contour line).

5 Search for Charged Higgs Boson Pair-Production

Searches are made for signatures of charged Higgs pair-production in the decay channels $c\bar{s}c$, $c\bar{s}\tau\nu$ and $\tau\nu\tau\nu$. A mass range between 20 GeV and the kinematic production threshold has been investigated. The mass region below 20 GeV had been excluded before the operation of the LEP accelerator [20].

5.1 Search in the $Z^0 \rightarrow H^+H^- \rightarrow c\bar{s}c$ Channel

The search for $Z^0 \rightarrow H^+H^- \rightarrow c\bar{s}c$ process is made in the hadronic event sample. In order to improve the jet energy resolution, the total event energy is rescaled to the known LEP center-of-mass energy. Events with 4 and 5-jets ($y_{\text{cut}} = 0.02$) are selected. The 5 jet events are transformed into 4-jets events by combining the two jets with the minimum invariant mass. Since Higgs events are expected to be more spherical, the cut $T < 0.95$ is applied.

5.1.1 Selection-Details

Cuts on the following variables are applied to search for an expected charged-Higgs signal. As an example the cuts and resolutions are given for a 40 GeV simulated Higgs signal:

- $\Delta m_{\text{rec}} = |m_{H^+}^{\text{rec}} - m_{H^-}^{\text{rec}}|$, where $m_{H^\pm}^{\text{rec}}$ are the reconstructed Higgs masses. The four jets can be combined into 2-jet pairs in three possible ways. In order to select the combination most likely to come from charged-Higgs production and decay, use is made of the fact that $m_{H^+} = m_{H^-}$. The combination with minimum Δm_{rec} is chosen and events with $\Delta m_{\text{rec}} \geq 6$ GeV are rejected.
- $|\cos \theta_p| \leq 0.5$ and $|\cos \theta_d| \leq 0.7$ are required and in order to exploit the back-to-back production of the Higgs it is required that $|\cos \theta_p(H^+) + \cos \theta_p(H^-)| \leq 0.3$. The production angle and the decay angle distributions for data, $Z^0 \rightarrow q\bar{q}$ background and expected Higgs signal are shown in Figures 20 and 21, respectively. As expected, the signal θ_p distribution exhibits a clear $\sin^2 \theta_p$ behavior and the $\cos \theta_d$ distribution is flat, whereas the data and $Z^0 \rightarrow q\bar{q}$ background distributions are peaked at large values in both variables.
- $\psi_{\text{pl}} \geq 0.7$ rad is required, where ψ_{pl} is the angle between the $H^+ \rightarrow c\bar{s}$ decay plane and the $H^- \rightarrow \bar{c}s$ decay plane. For the signal the ψ_{pl} distribution is expected to be flat whereas for the QCD background it is more peaked at small angles.
- Three mass-dependent cuts are applied on the variables $\sum M_{\text{jet}}^{\text{rec}}$, $E_{\text{jet}}^{\text{max}}/\sqrt{s}$ and $E_{\text{jet}}^{\text{min}}/\sqrt{s}$, where $\sum M_{\text{jet}}^{\text{rec}}$ is the sum of reconstructed jet masses, $E_{\text{jet}}^{\text{max}}/\sqrt{s}$, $E_{\text{jet}}^{\text{min}}/\sqrt{s}$ are the fractions of energies carried by the highest and lowest energy jets, respectively. In order to optimize the above cuts and determine the signal selection efficiency, 1600 signal events for $m_H = 20, 30$ and 40 GeV have been studied. The values of mass-dependent cuts are given in Table 19.
- To reduce the $Z \rightarrow b\bar{b}$ background, events with inclusive leptons (e or μ) as defined in the bbbb analysis, are rejected.

The percentages of surviving events with average reconstructed Higgs mass $m_H = 0.5 \times (m_{H^+}^{\text{rec}} + m_{H^-}^{\text{rec}})$ within 1 GeV of the generated Higgs mass are 3.8, 3.5 and 2.8% for $m_H = 20, 30$ and 40 GeV,

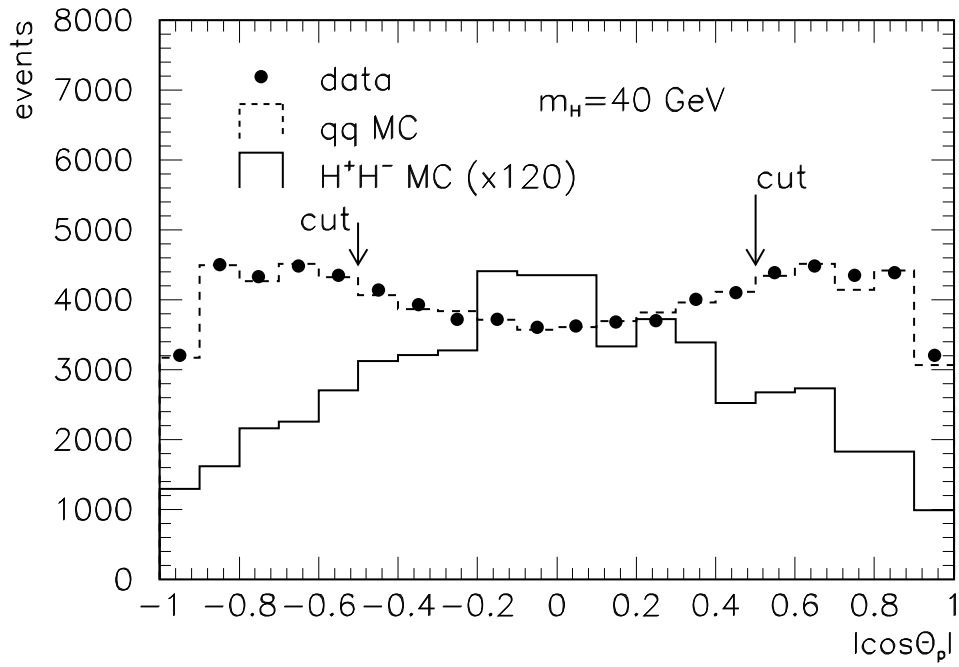


Figure 20: Distribution of the production angle for data, simulated background and Higgs signal in the cscs channel.

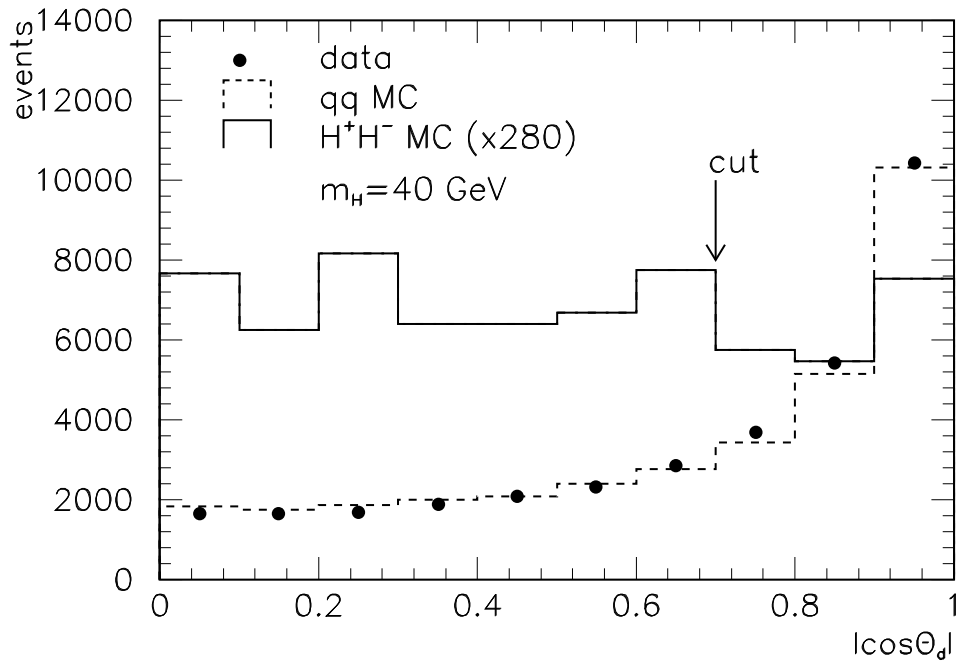


Figure 21: Decay angle θ_d distribution for data, simulated background and Higgs signal in the cscs channel.

cscs Channel			
Higgs mass (GeV)	20	30	40
$\sum M_{\text{jet}}^{\text{rec}} \leq$ (GeV)	22	28	30
$E_{\text{jet}}^{\text{max}}/\sqrt{s} \leq$	0.39	0.38	0.34
$E_{\text{jet}}^{\text{min}}/\sqrt{s} \geq$	0.10	0.12	0.14

Table 19: Values of Higgs-mass-dependent cuts applied in the cscs channel.

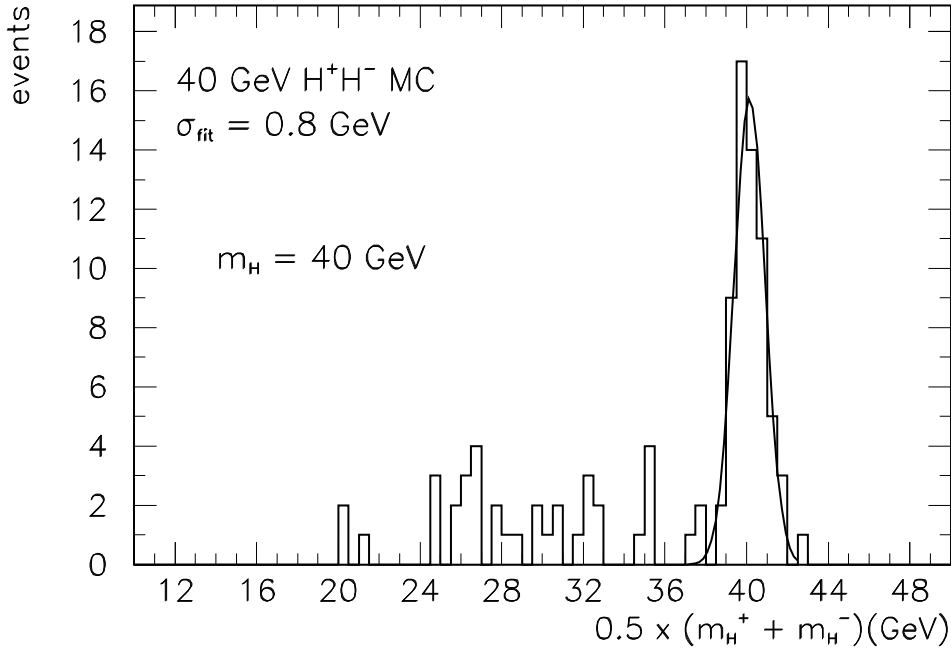


Figure 22: Expected mass resolution for a 40 GeV charged Higgs signal in the cscs channel.

respectively. The mass m_H distribution for the 40 GeV Higgs signal is shown in Figure 22. A mass resolution of 0.8 GeV is obtained, using the fact that both Higgs bosons must have the same mass and that the total visible energy must be the center-of-mass energy.

Linearly interpolating the mass-dependent cuts, the number of surviving events in the data and $Z^0 \rightarrow q\bar{q}$ background are determined in the range $m_H = 20$ to 43 GeV at 0.5 GeV intervals. The distribution of the average reconstructed Higgs mass, $0.5 \times (m_{H^+}^{\text{rec}} + m_{H^-}^{\text{rec}})$, is shown in Figure 23 together with the events expected from 40 GeV charged-Higgs production after taking into account the selection efficiency (2.8%) at this mass value. The distributions of data and $Z^0 \rightarrow q\bar{q}$ background are in good agreement and the number of surviving events in a 1 GeV bin is about 10 over the entire mass range. In Table 20 the cscs selection cuts and their effects on data, background and signal for 40 GeV charged Higgs are listed for the 1991 and 1990 detector configurations.

5.1.2 Results for $c\bar{s}cs$ Channel

The signal acceptances and a comparison between data and expected background events are given in Table 21. No signal has been found. The systematic errors and their effects on the

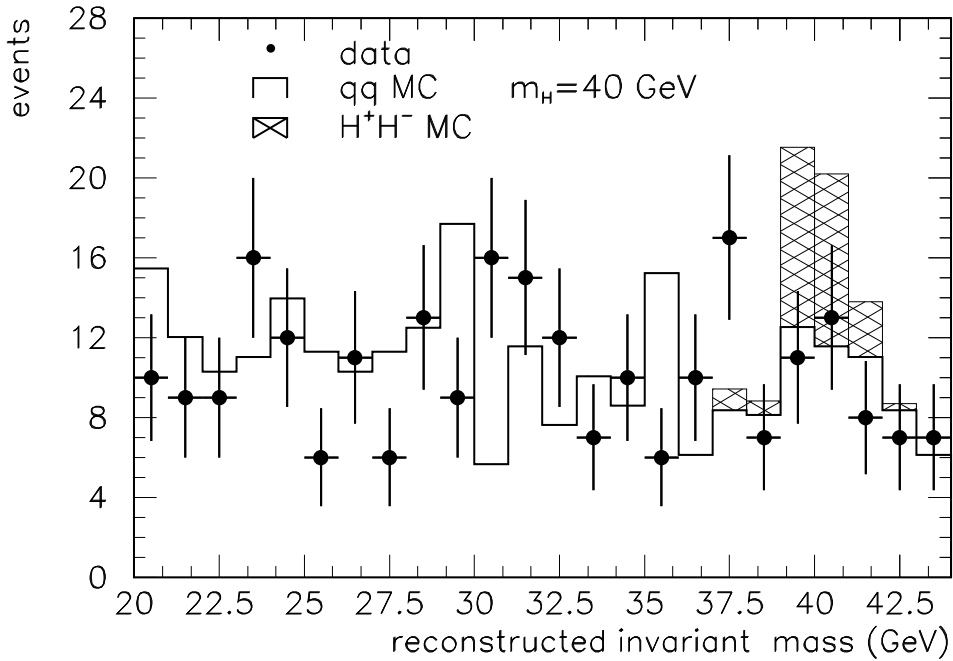


Figure 23: *Reconstructed invariant mass of data, simulated background and Higgs signal in the cscs channel.*

predicted signal acceptances for the cscs channel are given in Table 22. A 33% error, including 12% statistical error, on the number of expected events is taken into account in the evaluation of the excluded region. Figure 33 shows the excluded mass region as a function of the leptonic branching fraction and the charged-Higgs mass.

5.2 Search in the $Z^0 \rightarrow H^+H^- \rightarrow cs\tau\nu$ Channel

The signature for $Z^0 \rightarrow H^+H^- \rightarrow cs\tau\nu$ is one isolated tau and missing energy recoiling against a hadronic system. Signal events for different Higgs masses between 20 GeV and 44 GeV have been simulated. Background from $Z^0 \rightarrow q\bar{q}$ and $Z^0 \rightarrow \tau^+\tau^-$ have been studied. The describing the selection, cuts and resolutions are given for the search for a 40 GeV Higgs signal.

5.2.1 Selection-Details

We require large calorimetric cluster multiplicity, $N_{cl} \geq 20$ to remove pure leptonic events. Backgrounds from two-photon and beam-gas events are removed by requiring small longitudinal energy imbalance, $E_{||}/E_v < 0.60$, the thrust axis not pointing along the beam axis, $|\cos\theta_T| < 0.9$ and the total calorimetric energy in a range expected for the signal, $0.4 < E_v/\sqrt{s} < 0.75$. The upper cut removes much of the hadronic background. A cut on the thrust, $T \leq 0.95$, removes 2-jet events. After this preselection, about 4000 events from $Z^0 \rightarrow q\bar{q}$ background survive, keeping an efficiency of about 70% for the signal. The main selection consists of the following cuts:

- $N_{cl} \leq 30 + 0.5 \cdot \frac{m_H}{\text{GeV}}$. Expected signal events with smaller cluster multiplicity are preferentially selected and the $Z^0 \rightarrow q\bar{q}$ background is reduced by about 50%.

cscs Channel			
Selection Cuts	Signal Acc.(%)	$Z^0 \rightarrow q\bar{q}$ Events	Data Events
1991			
$m_H=40$ GeV			296 k
Preselection	85.8	59569	59569
$\Delta m_{\text{rec}} \leq 6$ GeV	48.6	22152	29075
$ \cos \theta_p \leq 0.5$	25.3	12790	12327
$ \cos \theta_d \leq 0.7$	13.0	1608	1510
$\psi_{\text{pl}} \geq 0.7$ rad	8.2	742	790
$\sum M_{\text{jet}}^{\text{rec}} \leq 30$ GeV	6.0	575	554
$0.14 \leq E_{\text{jet}} \leq 0.34$	6.0	255	227
incl. lepton rejection	4.5	254	223
$39 \text{ GeV} \leq m_H \leq 41 \text{ GeV}$	2.8	18	19
1990			
$m_H=40$ GeV			116k
Preselection	82.2	24947	24947
$\Delta m_{\text{rec}} \leq 6$ GeV	53.7	12283	12329
$ \cos \theta_p \leq 0.5$	27.2	5239	5145
$ \cos \theta_d \leq 0.7$	13.5	628	584
$\psi_{\text{pl}} \geq 0.7$ rad	8.7	301	295
$\sum M_{\text{jet}}^{\text{rec}} \leq 30$ GeV	8.7	215	198
$0.14 \leq E_{\text{jet}} \leq 0.34$	7.3	86	84
incl. lepton rejection	7.3	83	83
$39 \text{ GeV} \leq m_H \leq 41 \text{ GeV}$	2.7	6	7

Table 20: The cuts and the corresponding numbers of events in the different steps of the selection in the cscs channel for data and background compared with acceptances for a $m_H=40$ GeV signal for the 1991 and 1990 detector configurations, respectively. The details of the preselection are described in the text.

cscs Channel						
m_H (GeV)	Signal Acc.(%)	$Z^0 \rightarrow q\bar{q}$ Events	Data Events	Signal Acc.(%)	$Z^0 \rightarrow q\bar{q}$ Events	Data Events
	1990			1991		
20	4.2	6	5	3.8	18	19
30	4.2	5	9	2.9	18	16
40	2.7	6	7	2.8	18	19

Table 21: Surviving events after all cuts in the cscs channel. At each mass point 1500 Higgs events in 1991 have been simulated (600 events in 1990). The expected $Z^0 \rightarrow q\bar{q}$ background is normalized to the data.

cscs Channel		
Selection Cuts $m_H=40$ GeV	Variation	Acceptance Reduction (%)
Preselection	–	< 3
$N_J = 4$ or 5	20%	20
$\Delta m_{\text{rec}} \leq 6$ GeV	0.5 GeV	5
$ \cos \theta_p \leq 0.5$	0.04	7.2
$ \cos \theta_d \leq 0.7$	0.04	5.8
$\psi_{\text{pl}} \geq 0.7$ rad	0.08	8.0
$\sum M_{\text{jet}}^{\text{rec}} \leq 30$ GeV	1 GeV	9.4
$E_{\text{jet}}^{\text{max}}/\sqrt{s} \leq 0.34$	0.01	7.1
$E_{\text{jet}}^{\text{min}}/\sqrt{s} \geq 0.14$	0.01	6.5
$39 \text{ GeV} \leq m_H \leq 41 \text{ GeV}$	$\sigma \pm 30\%$	16
TOTAL		31

Table 22: Reduction of expected Higgs acceptance in the cscs channel due to modeling of the detector response for each quantity used in the analysis. For continuous quantities the variation is taken as one standard deviation on the measured quantity and for discrete quantities as one standard deviation on the normalization of the event rate. The reductions are summed in quadrature.

- $M \geq 0.2 + (\frac{m_H}{\text{GeV}} - 20) \cdot 0.0025$. The event major, M , is defined as:

$$M = \max_{\vec{n}_M} \frac{\sum_i |\vec{p}_i \cdot \vec{n}_M|}{\sum_i |\vec{p}_i|} \quad (22)$$

where the maximum is over all possible orientations of the axis \vec{n}_M perpendicular to the thrust axis. Only very spherical events pass this cut. The distribution of M is shown in Figure 24.

- One isolated tau in the event is required. Only one-prong tau decays are considered to reduce misidentification of low-multiplicity isolated hadronic jets from $Z^0 \rightarrow q\bar{q}$ background. Tau candidates are defined as isolated tracks with azimuthal angle $|\cos \theta_{is}| < 0.8$. We consider an inner cone of half angle 10° around the track and an outer cone of half angle θ_{is} . In the inner cone we require one track. The energy of the isolated tau candidate, E_τ , is the energy deposited in this cone. The isolation angle, θ_{is} , is defined as the maximum half angle for which the ratio of energy deposited between the inner and outer cones does not exceed 6%. The distribution of the isolation angle is shown in Figure 25. Tau candidates must have $\theta_{is} \geq 40^\circ$ and $2 \text{ GeV} \leq E_\tau \leq 25 \text{ GeV}$. The low-energy cut reduces background from fluctuations in fragmentation. Low visible energy is likely for tau candidates in signal events since neutrinos are produced in both the tau production and decay.
- $E_\perp/E_v > 0.01 \cdot (45 - \frac{m_H}{\text{GeV}})$ where E_\perp is the momentum imbalance perpendicular to the thrust axis. The imbalance is due to the neutrinos in the decay products of the charged Higgs bosons. For a heavy Higgs which decays almost at rest this cut becomes less efficient.

- $0.35 < E_h/\sqrt{s} < 0.60$ is required, where $E_h = E_v - E_\tau$. Then E_h is scaled to the beam energy (as expected for a charged-Higgs signal) to calculate the invariant mass of the hadronic system. The reconstructed mass distribution is shown in Figure 26. An energy resolution of 1.5 GeV is obtained for a 40 GeV Higgs signal. The reconstructed mass has to be within 10 GeV of the expected Higgs mass for a 20 GeV Higgs and the tolerance decreases linearly to 5.2 GeV for a 44 GeV Higgs.

For the 1990 detector configuration identical cuts are applied except that the cut on N_{cl} is slightly different:

- $16 \leq N_{cl} \leq 22 + 0.5 \cdot \frac{m_H}{\text{GeV}}$.

This change in the selection cut is due to the absence of BGO endcaps in 1990. Only a few data events survive, in agreement with the expected background. The selection efficiency for a 40 GeV Higgs is 13%. The cuts and their effects on data, background and signal for a 40 GeV Higgs signal are summarized in Table 23.

5.2.2 Results for $cs\tau\nu$ Channel

The signal acceptances and a comparison between data and expected background events are given in Table 24. The four remaining data events in the mass range 20 to 30 GeV are used to calculate constraints on the two-doublet Higgs model. The events have been scanned to determine their probable origins, with the conclusion that they are most likely fluctuations of the hadronic background.

In this mass range more than 700 charged-Higgs events are expected in the two-doublet Higgs model under investigation. No indication of a signal has been found. The systematic errors and their effects on the predicted signal acceptances for the $cs\tau\nu$ channel are given in Table 22. A 14% error, including 8% statistical error, on the number of expected events is taken into account in the exclusion plot shown in Figure 33.

The systematic errors and their effects on the predicted signal acceptances for the $cs\tau\nu$ channel are given in Table 25.

5.3 Search in the $Z^0 \rightarrow H^+H^- \rightarrow \tau^+\nu\tau^-\nu$ Channel

The $Z^0 \rightarrow H^+H^- \rightarrow \tau^+\nu\tau^-\nu$ events are characterized by a small particle multiplicity and large missing energy. For this channel, events from $Z^0 \rightarrow \tau^+\tau^-(\gamma)$, $Z^0 \rightarrow q\bar{q}$ and $e^+e^- \rightarrow e^+e^-\bar{f}\bar{f}$ where both fermions are detected and the electron pair is lost in the beam pipe, are sources of background.

5.3.1 Selection-Details

Hadronic events are largely suppressed by requiring $N_{cl} \leq 15$. In order to reject beam-gas and two-photon events with large energy deposit near the beam pipe, we require on the thrust axis $|\cos\theta_T| \leq 0.7$ and $E_{||}/E_v < 0.5$. Each jet ($y_{cut} = 0.02$) with azimuthal angle to the beam axis, θ_J , must fulfill $|\cos\theta_J| \leq 0.93$. A lower cut on the calorimetric energy, $0.2 < E_v/\sqrt{s}$, removes most of the remaining $e^+e^- \rightarrow e^+e^-\bar{f}\bar{f}$ events. In order to remove dimuon and Bhabha events, a cut on the visible energy (including the muon momenta) is applied: $E_v/\sqrt{s} < 0.8$. The remaining events have 2 or 3 jets. We require that at least two jets have an associated TEC track within a 50° half opening angle with the jet axis.

$c\bar{s}\tau\nu$ Channel			
Selection cuts	Signal Acc.(%)	$Z^0 \rightarrow q\bar{q}$ Events	Data Events
1991			
$m_H=40$ GeV			296k
Preselection	70.8	3843	3765
$N_{cl} \leq 50$	64.4	1574	1605
$M \geq 0.25$	60.5	426	420
1 isolated τ	15.5	6.6	9
$E_{\perp} > 0.05 \cdot E_{\nu}$	15.3	5.9	8
$0.35 < E_{had}/\sqrt{s} < 0.60$	12.7	2.6	4
$34 \text{ GeV} < m_{had} < 46 \text{ GeV}$	12.5	2.6	1
1990			
$m_H=40$ GeV			116k
Preselection	72.5	2276	2559
$N_{cl} \leq 42$	69.3	1014	1115
$M \geq 0.25$	63.0	301	321
1 isolated τ	18.0	5.8	8
$E_{\perp} > 0.05 \cdot E_{\nu}$	17.8	3.8	6
$0.35 < E_{had}/\sqrt{s} < 0.60$	15.8	1.9	3
$34 \text{ GeV} < m_{had} < 46 \text{ GeV}$	15.3	1.0	1

Table 23: The cuts and the corresponding numbers of events in the different steps of the selection in the $c\bar{s}\tau\nu$ channel for data and background compared with acceptances for $m_H=40$ GeV signal for the 1991 and 1990 detector configurations, respectively. The details of the preselection are described in the text.

$c\bar{s}\tau\nu$ Channel						
m_H (Gev)	Signal Acc. (%)	$Z^0 \rightarrow q\bar{q}$ Events	Data Events	Signal Acc. (%)	$Z^0 \rightarrow q\bar{q}$ Events	Data Events
1990			1991			
20	14.5%	0.0	1	14.0%	0.0	3
30	17.2%	0.0	1	16.9%	0.0	1
40	15.3%	1.0	1	12.5%	2.6	1
44	—	1.0	1	9.8%	1.4	1

Table 24: Surviving events after all cuts in the $c\bar{s}\tau\nu$ channel. At each mass point 1500 Higgs events in 1991 have been simulated (600 events in 1990). The expected $Z^0 \rightarrow q\bar{q}$ background is normalized to the data. Due to the chosen bin size in the last cut, events can be selected at more than one listed mass value. A total of 7 events pass the selection.

cs $\tau\nu$ Channel		
Selection cuts $m_H=40$ GeV	Variation	Acceptance Reduction (%)
Preselection	–	< 3
$N_{cl} \geq 20$	–1	2
$M \geq 0.25$	+0.02	2.8
1 isolated $\tau(40^\circ)$	3°	4.6
$E_\perp/E_\nu > 0.05$	+0.025	8.3
$0.35 < E_h/\sqrt{s} < 0.60$	± 0.5 GeV	2.2
$32 \text{ GeV} \leq m_{had} \leq 46 \text{ GeV}$	$\sigma \pm 30\%$	< 1
TOTAL		11

Table 25: Reduction of expected Higgs acceptance in the cs $\tau\nu$ channel due to modeling of the detector response for each quantity used in the analysis. For continuous quantities the variation is taken as one standard deviation on the measured quantity and for discrete quantities as one standard deviation on the normalization of the event rate. The reductions are summed in quadrature.

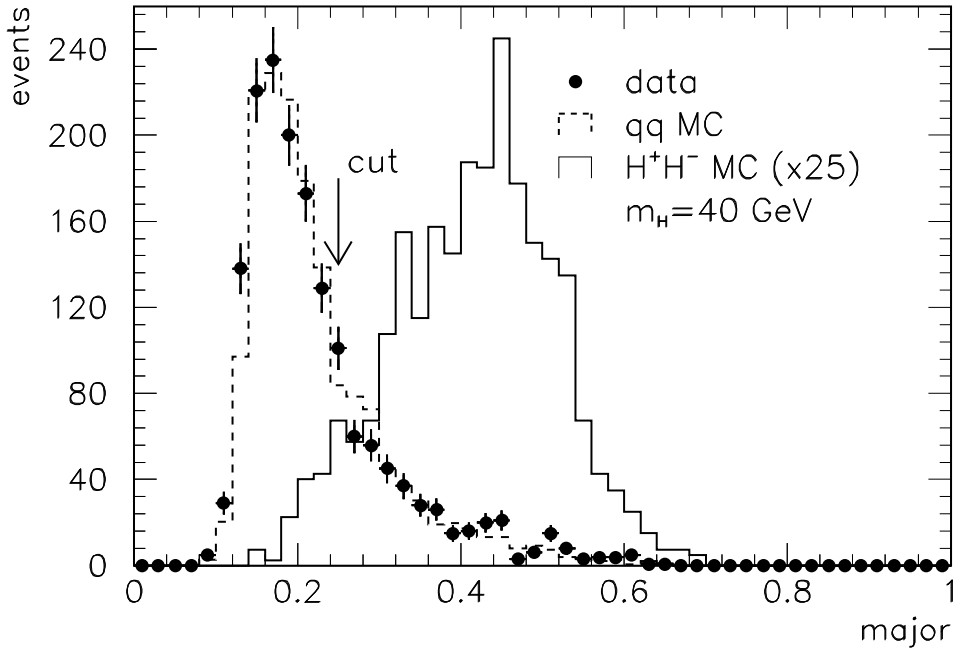


Figure 24: Major distribution for data, simulated background and Higgs signal in the cs $\tau\nu$ channel.

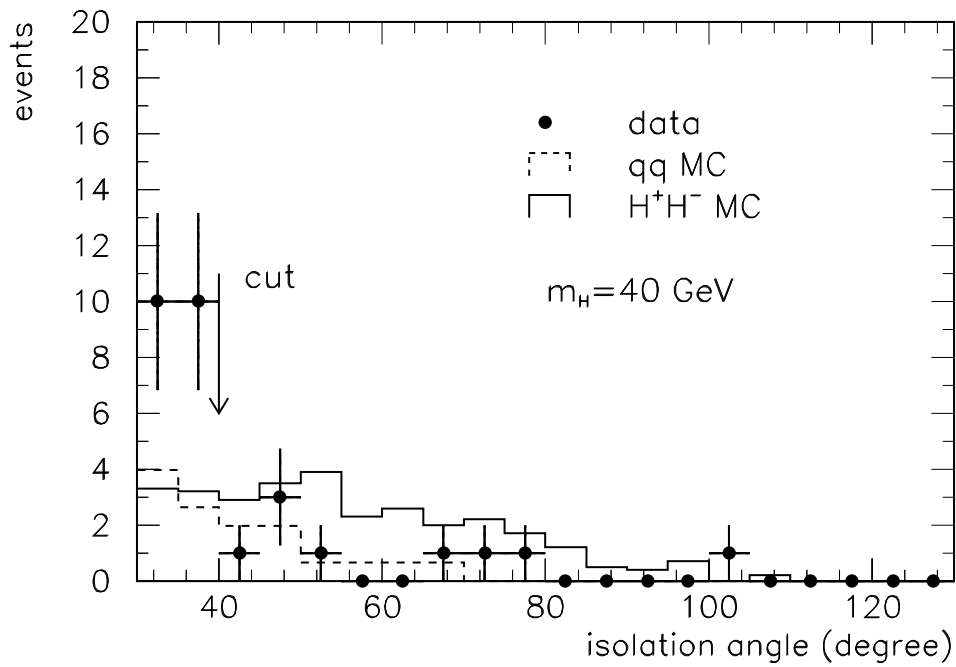


Figure 25: *Distribution of the isolation angle for tau candidates for data, simulated background and Higgs signal in the $c\tau\nu$ channel.*

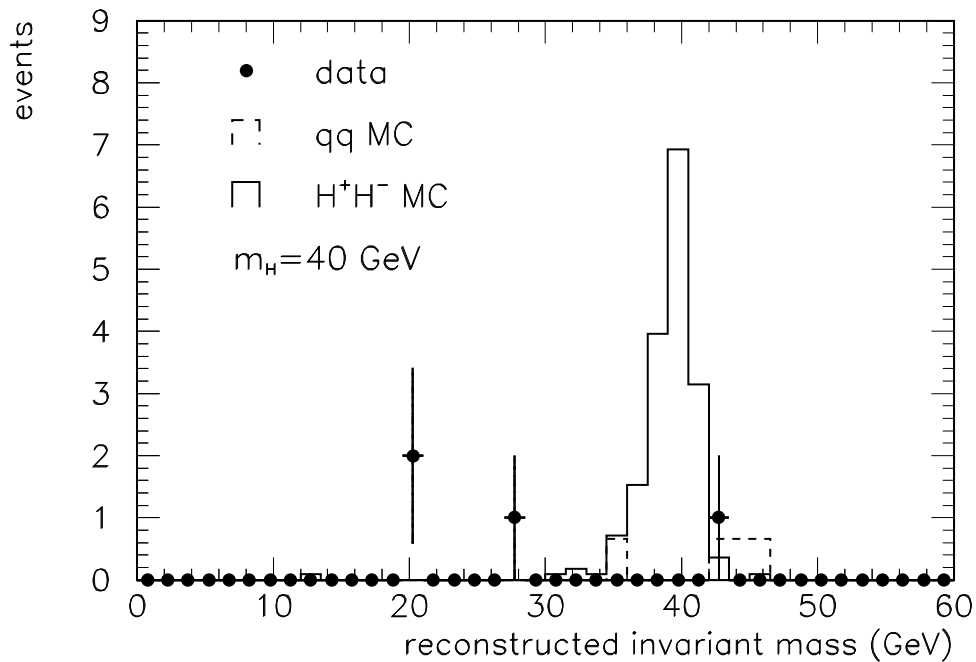


Figure 26: *Distribution of the reconstructed invariant mass for data, simulated background and Higgs signal in the $c\tau\nu$ channel.*

The following numbers correspond to the search for a 40 GeV Higgs signal. At this stage the signal efficiency is about 35% with about 3500 background events surviving. The remaining background consists of $Z^0 \rightarrow \tau^+\tau^-(\gamma)$ events. The trigger efficiency for signal events after the preselection cuts has been determined to be $\geq 99\%$. Further selection cuts are applied:

- $E_{\perp}/E_v > 0.2$, where E_{\perp} is the perpendicular energy imbalance.
- $\theta_{123} < 2.8$ rad, where θ_{123} is defined in section 3.1. The $Z^0 \rightarrow \tau^+\tau^-$ background is substantially reduced while for the expected signal 28% selection efficiency is maintained. The θ_{123} distributions for data, background and signal are shown in Figure 27.
- $\theta_a < 2.8$ rad, where the acoplanarity angle, θ_a , is defined as the angular difference of the two most energetic jets in the plane perpendicular to the beam axis. It removes $e^+e^- \rightarrow \tau^+\tau^-(\gamma)$ events with a radiative photon where the photon is lost in the beam pipe. The distributions for data, background and signal are shown in Figure 28.
- $M \geq 0.2$. This cut on the major, M , removes $Z^0 \rightarrow \tau^+\tau^-(\gamma)$ events in which the energy difference between the two taus is very large. Background events where one tau decays into an electron which travels in a direction opposite to the initial tau are rejected. The distributions in M for data, background and signal are shown in Figure 29.

The cuts and their effects on data, background and signal for a 40 GeV Higgs signal are shown in Table 26.

5.3.2 Results for $\tau^+\nu\tau^-\bar{\nu}$ Channel

The signal acceptances are shown in Table 27 for different charged-Higgs masses. No data events pass this selection. The systematic errors and their effects on the predicted signal acceptances for the $\tau\nu\tau\nu$ channel are given in Table 28. A 10% error, including 6% statistical error, on the number of expected events is taken into account in the exclusion plot shown in Figure 33.

$\tau\nu\tau\nu$ Channel			
Selection cuts	Signal Acc. (%)	$Z^0 \rightarrow \tau^+\tau^-$ Events	Data Events
1991			
$m_H=40$ GeV			296k
preselection	29.4	2821	2448
$E_{\perp}/E_v > 0.2$	27.0	1934	1753
$\theta_{123} < 2.8$ rad	24.2	119	97
$\theta_a > 2.8$ rad	21.6	26	26
$M \geq 0.2$	19.7	0	0
1990			
$m_H=40$ GeV			116k
preselection	30.8	1443	1750
$E_{\perp}/E_v > 0.2$	28.7	989	1219
$\theta_{123} < 2.8$ rad	25.2	60	51
$\theta_a > 2.8$ rad	22.2	13	9
$M \geq 0.2$	20.0	0	0

Table 26: The cuts and the corresponding numbers of events in the different steps of the selection in the $\tau\nu\tau\nu$ channel for data and background compared with acceptances for $m_H=40$ GeV signal for the 1991 and 1990 detector configurations, respectively. The details of the preselection are described in the text.

$\tau\nu\tau\nu$ Channel		
m_H (GeV)	Signal Acceptance(%)	Signal Acceptance(%)
	1990	1991
20	11.8	10.1
30	18.3	16.1
40	20.0	19.7
44	—	19.5

Table 27: Selection efficiencies for various Higgs masses in the $\tau\nu\tau\nu$ channel. No data events survive the selection.

$\tau\nu\tau\nu$ Channel		
Selection cuts $m_H=40$ GeV	Variation	Acceptance Reduction (%)
Preselection	—	< 5
$E_\perp/E_\nu > 0.2$	0.03	2.9
$\theta_{123} < 2.8$ rad	0.09	2.9
$\theta_a > 2.8$ rad	0.04	2.2
$M \geq 0.2$	0.025	4.4
TOTAL		8.1

Table 28: Reduction of expected Higgs acceptance in the $\tau\nu\tau\nu$ channel due to modeling of the detector response for each quantity used in the analysis. For continuous quantities the variation is taken as one standard deviation on the measured quantity and for discrete quantities as one standard deviation on the normalization of the event rate. The reductions are summed in quadrature.

6 Interpretation in the Two-Doublet Higgs Model

From the limits on the low-mass Higgs presented above and from previously presented searches optimized for high Higgs masses [3], a limit on $\sin^2(\beta - \alpha)$ as a function of m_h is obtained. We can also obtain limits on $\cos^2(\beta - \alpha)$ as a function of m_h and m_A from Z^0 line shape measurements. The detection efficiencies for the Higgs decay $h^0 \rightarrow A^0 A^0$ have been studied in addition to the minimal SM Higgs decays. The combination of the $\sin^2(\beta - \alpha)$ and $\cos^2(\beta - \alpha)$

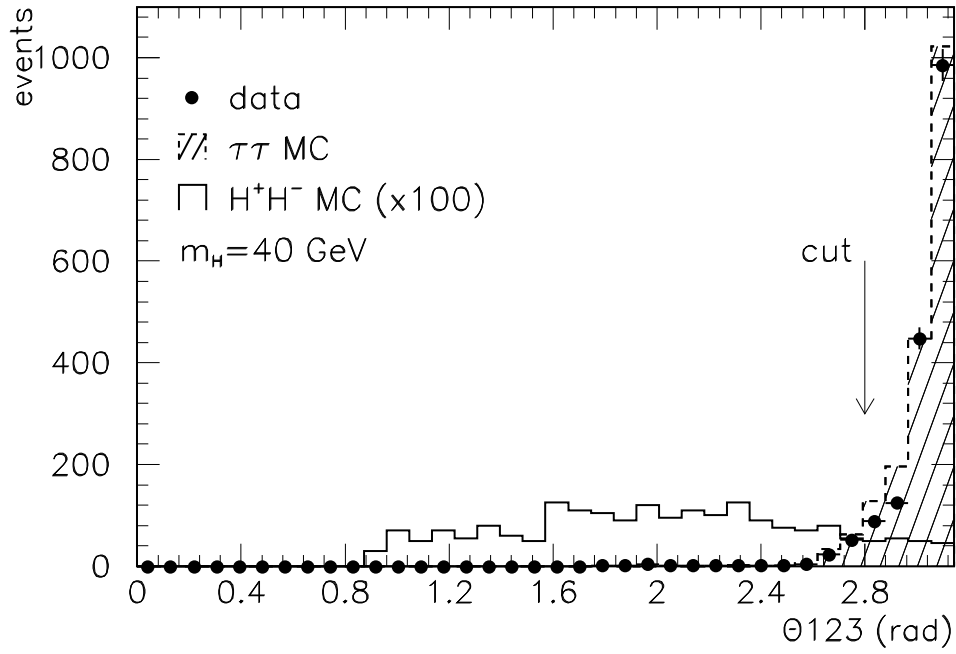


Figure 27: Distribution of θ_{123} for data, simulated background and Higgs signal in the $\tau\nu\tau\nu$ channel.

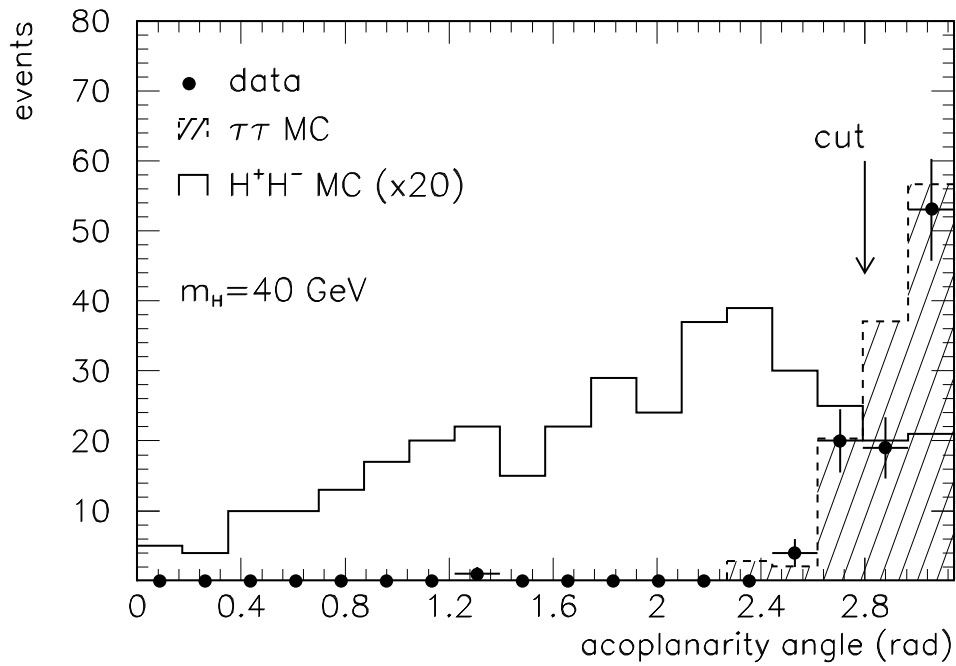


Figure 28: Acoplanarity angle distribution for data, simulated background and Higgs signal in the $\tau\nu\tau\nu$ channel.

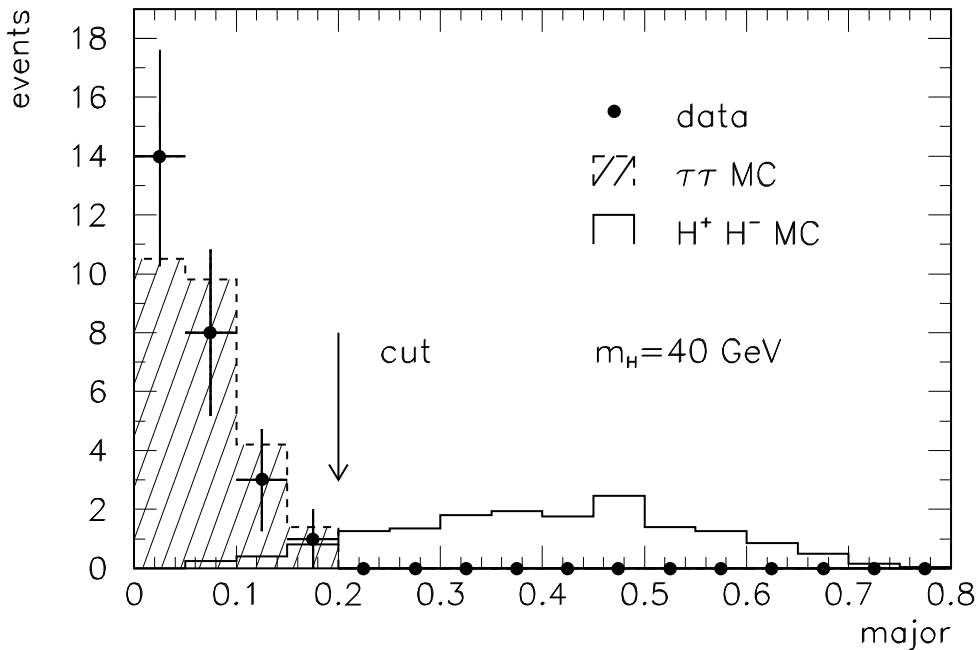


Figure 29: Major distribution for data, simulated background and Higgs signal in the $\tau\nu\tau\nu$ channel.

bounds are used to exclude a region in the (m_h, m_A) plane, which is independent of the α and β parameters.

6.1 Constraints from Higgs Bremsstrahlung

In the two-doublet Higgs model, a large range of $\sin^2(\beta - \alpha)$ can be excluded, based on the minimal Standard Model Higgs search [3]. Table 1 lists the detection efficiencies obtained in the minimal Standard Model Higgs search in the mass range 30 GeV to 60 GeV. For the reinterpretation of the minimal Standard Model Higgs search, the results are first presented under the assumption that the detection efficiencies for $Z^0 \rightarrow Z^{0*}h^0$ are identical to those for $Z^0 \rightarrow Z^{0*}H_{\text{SM}}^0$, but that the h^0 production cross section is suppressed by $\sin^2(\beta - \alpha)$. The effects of the $h^0 \rightarrow A^0A^0$ decay, which result in a smaller selection efficiency for h^0 are evaluated in section 3.4.

In the mass range where no events are observed, the limit on $\sin^2(\beta - \alpha)$ is given by:

$$\sin_{\text{max}}^2(\beta - \alpha) = \frac{N^l}{N^e}, \quad (23)$$

where N^e is the expected number of Higgs events for $\sin^2(\beta - \alpha) = 1$ and $N^l = 3.0$ for a 95% CL limit. The effect of the candidate event is taken into account in each channel by using Poisson statistics. The resulting limit on $\sin^2(\beta - \alpha)$ is shown in Figure 30.

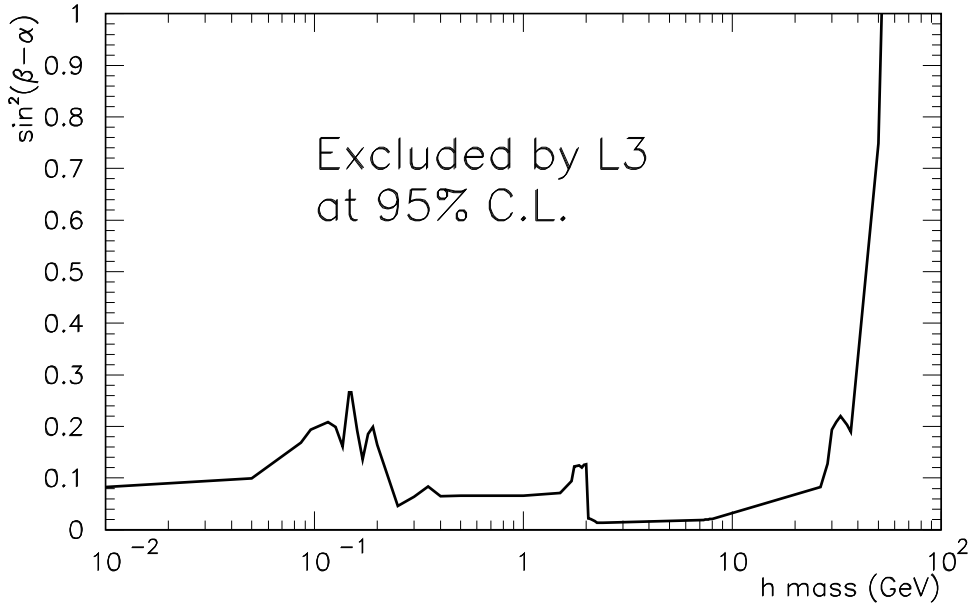


Figure 30: Limit on $\sin^2(\beta - \alpha)$ of the two-doublet Higgs model obtained by conversion of limits from searches for Higgs bremsstrahlung-type events.

6.2 Constraints from the Z^0 Line-Shape

In the general two-doublet model, a contribution from the $Z^0 \rightarrow h^0 A^0$ decay to the total Z^0 width is expected. The upper limit on the contribution to the Z^0 width from new physics, $\Gamma_Z^X < 40$ MeV [21], where Γ_Z^X is the non-Standard Model contribution to the Z^0 width, is used. A limit on $\cos^2(\beta - \alpha)$ for given (m_h, m_A) masses can be set from the constraints on Γ_Z^X :

$$\cos^2_{\max}(\beta - \alpha) = \frac{1}{2} \Gamma_Z^X \Gamma(Z^0 \rightarrow \nu\bar{\nu}) \lambda^{3/2} \left(\frac{m_h^2}{m_Z^2}, \frac{m_A^2}{m_Z^2} \right), \quad (24)$$

$$\lambda(a, b) = (1 - a - b)^2 - 4ab,$$

where $\Gamma(Z^0 \rightarrow \nu\bar{\nu}) = 166 \pm 2.7$ MeV [22].

Figure 31 shows the excluded range of $\cos^2(\beta - \alpha)$ as a function of m_h for $m_A = 20$ GeV.

6.3 Excluded Region in the (m_h, m_A) Plane

Using the lower limits on $\sin^2(\beta - \alpha)$ from the minimal Standard Model search and the lower limit on $\cos^2(\beta - \alpha)$, i.e. an upper limit on $\sin^2(\beta - \alpha)$, from the line shape constraint, a region in the (m_h, m_A) plane is excluded where the two limits are inconsistent with each other. The excluded (m_h, m_A) region is shown in Figure 32.

6.4 Combined Limit on Charged-Higgs Production

Combining the results in the three decay channels we can set a lower limit on the Higgs mass of 41 GeV independent of the Higgs decay mode. In order to smooth the exclusion line in the cscs channel the average of data and background over three neighboring mass points is used.

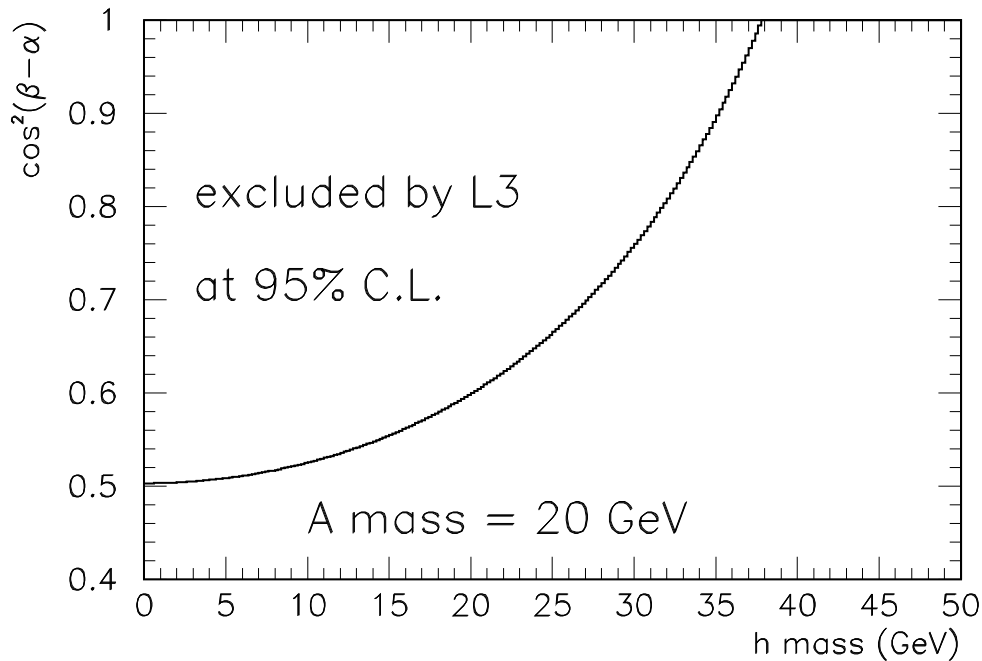


Figure 31: Limit on $\cos^2(\beta - \alpha)$ as a function of m_h for $m_A = 20$ GeV. The exclusion limit (95% CL) is based on constraints by the line-shape measurements which constrain additional contributions to the total Z^0 width from the reaction $Z^0 \rightarrow h^0 A^0$.

Figure 33 shows the excluded regions for the $cscs$, $cs\tau\nu$ and $\tau\nu\tau\nu$ signatures separately. From the three independent searches a combined excluded region is determined. Independent of the Higgs decay branching ratio a charged Higgs with mass lighter than 41 GeV is excluded.

7 Interpretation in the Minimal Supersymmetric Standard Model

In the framework of the Minimal Supersymmetric extension of the Standard Model, only the search for the neutral scalar h^0 and the neutral pseudoscalar A^0 is possible at LEP due to mass relations [4] in this model. For example $m_{H^\pm} > m_{W^\pm}$ is predicted. In the MSSM the parameters α and $\tan\beta$ are related to the Higgs masses and only two free parameter of the model remain. We choose (m_h, m_A) as the independent parameters of the model. The MSSM also predicts the branching ratios of the various allowed Higgs decays as a function of (m_h, m_A) .

The importance of radiative corrections for the Higgs mass spectrum in the MSSM was recently pointed out by several authors [23]. Due to these corrections the neutral Higgs boson masses can increase by several tens of GeV and the Higgs couplings can change substantially. When radiative corrections in this model are considered, the tree level mass relations as $m_h < m_Z$ or $m_h < m_A$ are no longer valid. Previous studies of radiative corrections in the MSSM did not take into account the possibility that the top quark mass and its supersymmetric partner, the stop, could be large [24]. The important implications of radiative corrections in the MSSM for the Higgs search can be extracted by making the following assumptions [25]. When top and the stop quarks have large masses, they contribute most to corrections to the tree level

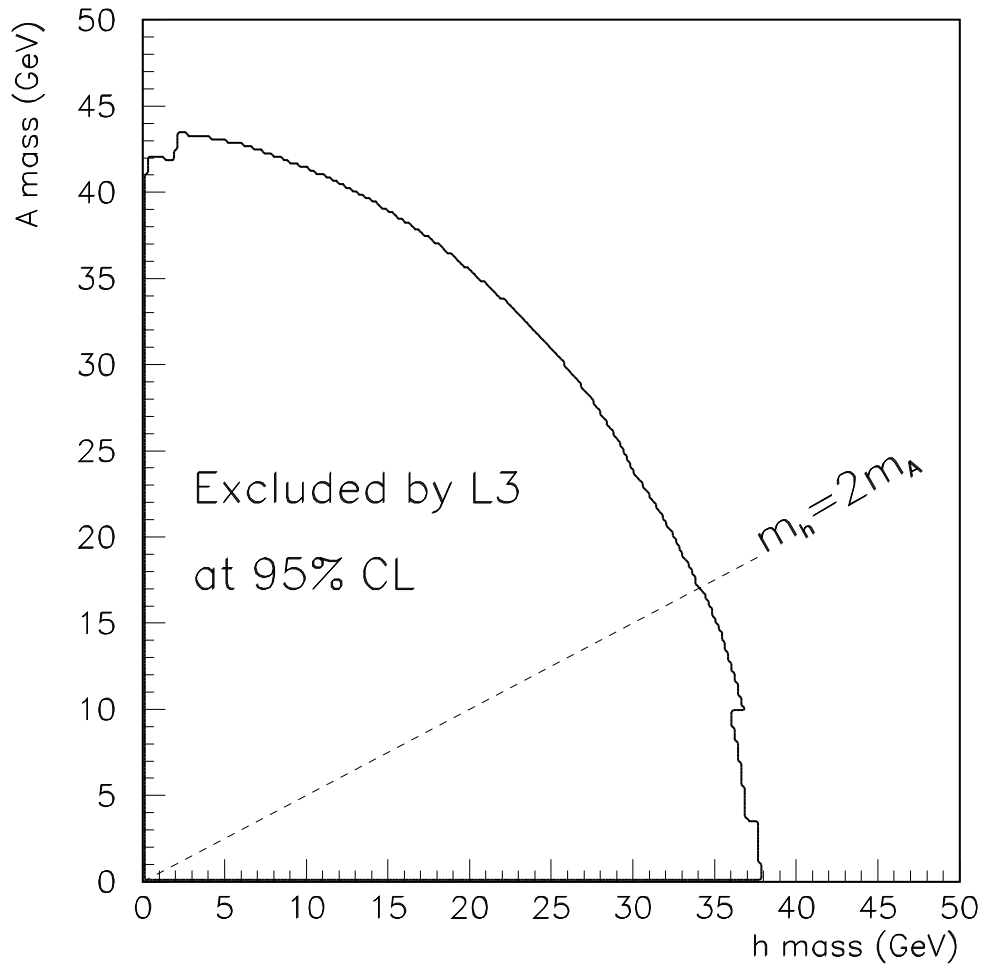


Figure 32: Exclusion in the (m_h, m_A) plane of the two-doublet Higgs model obtained by combining the limits from Higgs bremsstrahlung searches with the limits from the Z^0 line-shape measurements.

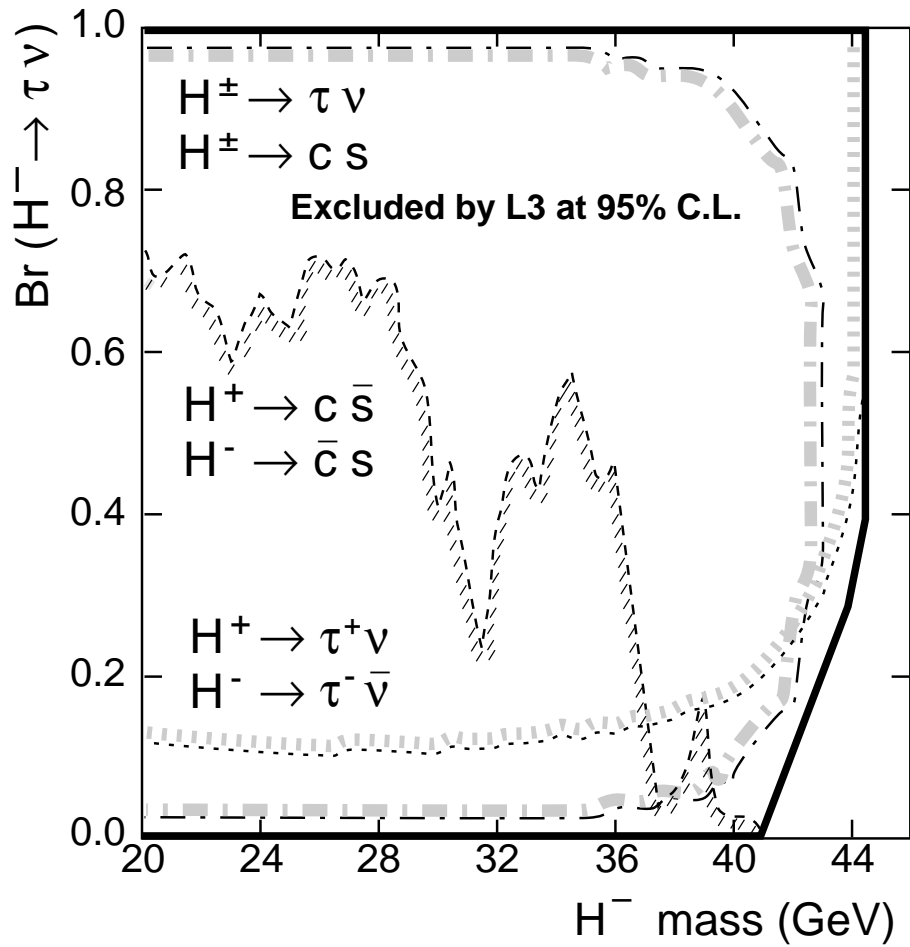


Figure 33: Excluded regions of pair produced charged Higgs in the channels $c\bar{c}s$, $cs\tau\nu$ and $\tau^+\nu\tau^-\bar{\nu}$ as a function of the charged Higgs mass and the leptonic Higgs branching fraction. The thick black line defines the combined excluded region.

calculations. The radiative corrections to the Higgs potential include m_{top} independent terms, and terms proportional to m_{top}^2 and m_{top}^4 . Only one term depends on m_{top}^4 . Due to the large top mass, only this term is considered to give the leading effect. Since the m_{top}^4 term concerns only the neutral Higgs sector, the effects of radiative corrections to the charged-Higgs sector are small in this approximation. It is further assumed that the value of $\tan \beta$ is not too large ($\tan \beta \leq m_{\text{top}}/m_b \approx 30$), otherwise, bottom and sbottom couplings to the Higgs are large and the bottom-sbottom loops can no longer be neglected. In addition, it is assumed that all Supersymmetric partners of the SM particles are degenerate in mass and do not mix. Their common mass, $m_{\tilde{q}}$, is related to the Supersymmetry breaking mass scale, m , by $m_{\tilde{q}}^2 = m_{\text{top}}^2 + m^2$,

Under the above assumptions, the effects of radiative corrections to tree level calculations can be summarized with a single dimensionless parameter, ϵ , for a given m_{top} and $m_{\text{stop}} = m_{\tilde{q}}$:

$$\epsilon \equiv \frac{3\alpha_W}{2\pi} \frac{m_{\text{top}}^4}{m_W^2 m_Z^2} \ln\left(\frac{m_{\text{stop}}^2}{m_{\text{top}}^2}\right), \quad (25)$$

where $\alpha_W = \alpha/\sin^2 \theta_W$. Radiative corrections modify the tree-level mass relations and the mass mixing angle. The correction $m_Z^2 \epsilon/\sin \beta$ is added to the squared mass mixing matrix for the neutral scalars. The physical Higgs masses are given by:

$$m_{\text{H,h}}^2 = \frac{1}{2}[m_A^2 + m_Z^2(1 + \frac{\epsilon}{\sin \beta}) \pm \Delta], \quad \text{where} \quad (26)$$

$$\begin{aligned} \Delta = & [(m_A^2 + m_Z^2(1 + \frac{\epsilon}{\sin \beta}))^2 - 4m_A^2 m_Z^2 \cos^2 2\beta \\ & - 4\frac{\epsilon}{\sin \beta} m_A^2 m_Z^2 \sin \beta - 4\frac{\epsilon}{\sin \beta} m_Z^4 \cos^2 \beta]^{1/2}. \end{aligned} \quad (27)$$

The mixing angle α and $\tan \beta$ are related by:

$$\sin 2\alpha = \frac{-(m_A^2 + m_Z^2) \sin 2\beta}{\Delta}. \quad (28)$$

After including radiative corrections, the expected number of pair-produced Higgs events depending on α and β , has changed compared to the tree level prediction.

In order to evaluate the effects of radiative corrections on the expected Higgs signal, a conservative mass range of the top and stop masses is chosen:

$$90 < m_{\text{top}} < 250 \text{ GeV}, \quad m_{\text{top}} < m_{\text{stop}} < 1000 \text{ GeV}. \quad (29)$$

This mass range corresponds to an ϵ range of $0 < \epsilon < 1.45$.

The theoretically preferred parameterization $(m_A, \tan \beta)$ of the available phase space is transformed into the (m_h, m_A) plane. Without radiative corrections, there is a one to one correspondence. However, with radiative corrections, one or two (m_h, m_A) pairs can correspond to one given $(m_A, \tan \beta)$ pair, while $\tan \beta$ is constrained to the range: $1.0 < \tan \beta \leq 50$ where the effect of the radiative correction is maximal. This ambiguity exists only in a small (m_h, m_A) region. Conservatively, for the prediction of the number of expected events, the $\tan \beta$ value which corresponds to the smaller Higgs production cross-section is chosen.

A given mass point in the (m_h, m_A) plane is excluded if, for all allowed values of ϵ , the model fails at least one of the direct searches or is excluded by the minimal Standard Model Higgs search or by the constraint from the Z^0 -lineshape limit. Figure 34 shows the excluded mass region in the (m_h, m_A) plane at 95% CL.

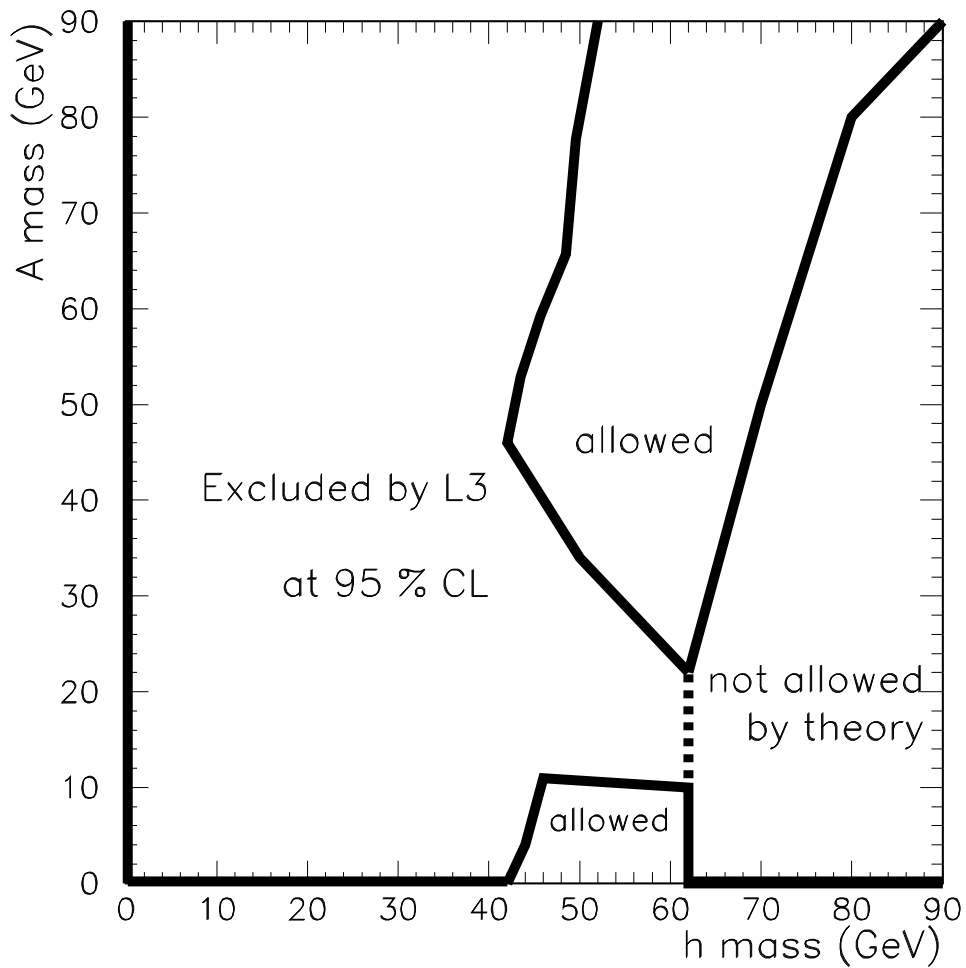


Figure 34: Excluded region at 95% confidence level in the (m_h, m_A) parameter region in the MSSM. A given mass point is excluded if for all allowed radiative correction effects the model fails at least one of the direct searches or is excluded by the minimal Standard Model Higgs search or by the constraint from the Z^0 -lineshape limit.

8 Conclusions

No indication for the production of Higgs bosons predicted in non-minimal models has been found. The following limits on the Higgs masses and other parameters of the two-doublet Higgs model are obtained:

- An upper limit on the branching ratio of Higgs bremsstrahlung of 3×10^{-5} to 2×10^{-4} is set depending on the Higgs mass in the mass range 0 to 60 GeV (see Figure 7).
- For pair-produced neutral Higgs bosons, a search of the dominant decay channels yields limits on allowed h^0 and A^0 mass ranges even for small branching ratios. (see Figures 11, 17 and 19).
- In the two-doublet Higgs model, the limit obtained from Higgs bremsstrahlung searches is expressed as an upper limit on $\sin^2(\beta - \alpha)$ of about 0.1 for Higgs masses up to about 30 GeV (see Figure 30).
- Limits on non-standard contributions to the Z^0 width as well as a direct search for Higgs bremsstrahlung including $h^0 \rightarrow A^0 A^0$ decays exclude a region $m_h^2 + m_A^2 \leq (40 \text{ GeV})^2$ in the framework of the two-doublet Higgs model (see Figure 32).
- For charged Higgs bosons of the two-doublet Higgs model, a lower limit of 41 GeV is obtained at 95% CL independent of the Higgs decay modes (see Figure 33).
- The interpretation of the results in the context of the Minimal Supersymmetric extension of the Standard Model includes radiative corrections. Nearly the entire (m_h, m_A) mass region which is kinematically allowed at present LEP energies is excluded (see Figure 34).

Acknowledgments

We wish to express our gratitude to the CERN accelerator divisions for the excellent performance of the LEP machine. We acknowledge the contributions of all the engineers and technicians who have participated in the construction and maintenance of this experiment.

The L3 Collaboration:

O. Adriani,¹⁴ M. Aguilar-Benitez,²³ S. Ahlen,⁹ J. Alcaraz,¹⁵ A. Aloisio,²⁶ G. Alverson,¹⁰ M.G. Alviggi,²⁶ G. Ambrosi,³¹ Q. An,¹⁶ H. Anderhub,⁴⁵ A.L. Anderson,¹³ V.P. Andreev,³⁵ T. Angelov,¹³ L. Antonov,³⁹ D. Antreasyan,⁷ P. Arce,²³ A. Arefev,²⁵ A. Atamanchuk,³⁵ T. Azemoon,³ T. Aziz,^{8,1} P.V.K.S. Baba,¹⁶ P. Bagnaia,³⁴ J.A. Bakken,³³ L. Baksay,⁴¹ R.C. Ball,³ S. Banerjee,⁸ J. Bao,⁵ R. Barillère,¹⁵ L. Barone,³⁴ A. Baschirotto,²⁴ R. Battiston,³¹ A. Bay,¹⁷ F. Becattini,¹⁴ U. Becker,^{13,45} F. Behner,⁴⁵ J. Behrens,⁴⁵ S. Beingessner,⁴ Gy.L. Bencze,¹¹ J. Berdugo,²³ P. Berges,¹³ B. Bertucci,³¹ B.L. Betev,^{39,45} M. Biasini,³¹ A. Biland,⁴⁵ G.M. Bilei,³¹ R. Bizzarri,³⁴ J.J. Blaising,⁴ G.J. Bobbink,^{15,2} M. Bocciaolini,¹⁴ R. Bock,¹ A. Böhm,¹ B. Borgia,³⁴ M. Boseti,²⁴ D. Bourilkov,²⁸ M. Bourquin,¹⁷ D. Boutigny,⁴ B. Bouwens,² E. Brambilla,²⁶ J.G. Branson,³⁶ I.C. Brock,³² M. Brooks,²¹ C. Buisson,²² A. Bujak,⁴² J.D. Burger,¹³ W.J. Burger,¹⁷ J. Busenitz,⁴¹ X.D. Cai,¹⁶ M. Capell,²⁰ M. Caria,³¹ G. Carlino,²⁶ F. Carminati,¹⁴ A.M. Cartacci,¹⁴ R. Castello,²⁴ M. Cerrada,²³ F. Cesaroni,³⁴ Y.H. Chang,¹³ U.K. Chaturvedi,¹⁶ M. Chemarin,²² A. Chen,⁴⁷ C. Chen,⁶ G.M. Chen,⁶ H.F. Chen,¹⁸ H.S. Chen,⁶ J. Chen,¹³ M. Chen,¹³ M.L. Chen,³ W.Y. Chen,¹⁶ G. Chiefari,²⁶ C.Y. Chien,⁵ M. Chmeissani,³ M.T. Choi,⁴⁰ S. Chung,¹³ C. Cividini,¹⁴ I. Clare,¹³ R. Clare,¹³ T.E. Coan,²¹ H.O. Cohn,²⁹ G. Coignet,⁴ N. Colino,¹⁵ A. Contin,⁷ F. Crijns,²⁸ X.T. Cui,¹⁶ X.Y. Cui,¹⁶ T.S. Dai,¹³ R.D. Alessandro,¹⁴ R. de Asmundis,²⁶ A. Degré,⁴ K. Deiters,¹³ E. Dénes,¹¹ P. Denes,³³ F. De Notaristefani,³⁴ M. Dhina,⁴⁵ D. Di Bitonto,⁴¹ M. Diemoz,³⁴ H.R. Dimitrov,³⁹ C. Dionisi,^{34,15} M.T. Dova,¹⁶ E. Drago,²⁶ T. Drierer,²⁸ D. Duchesneau,¹⁷ P. Duinker,² I. Duran,³⁷ S. Easo,³¹ H. El Mamouni,²² A. Engler,³² F.J. Epling,¹³ F.C. Erné,² P. Extermann,¹⁷ R. Fabbretti,⁴³ M. Fabre,⁴³ S. Falciano,³⁴ S.J. Fan,³⁸ O. Fackler,²⁰ J. Fay,²² M. Felcini,¹⁵ T. Ferguson,³² D. Fernandez,²³ G. Fernandez,²³ F. Ferroni,³⁴ H. Fesefeldt,¹ E. Fiandrini,³¹ J. Field,¹⁷ F. Filthaut,²⁸ G. Finocchiaro,³⁴ P.H. Fisher,⁵ G. Forconi,¹⁷ T. Foreman,² K. Freudenreich,⁴⁵ W. Friebel,⁴⁴ M. Fukushima,¹³ M. Gaillard,¹⁹ Yu. Galaktionov,^{25,13} E. Gallo,¹⁴ S.N. Ganguli,^{15,8} P. Garcia-Abia,²³ S.S. Gau,⁴⁷ D. Gele,²² S. Gentile,^{34,15} S. Goldfarb,¹⁰ Z.F. Gong,¹⁸ E. Gonzalez,²³ P. Göttlicher,¹ A. Gougas,⁵ D. Goujon,¹⁷ G. Gratta,³⁰ C. Grinnell,¹³ M. Gruenewald,³⁰ C. Gu,¹⁶ M. Guanzioli,¹⁶ J.K. Guo,³⁸ V.K. Gupta,³³ A. Gurtu,⁸ H.R. Gustafson,³ L.J. Gutay,⁴² K. Hangarter,¹ A. Hasan,¹⁶ D. Hauschildt,² C.F. He,³⁸ T. Hebbeker,¹ M. Hebert,³⁶ G. Herten,¹³ U. Herten,¹ A. Hervé,¹⁵ K. Hilgers,¹ H. Hofer,⁴⁵ H. Hoorani,¹⁷ G. Hu,¹⁶ G.Q. Hu,³⁸ B. Ille,²² M.M. Ilyas,¹⁶ V. Innocente,¹⁵ H. Janssen,¹⁵ S. Jezequel,¹⁵ B.N. Jin,⁶ L.W. Jones,³ A. Kasser,¹⁹ R.A. Khan,¹⁶ Yu. Kamyshev,²⁹ P. Kapinos,^{35,44} J.S. Kapustinsky,²¹ Y. Karyotakis,¹⁵ M. Kaur,¹⁶ S. Khokhar,¹⁶ M.N. Kienzle-Focacci,¹⁷ J.K. Kim,⁴⁰ S.C. Kim,⁴⁰ Y.G. Kim,⁴⁰ W.W. Kinnison,²¹ D. Kirkby,³⁰ S. Kirsch,⁴⁴ W. Kittel,²⁸ A. Klimentov,^{13,25} A.C. König,²⁸ E. Koffeman,² O. Kornadt,¹ V. Koutsenko,^{13,25} A. Koulbardi,³⁵ R.W. Kraemer,³² T. Kramer,¹³ V.R. Krastev,^{39,31} W. Krenz,¹ A. Krivshich,³⁵ H. Kuijten,²⁸ K.S. Kumar,¹² A. Kunin,^{12,25} G. Landi,¹⁴ D. Lanske,¹ S. Lanzano,²⁶ P. Lebrun,²² P. Lecomte,⁴⁵ P. Lecoq,¹⁵ P. Le Coultre,⁴⁵ D.M. Lee,²¹ I. Leedom,¹⁰ J.M. Le Goff,¹⁵ R. Leiste,⁴⁴ M. Lenti,¹⁴ E. Leonardi,³⁴ J. Lettry,⁴⁵ X. Leytens,² C. Li,^{18,16} H.T. Li,⁶ P.J. Li,³⁸ X.G. Li,⁶ J.Y. Liao,³⁸ W.T. Lin,⁴⁷ Z.Y. Lin,¹⁸ F.L. Linde,¹⁵ B. Lindemann,¹ D. Linnhofer,⁴⁵ L. Lista,²⁶ Y. Liu,¹⁶ W. Lohmann,^{44,15} E. Longo,³⁴ Y.S. Lu,⁶ J.M. Lubbers,¹⁵ K. Lübelmeyer,¹ C. Luci,³⁴ D. Luckey,^{7,13} L. Ludovici,³⁴ L. Luminari,³⁴ W. Lustermaun,⁴⁴ J.M. Ma,¹⁸ W.G. Ma,¹⁸ M. MacDermott,⁴⁵ P.K. Malhotra,^{8,1} R. Malik,¹⁶ A. Malinin,^{4,25} C. Mañá,²³ D.N. Mao,³ Y.F. Mao,⁶ M. Maolinbay,⁴⁵ P. Marchesini,⁴⁵ F. Marion,⁴ A. Marin,⁹ J.P. Martin,²² L. Martinez-Laso,²³ F. Marzano,³⁴ G.G.G. Massaro,¹³ T. Matsuda,¹³ K. Mazumdar,⁸ P. McBride,¹² T. McMahon,⁴² D. McNally,⁴⁵ M. Merk,²⁸ L. Merola,²⁶ M. Meschini,¹⁴ W.J. Metzger,²⁸ Y. Mi,¹⁹ G.B. Mills,²¹ Y. Mir,¹⁶ G. Mirabelli,³⁴ J. Mnich,¹ M. Möller,¹ B. Monteleoni,¹⁴ R. Morand,⁴ S. Morganti,³⁴ N.E. Moulai,¹⁶ R. Mout,³⁰ S. Müller,¹ A. Nadochty,³⁵ E. Nagy,¹¹ M. Napolitano,²⁶ H. Newman,³⁰ C. Neyer,⁴⁵ M.A. Niaz,¹⁶ A. Nippe,¹ H. Nowak,⁴⁴ G. Organtini,³⁴ D. Pandoulas,¹ S. Paoletti,¹⁴ P. Paolucci,²⁶ G. Passaleva,^{14,31} S. Patricelli,²⁶ T. Paul,⁵ M. Pauluzzi,³¹ F. Pauss,⁴⁵ Y.J. Pei,¹ S. Pensotti,²⁴ D. Perret-Gallix,⁴ J. Perrier,¹⁷ A. Pevsner,⁵ D. Piccolo,²⁶ M. Pieri,¹⁵ P.A. Piroué,³³ F. Plasil,²⁹ V. Plyaskin,²⁵ M. Pohl,⁴⁵ V. Poggiadaev,^{25,14} N. Produit,¹⁷ J.M. Qian,³ K.N. Qureshi,¹⁶ R. Raghavan,⁸ G. Rahal-Callot,⁴⁵ P.G. Rancoita,²⁴ M. Rattaggi,²⁴ G. Raven,² P. Raziš,²⁷ K. Read,²⁹ D. Ren,⁴⁵ Z. Ren,¹⁶ M. Rescigno,³⁴ S. Reucroft,¹⁰ A. Ricker,¹ S. Riemann,⁴⁴ W. Riemers,⁴² K. Riles,³ O. Rind,³ H.A. Rizvi,¹⁶ F.J. Rodriguez,²³ B.P. Roe,³ M. Röhner,¹ S. Röhner,¹ L. Romero,²³ J. Rose,¹ S. Rosier-Lees,⁴ R. Rosmalen,²⁸ Ph. Rosselet,¹⁹ A. Rubbia,¹³ J.A. Rubio,¹⁵ H. Rykaczewski,⁴⁵ M. Sachwitz,⁴⁴ E. Sajan,³¹ J. Salicio,¹⁵ J.M. Salicio,²³ G.S. Sanders,²¹ A. Santocchia,³¹ M.S. Sarakinos,¹³ G. Sartorelli,^{7,16} M. Sassowsky,¹ G. Sauvage,⁴ V. Schegelsky,³⁵ D. Schmitz,¹ P. Schmitz,¹ M. Schneegans,⁴ H. Schopper,⁴⁶ D.J. Schotanus,²⁸ S. Shotkin,¹³ H.J. Schreiber,⁴⁴ J. Shukla,³² R. Schulte,¹ S. Schulte,¹ K. Schultze,¹ J. Schwenke,¹ G. Schwering,¹ C. Sciacca,²⁶ I. Scott,¹² R. Sehgal,¹⁶ P.G. Seiler,⁴³ J.C. Sens,^{15,2} L. Servoli,³¹ I. Sheer,³⁶ D.Z. Shen,³⁸ S. Shevchenko,³⁰ X.R. Shi,³⁰ E. Shumilov,²⁵ V. Shoutko,²⁵ E. Soderstrom,³³ D. Son,⁴⁰ A. Sopczak,³⁶ C. Spartiotis,⁵ T. Spickermann,¹ P. Spillantini,¹⁴ R. Starosta,¹ M. Steuer,^{7,13} D.P. Stickland,³³ F. Sticozzi,¹³ H. Stone,¹⁷ K. Strauch,¹² B.C. Stringfellow,⁴² K. Sudhakar,⁸ G. Sultanov,¹⁶ R.L. Sumner,³³ L.Z. Sun,^{18,16} H. Suter,⁴⁵ R.B. Sutton,³² J.D. Swain,¹⁶ A.A. Syed,¹⁶ X.W. Tang,⁶ L. Taylor,¹⁰ G. Terzi,²⁴ C. Timmermans,²⁸ Samuel C.C. Ting,¹³ S.M. Ting,¹³ M. Tonutti,¹ S.C. Tonwar,⁸ J. Tóth,¹¹ A. Tsaregorodtsev,³⁵ G. Tsipolitis,³² C. Tully,³⁰ K.L. Tung,⁶ J. Ulbricht,⁴⁵ L. Urbán,¹¹ U. Uwer,¹ E. Valente,³⁴ R.T. Van de Walle,²⁸ I. Vetlitsky,²⁵ G. Viertel,⁴⁵ P. Vikas,¹⁶ U. Vikas,¹⁶ M. Vivargent,⁴ H. Vogel,³² H. Vogt,⁴⁴ I. Vorobiev,²⁵ A.A. Vorobyov,³⁵ L. Vuilleumier,¹⁹ M. Wadhwa,¹⁶ W. Wallraff,¹ C.R. Wang,¹⁸ G.H. Wang,³² J.H. Wang,⁶ X.L. Wang,¹⁸ Y.F. Wang,¹³ Z.M. Wang,^{16,18} A. Weber,¹ J. Weber,⁴⁵ R. Weill,¹⁹ T.J. Wenaus,²⁰ J. Wenninger,¹⁷ M. White,¹³ C. Willmott,²³ F. Wittgenstein,¹⁵ D. Wright,³³ R.J. Wu,⁶ S.X. Wu,¹⁶ Y.G. Wu,⁶ B. Wyslouck,¹³ Y.Y. Xie,³⁸ Y.D. Xu,⁶ Z.Z. Xu,¹⁸ Z.L. Xue,³⁸ D.S. Yan,³⁸ X.J. Yan,¹³ B.Z. Yang,¹⁸ C.G. Yang,⁶ G. Yang,¹⁶ K.S. Yang,⁶ Q.Y. Yang,⁶ Z.Q. Yang,³⁸ C.H. Ye,¹⁶ J.B. Ye,¹⁸ Q. Ye,¹⁶ S.C. Yeh,⁴⁷ Z.W. Yin,³⁸ J.M. You,¹⁶ N. Yunus,¹⁶ M. Yzerman,² C. Zaccardelli,³⁰ P. Zemp,⁴⁵ M. Zeng,¹⁶ Y. Zeng,¹ D.H. Zhang,² Z.P. Zhang,^{18,16} B. Zhou,⁹ J.F. Zhou,¹ R.Y. Zhu,³⁰ H.L. Zhuang,⁶ A. Zichichi,^{7,15,16} B.C.C. van der Zwaan,²

-
- 1 I. Physikalisches Institut, RWTH, W-5100 Aachen, FRG[§]
 - III. Physikalisches Institut, RWTH, W-5100 Aachen, FRG[§]
 - 2 National Institute for High Energy Physics, NIKHEF, NL-1009 DB Amsterdam, The Netherlands
 - 3 University of Michigan, Ann Arbor, MI 48109, USA
 - 4 Laboratoire d'Annecy-le-Vieux de Physique des Particules, LAPP,IN2P3-CNRS, BP 110, F-74941 Annecy-le-Vieux CEDEX, France
 - 5 Johns Hopkins University, Baltimore, MD 21218, USA
 - 6 Institute of High Energy Physics, IHEP, Beijing, China
 - 7 INFN-Sezione di Bologna, I-40126 Bologna, Italy
 - 8 Tata Institute of Fundamental Research, Bombay 400 005, India
 - 9 Boston University, Boston, MA 02215, USA
 - 10 Northeastern University, Boston, MA 02115, USA
 - 11 Central Research Institute for Physics of the Hungarian Academy of Sciences, H-1525 Budapest 114, Hungary[‡]
 - 12 Harvard University, Cambridge, MA 02139, USA
 - 13 Massachusetts Institute of Technology, Cambridge, MA 02139, USA
 - 14 INFN Sezione di Firenze and University of Florence, I-50125 Florence, Italy
 - 15 European Laboratory for Particle Physics, CERN, CH-1211 Geneva 23, Switzerland
 - 16 World Laboratory, FBLJA Project, CH-1211 Geneva 23, Switzerland
 - 17 University of Geneva, CH-1211 Geneva 4, Switzerland
 - 18 Chinese University of Science and Technology, USTC, Hefei, Anhui 230 029, China
 - 19 University of Lausanne, CH-1015 Lausanne, Switzerland
 - 20 Lawrence Livermore National Laboratory, Livermore, CA 94550, USA
 - 21 Los Alamos National Laboratory, Los Alamos, NM 87544, USA
 - 22 Institut de Physique Nucléaire de Lyon, IN2P3-CNRS, Université Claude Bernard, F-69622 Villeurbanne Cedex, France
 - 23 Centro de Investigaciones Energeticas, Medioambientales y Tecnologicas, CIEMAT, E-28040 Madrid, Spain
 - 24 INFN-Sezione di Milano, I-20133 Milan, Italy
 - 25 Institute of Theoretical and Experimental Physics, ITEP, Moscow, Russia
 - 26 INFN-Sezione di Napoli and University of Naples, I-80125 Naples, Italy
 - 27 Department of Natural Sciences, University of Cyprus, Nicosia, Cyprus
 - 28 University of Nymegen and NIKHEF, NL-6525 ED Nymegen, The Netherlands
 - 29 Oak Ridge National Laboratory, Oak Ridge, TN 37831, USA
 - 30 California Institute of Technology, Pasadena, CA 91125, USA
 - 31 INFN-Sezione di Perugia and Università Degli Studi di Perugia, I-06100 Perugia, Italy
 - 32 Carnegie Mellon University, Pittsburgh, PA 15213, USA
 - 33 Princeton University, Princeton, NJ 08544, USA
 - 34 INFN-Sezione di Roma and University of Rome, "La Sapienza", I-00185 Rome, Italy
 - 35 Nuclear Physics Institute, St. Petersburg, Russia
 - 36 University of California, San Diego, CA 92182, USA
 - 37 Dept. de Fisica de Particulas Elementales, Univ. de Santiago, E-15706 Santiago de Compostela, Spain
 - 38 Shanghai Institute of Ceramics, SIC, Shanghai, China
 - 39 Bulgarian Academy of Sciences, Institute of Mechatronics, BU-1113 Sofia, Bulgaria
 - 40 Center for High Energy Physics, Korea Advanced Inst. of Sciences and Technology, 305-701 Taejon, Republic of Korea
 - 41 University of Alabama, Tuscaloosa, AL 35486, USA
 - 42 Purdue University, West Lafayette, IN 47907, USA
 - 43 Paul Scherrer Institut, PSI, CH-5232 Villigen, Switzerland
 - 44 DESY-Institut für Hochenergiephysik, O-1615 Zeuthen, FRG
 - 45 Eidgenössische Technische Hochschule, ETH Zürich, CH-8093 Zürich, Switzerland
 - 46 University of Hamburg, W-2000 Hamburg, FRG
 - 47 High Energy Physics Group, Taiwan, China
- § Supported by the German Bundesministerium für Forschung und Technologie
‡ Supported by the Hungarian OTKA fund under contract number 2970.
† Deceased.

References

- [1] S.L. Glashow, *Nucl. Phys.* **22** (1961) 579,
A. Salam, *Phys. Rev.* **127** (1962) 331,
A. Salam, in: “Elementary Particle Theory”, ed. N. Svartholm (Stockholm, 1968), 361,
S. Weinberg, *Phys. Rev. Lett.* **19** (1967) 1264.
- [2] P.W. Higgs, *Phys. Lett.* **12** (1964) 132,
P.W. Higgs, *Phys. Rev. Lett.* **13** (1964) 508,
P.W. Higgs, *Phys. Rev.* **145** (1966) 1156,
F. Englert and R. Brout, *Phys. Rev. Lett.* **13** (1964) 321,
G.S. Guralnik, C.S. Hagen and T.W.B. Kibble, *Phys. Rev. Lett.* **13** (1964) 585.
- [3] L3 Collaboration, B. Adeva *et al.*, *Phys. Lett.* **B 283** (1992) 454.
- [4] For a review see S. Dawson, J.F. Gunion, H.E. Haber and G.L. Kane, “The Physics of the Higgs bosons: Higgs Hunter’s Guide” (Addison Wesley, Menlo Park, 1989).
- [5] M. Aguilar-Benitez *et al.*, “Review of Particle Properties”, *Phys. Rev.* **D 45** (1992) 1.
- [6] Y.A. Golfand and E.P. Likhtman, *JETP Lett.* **13** (1971) 323,
D.V. Volkov and V.P. Akulov, *Phys. Lett.* **B 46** (1973) 109,
J. Wess and B. Zumino, *Nucl. Phys.* **B 70** (1974) 39,
P. Fayet and S. Ferrara, *Phys. Rep.* **32** (1977) 249,
A. Salam and J. Strathdee, *Fortschr. Phys.* **26** (1978) 57,
H.P. Nilles, *Phys. Rep.* **110** (1984) 1.
- [7] ALEPH Collaboration, D. Decamp *et al.*, *Phys. Lett.* **B 245** (1990) 289,
DELPHI Collaboration, P. Abreu *et al.*, *Phys. Lett.* **B 343** (1990) 1,
OPAL Collaboration, P.D. Acton *et al.*, *Phys. Lett.* **B 251** (1990) 211,
L3 Collaboration, B. Adeva *et al.*, *Phys. Lett.* **B 252** (1990) 518.
- [8] ALEPH Collaboration, D. Decamp *et al.*, *Phys. Lett.* **B 265** (1991) 475,
DELPHI Collaboration, P. Abreu *et al.*, *Nucl. Phys.* **B 373** (1992) 3,
OPAL Collaboration, M.Z. Akrawi *et al.*, *Z. Phys.* **C 49** (1991) 1,
L3 Collaboration, B. Adeva *et al.*, *Phys. Lett.* **B 251** (1990) 331.
- [9] ALEPH Collaboration, D. Decamp *et al.*, *Phys. Lett.* **B 241** (1990) 623,
DELPHI Collaboration, P. Abreu *et al.*, *Nucl. Phys.* **B 241** (1990) 449,
OPAL Collaboration, M.Z. Akrawi *et al.*, *Phys. Lett.* **B 242** (1990) 299,
L3 Collaboration, B. Adeva *et al.*, *Phys. Lett.* **B 252** (1990) 511.
- [10] L3 Collaboration, B. Adeva *et al.*, *Nucl. Instrum. Methods* **A 289** (1990) 35.
- [11] GEANT Version 3.13, September, 1989.
See R. Brun *et al.*, “GEANT 3”, CERN DD/EE/84-1 (Revised), Sept. 1987.
- [12] H. Fesefeldt, RWTH Aachen Report PITHA 85/02 (1985).
- [13] M. Bengtsson and T. Sjöstrand, *Comput. Phys. Commun.* **43** (1987) 367,
T. Sjöstrand, “Z Physics at LEP 1”, eds. G. Altarelli, R. Kleiss and C. Verzegnassi, CERN Report CERN-89-08 (1989), Vol. 3, p. 143.

- [14] S. Jadach *et al.*, “Z Physics at LEP 1”, eds. G. Altarelli, R. Kleiss and C. Verzegnassi, CERN Report CERN-89-08 (1989), Vol. 3, p. 69.
- [15] F.A. Berends, P.H. Daverveldt and R. Kleiss, *Nucl. Phys.* **B 253** (1985) 441.
- [16] H.-U. Bengtsson and T. Sjöstrand, *Comput. Phys. Commun.* **46** (1987) 43.
- [17] Z. Kunszt, *Phys. Lett.* **B 99** (1981) 429,
J.A.M. Vermaseren, K.J.F. Gaemers and S.J. Oldham, *Nucl. Phys.* **B187** (1981) 301.
- [18] L3 Collaboration, B. Adeva *et al.*, *Phys. Lett.* **B 248** (1990) 203.
- [19] L3 Collaboration, B. Adeva *et al.*, Preprint, CERN, PPE/92-84 (1992).
- [20] L3 Collaboration, B. Adeva *et al.*, *Phys. Lett.* **B 252** (1990) 511.
- [21] L3 Collaboration, Contributed paper to the “XXVI International Conference on High Energy Physics”, Dallas, USA (6 – 12 August, 1992).
- [22] L3 Collaboration, B. Adeva *et al.*, *Z. Phys.* **C 51** (1991) 179.
- [23] J. Ellis, G. Ridolfi and F. Zwirner, *Phys. Lett.* **B 257** (1991) 83,
H.E. Haber and R. Hempfling, *Phys. Rev. Lett.* **66** (1991) 1815,
Y. Okada, M. Yamaguchi and T. Yanagida, *Prog. Theor. Phys. Lett.* **85** (1991) 1.
- [24] S.P. Li and M. Sher, *Phys. Lett.* **B 140** (1984) 339,
J.F. Gunion and A. Turski, *Phys. Rev.* **D 39** (1989) 2701,
J.F. Gunion and A. Turski, *Phys. Rev.* **D 40** (1989) 2325,
J.F. Gunion and A. Turski, *Phys. Rev.* **D 40** (1989) 2333,
M.S. Berger, *Phys. Rev.* **D 41** (1990) 225.
- [25] R. Barbieri and M. Frigeni, *Phys. Lett.* **B 258** (1991) 395,
A. Brignole, J. Ellis, G. Ridolfi and F. Zwirner, *Phys. Lett.* **B 271** (1991) 123,
J. Ellis, G. Ridolfi and F. Zwirner, *Phys. Lett.* **B 262** (1991) 477.